Bit error rate performance of CDMA mobile systems

BIT ERROR RATE PERFORMANCE OF CDMA MOBILE SYSTEMS

Prepared for the Communications Research Centre, Department of Communications

NovAtel Communications Ltd.

September 11, 1991

DSS Contract No: 36001-0-3593/1

CRC SC. AUTH.: MOHER, M.

Abstract

The effects of radio channel fading, multipath interference, multi-user interference, and additive white Gaussian noise on the bit error rate performance of a BPSK/DPSK modulated, direct sequence spread spectrum, code division multiple access (CDMA) mobile communication system are studied by computer simulation. Expressions for the decision statistic are derived in terms of the system parameters for both coherent and differential single path receivers, as well as differential RAKE receiver. These expressions form the basis of the bit error rate simulation package that is developed.

Results of several simulations with different system parameters are presented. The results suggest that if there are interference and fading conditions, then long spreading codes, diversity, and/or error correction coding are required for the CDMA mobile system to be of use as a practical communication system.

Table of Contents

1.0 Introduction

The application of spread spectrum techniques to mobile communication systems is of increasing interest in recent years, principally because of its potential for enhanced capacity. The current study is motivated by a need to fully understand the effects of the mobile radio environment and multi-user interference on the performance of direct sequence spread spectrum code division multiple access (DS-SS-CDMA) mobile communication systems. An appreciation of the effects of the mobile radio environment and multi-user interference is desired to enable an objective assessment of CDMA mobile system performance in terms of its limitations and capabilities, as well as facilitate the selection of optimum system parameters.

This study is concerned with the investigation of the effects of radio channel fading, multipath distortion, interference from other users, and thermal noise on the performance of CDMA mobile systems that use binary phase shift keying (BPSK) or differential phase shift keying (DPSK) modulation - as specified in the statement of work [1]. For both the coherent and differential single path receivers, as well as the differential RAKE receiver, expressions for the decision statistic are derived in terms of the multipath radio channel parameters, correlation properties of the spreading sequence, transmitted data bit sequence, number of simultaneous users, and additive white Gaussian noise. The expressions for the decision statistic are then used to predict through simulation the bit error rate for Rayleigh and Rician fading channels.

The remainder of the report is organized as follows. Section 2 describes the CDMA system to be simulated, the modeling assumptions, and a detailed analysis of the decision statistic for the different receiver structures considered. Section 3 describes the simulation assumptions and structure. In section 4 sample simulation results are presented and discussed as to their relation to the system design, and section 5 contains the conclusions. Appendix I describes the simulation software design and Appendix II contains the user guide and simulation source codes.

2.0 System Modeling and Analysis

2.1 System Block Diagram

The block diagram of the simulated system is shown in Figure 1.

2.2 System Description

The function of each block in Fig. 1 is described as follows.

Data Generator Generates a pseudo-random data bit sequence.

Spreading Code A set of Gold codes with a chip rate of 31 times the symbol rate, and a set of Kasami codes with a chip rate of 255 times the symbol rate are selected because of their low cross-correlation properties. Independent spreading codes are selected for different users.

BPSK Modulator Produces one of two signals that differ in phase by π radians at every data symbol interval. The DPSK modulator is realized by adding a differential encoding function to the BPSK modulator. As the number of signal levels is equal to two for both BPSK and DPSK, the data symbol rate equals the data bit rate. This study assumes no form of channel encoding [1], hence the terms "data bit", "data symbol" and "channel symbol" all have the same meaning and as such, "bit" and "symbol" are used interchangeably.

Channel A fading channel which will simulate each of the following scenarios [1]:

1) Rayleigh flat fading with:
   - chip rate to symbol rate of 31 and 255.
   - chip rate to coherence bandwidth < 0.1.
   - Doppler bandwidth to symbol rate of 0.1 and 0.01.

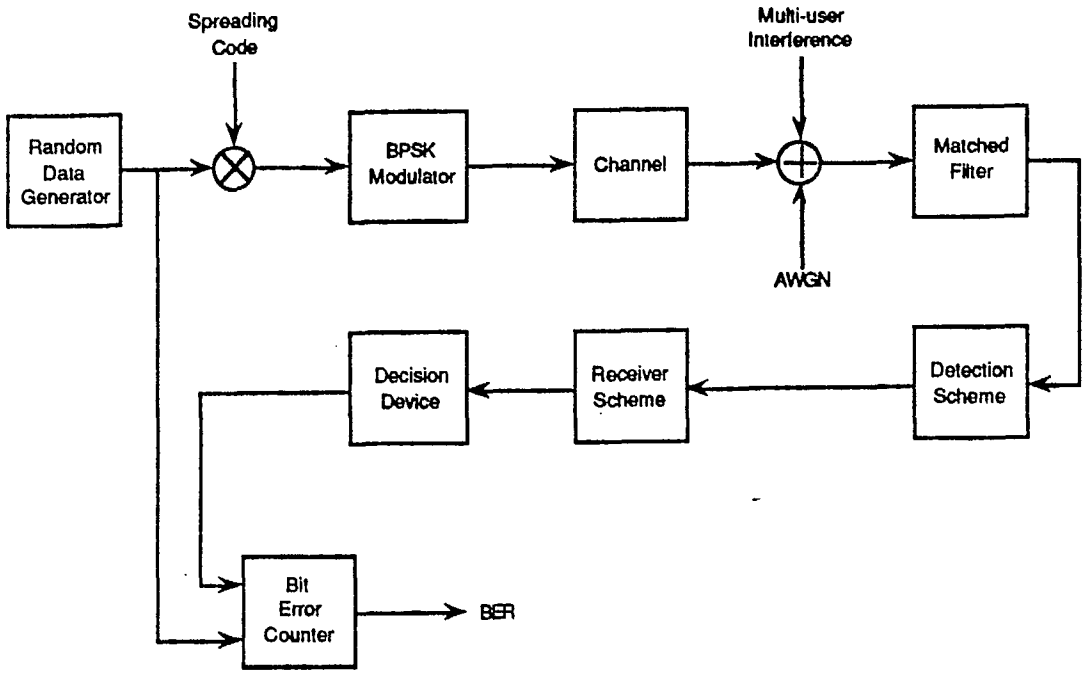

Fig.1 System block diagram

2) Rician flat fading with:
   - chip rate to symbol rate of 31 and 255.
   - chip rate to coherence bandwidth < 0.1.
   - Doppler bandwidth to symbol rate of 0.1 and 0.01.
   - Rice factor of -100 dB and -5 dB.

3) Rayleigh frequency selective fading with:
   - chip rate to symbol rate of 31 and 255.
   - chip rate to coherence bandwidth of 10 and 50.
   - Doppler bandwidth to symbol rate of 0.01 and 0.001.

4) Rician frequency selective fading with:
   - chip rate to symbol rate of 31 and 255.
   - chip rate to coherence bandwidth of 10 and 50.
   - Doppler bandwidth to symbol rate of 0.01 and 0.001.
   - Rice factor of -100 dB and -5 dB.

Multi-user Interference Results from other CDMA users, whose transmitted signals have propagated through independent fading channels which have the same channel statistics as that of the desired user.

Matched Filter Performs a correlation of the received signal with the locally generated spreading code waveform of the desired user. The resulting correlation peak is sampled by the detection device.

Detection scheme The detection scheme to be used depends on the fading channel scenario as specified in [1]:

1) Coherent Detection
   - Rician flat fading channel
   - Rician frequency selective fading channel

2) Differential Detection
   - Rayleigh flat fading channel
   - Rayleigh frequency selective fading channel

Receiver Scheme The receiver is either a single path receiver or a 10 or 20 tap differential RAKE receiver used only for the Rayleigh frequency selective fading channel.

Bit Error Rate (BER) Counter Compares the received symbol with the transmitted symbol and increments the error count if an error has occurred.

2.3 Definition of Variables

To simplify the presentation, the following variables and notations employed in system modeling and analysis are defined below:

$\{a_j^{(k)}\}_{j=0}^{N-1}$	spreading code sequence for user k
$a_k(.)$	spreading code waveform for user k
A_k	amplitude of the transmitted signal by user k
A	(generic) amplitude of transmitted signal
AWGN	additive white Gaussian noise
$\{b_j^{(k)}\}_{j=-\infty}^{\infty}$	data bit (symbol) sequence for user k
$b_0^{(k)}$	current transmitted bit by user k
$b_{-1}^{(k)}$	previous transmitted bit by user k, i.e. bit before $b_0^{(k)}$
$b_{+1}^{(k)}$	next transmitted bit by user k, i.e. bit after $b_0^{(k)}$
$b_k(.)$	data bit waveform for user k
$\widehat{b_0^{(k)}}$	detected estimate for $b_0^{(k)}$
$\vec{b}_k$	data bit vector for user k
B_d	Doppler bandwidth
B_{eq}	noise equivalent bandwidth
BER	bit error rate
$B_{ki}(.,.)$	mutual interference factor between user k and user i
$C_{ki}(.)$	discrete aperiodic cross-correlation function of the kth and ith user spreading sequences

exp	exponential function
E_b	energy per transmitted bit
f(.)	low-pass impulse response of the matched filter
G(0,1)	standard Gaussian source having zero mean and unity variance
$h_k(.)$	complex, low-pass impulse response of user k's radio channel
H(.)	fading filter transfer function
$I_{ii}(.,.)$	self interference for user i
$I_{ki}(.,.)$	mutual interference between user k and user i
Im[.]	imaginary part of .
I_o	Bessel function of order zero
K	number of users (mobile stations) in the simulated system
ln[.]	natural logarithm of .
L_k	number of discrete channel paths (user k)
min(...)	minimum value of ...
M	number of symbols to process in one simulation run
n(.)	additive white Gaussian noise (AWGN), a bandpass signal
$\tilde{n}(.)$	complex, low-pass equivalent of n(.)
N	number of chips in a spreading sequence (processing gain)
N_o	noise power spectral density
p(.)	data bit pulse
P_k	power in the transmitted signal by user k
P	power in the transmitted signal by a generic user
r(.)	total bandpass signal at the receiver input
$\tilde{r}(.)$	complex, low-pass equivalent of r(.)
Re[.]	real part of .
$R^-_{ki}(.)$	continuous-time partial cross-correlation function for the kth and ith user spreading sequence waveforms
$R^+_{ki}(.)$	continuous-time partial cross-correlation function for the kth and ith user spreading sequence waveforms
$s_k(.)$	spread spectrum modulated signal transmitted by user k
S	number of successive symbols to process (for each user) in the simulation
t	time variable
tot	total number of taps in a given RAKE window
T	symbol duration

T_c	chip duration
$U(.)$	indicator function
U_k	user k
w_i	weight for RAKE receiver tap number i
$W(.)$	weighting function for the total received signal
$\tilde{Z}(.)$	complex, low-pass matched filter output if $b_0^{(i)}$ is transmitted
$\tilde{Z}_{-1}(.)$	complex, low-pass matched filter output if $b_{-1}^{(i)}$ is transmitted
α	generic fading filter scaling factor
α_{Ray}	fading filter scaling factor for a Rayleigh fading path
α_{Rice}	fading filter scaling factor for a Rician fading path
$\beta(.)$	generic path gain at time .
β_i	path gain (only 1 path) for user i
β_{lk}	lth path gain for user k
$\hat{\beta}_{lk}$	estimate of β_{lk}
$\gamma(.)$	generic path phase at time .
γ_{lk}	lth path phase for user k
$\delta(.)$	Dirac delta function
Δ_W	RAKE window
ζ	decision statistic at the detector output
$\zeta_l(.)$	decision statistic at the differential detector output for path l
η	normalized zero mean AWGN, in-phase component
θ_k	carrier phase for user k
μ^2	average power in the dominant, nonfading subpath of the Rician fading path
ν	normalized zero mean AWGN, quadrature component
σ^2	half the average power of the fading subpaths of a channel path
τ	generic path delay
τ_{lk}	lth path delay for user k
τ'_{lk}	τ_{lk} relative to τ_{ji}
τ'_k	τ'_{lk} when there is only one path
ϕ	generic resultant path phase
ϕ_{lk}	resultant lth path phase for user k

ϕ'_{lk}	ϕ_{lk} relative to ϕ_{ji}
ϕ'_{k}	ϕ'_{lk} when there is only one path
$\psi(.)$	chip pulse
ω_c	carrier frequency
Ω	Rice factor
$\lvert . \rvert$	absolute value of .
$\lfloor . \rfloor$	floor of ., i.e. the greatest integer smaller than or equal to .
$\sum$	summation symbol
$\otimes$	convolution symbol
$\sqrt{}$	square root symbol
*	complex conjugate symbol

2.4 System Modeling Assumptions

In order to formulate a tractable analytic model for the CDMA system, the following assumptions are made concerning the transmitter, the radio channel, and the receiver.

2.4.1 Transmitter Assumptions

T1) The system consists of K users (mobile stations) all transmitting to one base station receiver.

T2) All the mobiles transmit at equal power level of P Watts.

T3) The data bit pulse is of a rectangular shape with a duration of T seconds.

T4) Transmitted data bits are from a binary sequence of independent and identically distributed, equally probable, antipodal (-1, +1) random variables.

T5) Each mobile is assigned a unique spreading sequence, and the base station receiver always has perfect knowledge of the spreading sequence of the desired mobile transmitter.

T6) Spreading codes consisting of (-1, +1) chips are selected from the Gold and Kasami codes.

T7) The chip pulse has rectangular shape of duration T_c seconds, and the power in the pulse is normalized to unity.

T8) A spreading code is periodic with period N, which is the length of the spreading code.

T9) Each data bit is encoded with N chips, hence $T = NT_c$.

2.4.2 Radio Channel Assumptions

C1) The signal transmitted by user k arrives at the receiver input via a fixed number of discrete paths, L_k.

C2) The channel parameters $\{\beta_{lk}\}_{l=1}^{L_k}$, $\{\gamma_{lk}\}_{l=1}^{L_k}$, and $\{\tau_{lk}\}_{l=1}^{L_k}$ are independent sets of random variables, and all the variables in each set are mutually independent and identically distributed.

C3) Each path is a vector sum of infinite number of subpaths arriving uniformly from all directions. For path l (user k), $1 \le l \le L_k$, the path gain (or received signal envelope) is either Rayleigh or Rician distributed. If the gain for path l is Rician distributed and $L_k > 1$, then the lth path delay is such that $\tau_{lk} = \min(\tau_{1k}, \tau_{2k}, \ldots, \tau_{L_k,k})$.

C4) The average power delay profile has a constant shape, i.e. all the paths have the same average power.

C5) The delay of each path is uniformly distributed over [0, T].

C6) The absolute difference between the delays for paths l and j ($l \neq j$) for user k

must satisfy the constraint $|\tau_{lk} - \tau_{jk}| \geq T_c$ for paths l and j to be resolvable.

C7) The channel fading rate is slow compared to the data rate.

C8) The K user channels are independent of each other, i.e. the channel parameters for user m are completely independent from the corresponding parameters for user n, ($m \neq n$).

C9) The transmitted signal is corrupted by additive white Gaussian noise (AWGN) with a double-sided power spectral density of $N_0/2$ Watts/Hz.

Remarks: Assumptions C1 and C4 are made to simplify the analysis because in a realistic mobile environment, the number of paths is not fixed and one would expect a decrease in average path power with increasing path delay. Assumption C5 means that the data symbol rate is less than the channel coherence bandwidth, which implies that for a given symbol, intersymbol interference (ISI) arises from only the immediate preceding and succeeding transmitted symbols. Actually, the assumption is made for notational convenience as the analysis can handle any range of propagation delay greater than T. For such a range, more adjacent bits will then account for ISI .

2.4.3 Receiver Assumptions

R1) A matched filter receiver is used, with the receiver matched to the spreading code waveform of the desired user.

R2) The sampling instant occurs at the end of the data bit pulse duration.

R3) For the single path receiver structure, the receiver always locks on to a path of the signal from the desired mobile transmitter.

R4) For the RAKE receiver, path combining is performed non-coherently and the receiver always has perfect knowledge of the channel parameters.

2.5 System Analysis

2.5.1 Transmitter Analysis

For BPSK/DPSK modulation, the spread spectrum modulated signal transmitted by user k, $1 \le k \le K$, is given by [2]

$$s_k(t) = A_k\, a_k(t)\, b_k(t) \cos(\omega_c t + \theta_k) \tag{1}$$

where $a_k(t) = \sum_{j=0}^{N-1} a_j^{(k)} \psi(t - jT_c)$ and $b_k(t) = \sum_{j=-\infty}^{\infty} b_j^{(k)} p(t - jT)$.

A_k is related to P_k, the power of the transmitted signal by user k. Under the assumption of no power control, $P_1 = P_2 = \ldots = P_K = P$, so that

$$s_k(t) = A\, a_k(t)\, b_k(t) \cos(\omega_c t + \theta_k) \tag{2}$$

2.5.2 Radio Channel Analysis

The complex, low-pass impulse response of the radio channel seen by user k's transmitted signal is defined by [3]

$$h_k(t) = \sum_{l=1}^{L_k} \beta_{lk}(t) \exp(j\gamma_{lk}(t))\delta(t - \tau_{lk}) \tag{3}$$

where L_k, $\beta_{lk}(.)$, $\gamma_{lk}(.)$ and τ_{lk} are the channel parameters for the kth user with statistics as defined in Section 2.4.2. The schematic diagram for the fading channel simulator used for generating samples for $\beta_{lk}(t)$ and $\gamma_{lk}(t)$ is shown in Figure 2 where the variates of two independent standard Gaussian sources are separately filtered (to give the desired correlation properties of the fading process), scaled (according to path gain distribution and average path power) and then added in quadrature. The output of the channel simulator is a complex Gaussian signal given by $\beta(t) \exp(j\gamma(t))$ where for path l of user k:

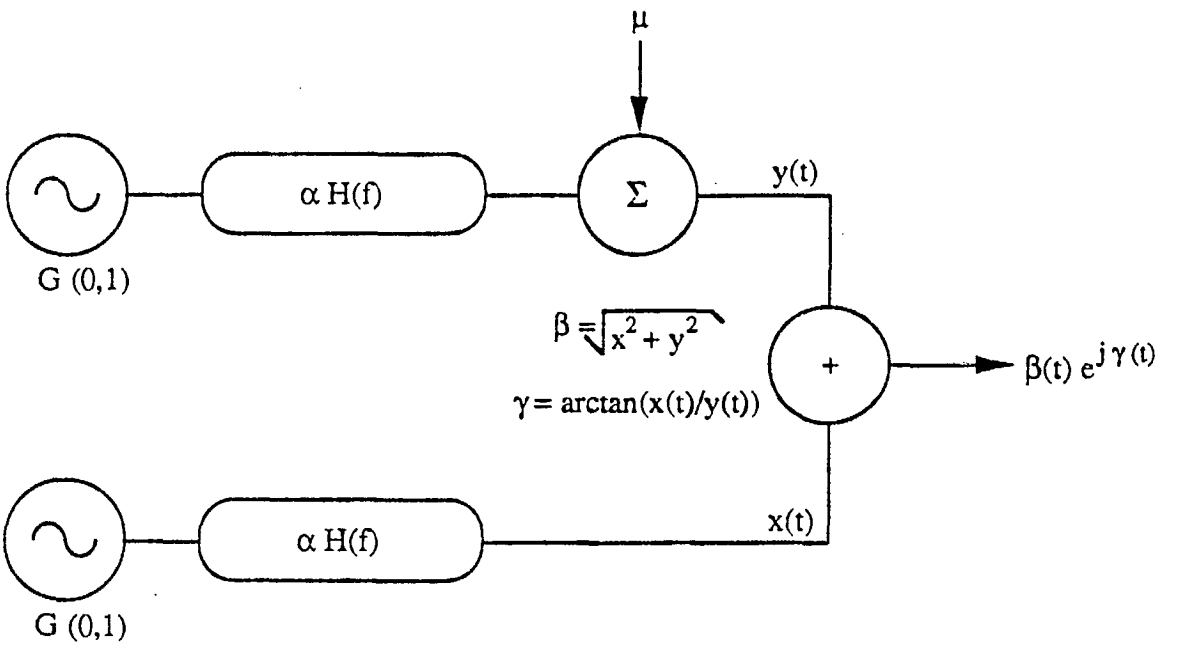

Fig.2 Fading channel simulator

$$\beta_{lk}(t) \equiv \beta(t) = \sqrt{(x(t))^2 + (y(t))^2} \tag{4a}$$

and

$$\gamma_{lk}(t) \equiv \gamma(t) = \tan^{-1}(x(t)/y(t)) \tag{4b}$$

The fading filter transfer function used is that suggested by Ball [5], where the filter response was shown to closely fit the land mobile fading spectrum. In [5], the filter transfer function was given as

$$H(s) = \frac{1}{(0.897s^2 + 0.31s + 1)(1.543s^2 + 0.841s + 1)(1.944s + 1)} \tag{5}$$

where $s = j2\pi f$ and $j = \sqrt{-1}$.

Note that a path having Rician distributed gain is assumed to consist of a dominant, nonfading subpath with average power μ^2, and many fading subpaths with total average power $2\sigma^2$; the delay of each fading subpath relative to that of the direct subpath is only a small faction of the chip duration so that all the subpaths constitute the Rician fading path. A measure of the severity of fading is the Rice factor, Ω defined as

$$\Omega = \frac{2\sigma^2}{\mu^2} \tag{6}$$

If the total average power of the Rician fading path is normalized to unity, μ is given as

$$\mu = \sqrt{\frac{1}{\Omega + 1}} \tag{7}$$

and the filter scaling factor, α_{Rice} is

$$\alpha = \alpha_{Rice} = \sqrt{\frac{\Omega}{2\,B_{eq}\,(\Omega + 1)}} \tag{8}$$

where B_{eq} is the noise equivalent bandwidth corresponding to a specified fading (Doppler) bandwidth and sampling rate.

When a path consists of only the fading subpaths with no dominant subpath (i.e. $\mu = 0$ in Fig. 2), then the path gains are Rayleigh distributed. By also assuming an average path power of unity, the filter scaling factor is found to be

$$\alpha = \alpha_{Ray} = \sqrt{\frac{1}{2\,B_{eq}}} \tag{9}$$

2.5.3 Receiver Analysis

Without loss of generality, let i denote the index of the desired mobile transmitter whose data symbol transmission is to be detected by the base station receiver. Also assume the time origin to be at the beginning of reception of the current symbol transmitted by user i, $b_0^{(i)}$. The total bandpass signal at the base station receiver input, r(t) consists of user i's signal, interfering signals from the other (K-1) users and thermal noise, n(t). Mathematically, from Figure 3

$$r(t) = n(t) + \sum_{k=1}^{K} s_k(t) \otimes h_k(t) \tag{10}$$

The complex, low-pass equivalent of the total received signal, $\tilde{r}(t)$ can be written as

$$\tilde{r}(t) = \sum_{k=1}^{K} \sum_{l=1}^{L_k} W(t - \tau_{lk}) \cos\phi_{lk} + Re[\tilde{n}(t)] + j\left(\sum_{k=1}^{K} \sum_{l=1}^{L_k} W(t - \tau_{lk}) \sin\phi_{lk} + Im[\tilde{n}(t)]\right) \tag{11}$$

where

$$W(t - \tau_{lk}) = A\,\beta_{lk}\,a_k(t - \tau_{lk})\,b_k(t - \tau_{lk}) \tag{12a}$$

and

$$\phi_{lk} = \theta_k - \omega_c \tau_{lk} + \gamma_{lk}(t) \tag{12b}$$

ϕ_{lk} is referred to as the resultant lth path phase for user k. For a given value of lth

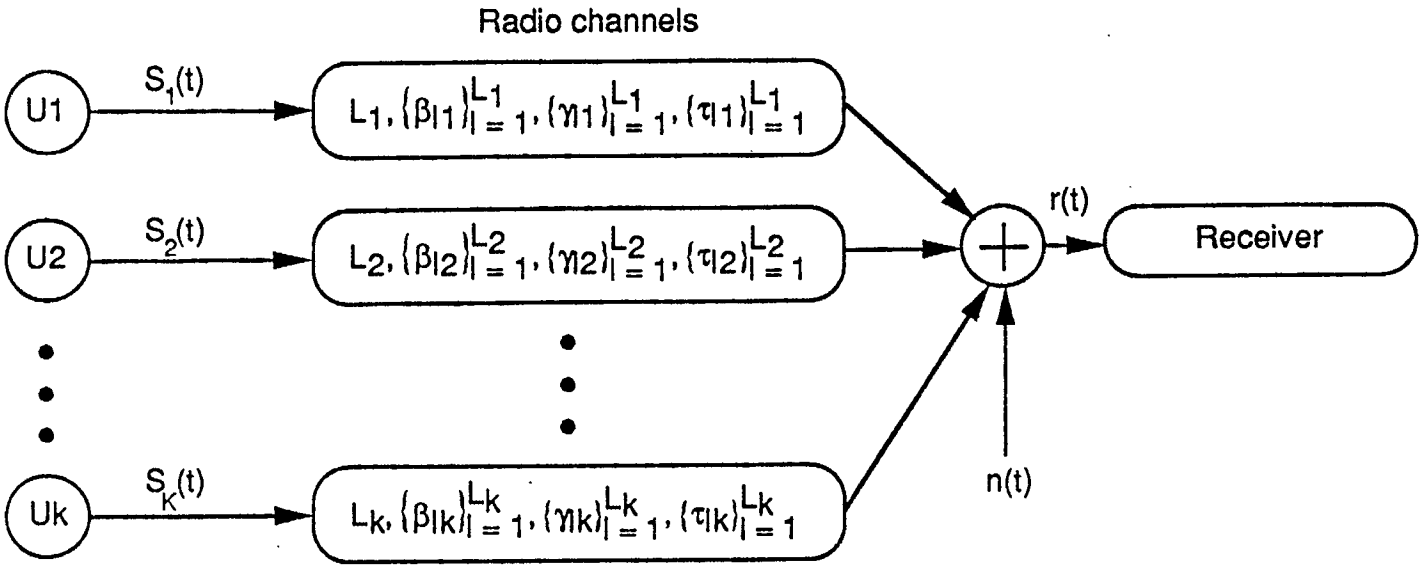

Fig.3 System Structure for analysis

path delay τ_{lk}, $(\theta_k - \omega_c\tau_{lk})$ is constant but is assumed to vary randomly over $[0, 2\pi]$. It is seen from (4b) that $\gamma_{lk}(t)$ is time dependent hence ϕ_{lk} is also a function of time, however, the time variable in ϕ_{lk} is not included in (12b) and in subsequent analysis for simplicity of notation. By assumption R1, the equivalent low-pass impulse response of the matched filter, is defined by

$$f(t) = a_i(T - t) \quad , \; 0 \le t \le T \tag{13}$$

and the signal at the matched filter output is obtained as

$$\tilde{Z}(t) = \int_0^t \tilde{r}(u)\, a_i(u - t)\, du \tag{14}$$

which at the sampling instant at $t = T$ (assumption R2) becomes

$$\tilde{Z}(T) = \int_0^T \tilde{r}(u)\, a_i(u)\, du \tag{15}$$

Note that the periodicity assumption of $a_i(.)$ has been used to arrive at (14) and (15).

2.5.3.1 Single Path Receiver

The purpose of the single path receiver structure in a multipath environment is to discriminate against multipath by basing the decision statistic on the contribution from only one path. This presumes that the single path receiver can lock on exactly to one of the L_i signal replicas of symbol $b_0^{(i)}$ that reach the receiver input. The lock-on criterion can be the signal replica with either the maximum gain or the shortest delay, the latter criterion is assumed in this study. Without loss of generality, let the jth signal replica be that to which the receiver is locked on to. Substituting (11) into (15) and after some algebraic manipulations, the signal at the matched filter output, normalized by AT is obtained as

$$\mathrm{Re}[\tilde{Z}(T)] = \eta + [\beta_{ji}\, b_0^{(i)} \cos\phi_{ji} + \sum_{\substack{l=1 \\ l \neq j}}^{L_i} \beta_{li} I_{ji}(\vec{b_i}, \tau_{li}) \cos\phi_{li} + \sum_{\substack{k=1 \\ k \neq i}}^{K} \sum_{l=1}^{L_k} \beta_{lk} I_{ki}(\vec{b_k}, \tau_{lk}) \cos\phi_{lk}] \tag{16a}$$

and

$$\mathrm{Im}[\tilde{Z}(T)] = \nu + [\beta_{ji}\, b_0^{(i)} \sin\phi_{ji} + \sum_{\substack{l=1 \\ l\neq j}}^{L_j} \beta_{li} I_{ji}(\vec{b_i}, \tau_{li}) \sin\phi_{li} + \sum_{\substack{k=1 \\ k\neq i}}^{K} \sum_{l=1}^{L_k} \beta_{lk} I_{ki}(\vec{b_k}, \tau_{lk}) \sin\phi_{lk}] \qquad (16b)$$

where η and ν are zero mean AWGN with identical variance $(2E_b/N_o)^{-1}$, $I_{ji}(.,.)$ is the self interference for user i, $I_{ki}(.,.)$ is the mutual interference between user k and user i and the data bit vector for user k, $\vec{b_k} = (b_{-1}^{(k)}, b_0^{(k)}, b_{+1}^{(k)})$, which accounts for lagging and leading path delays and also follows from assumption C5.

Finally, $I_{ki}(.,.)$ is given by:

$$I_{ki}(\vec{b_k},\tau) = T^{-1}[B_{ki}(\vec{b_k},\tau)] \qquad (17)$$

where the interference factor is defined by:

$$B_{ki}(\vec{b_k},\tau) = U(\tau > 0)[b_{-1}^{(k)} R_{ki}^{-}(\tau) + b_0^{(k)} R_{ki}^{+}(\tau)] + U(\tau < 0)[b_0^{(k)} R_{ki}^{-}(T - |\tau|) + b_{+1}^{(k)} R_{ki}^{+}(T - |\tau|)] \qquad (18)$$

The continuous-time partial cross-correlation functions of the kth and ith spreading sequence waveforms are defined as [2]

$$R_{ki}^{-}(\tau) = \begin{cases} \int_0^{\tau} a_k(u + T - \tau)\, a_i(u)\, du, & 0 \le \tau \le T \\ 0, & \text{otherwise} \end{cases} \qquad (19a)$$

$$R_{ki}^{+}(\tau) = \begin{cases} \int_{\tau}^{T} a_k(u - \tau)\, a_i(u)\, du, & 0 \le \tau \le T \\ 0, & \text{otherwise} \end{cases} \qquad (19b)$$

For a generic path delay τ, where $nT_c \le \tau < (n+1)T_c$ and $n = \lfloor \tau/T_c \rfloor$, then by assumption T7, $R_{ki}^{-}(\tau)$ and $R_{ki}^{+}(\tau)$ are found respectively to be [2]:

$$R_{ki}^{-}(\tau) = T_c C_{ki}(n - N) + (\tau - nT_c)[C_{ki}(n + 1 - N) - C_{ki}(n - N)] \quad (20a)$$

$$R_{ki}^{+}(\tau) = T_c C_{ki}(n) + (\tau - nT_c)[C_{ki}(n + 1) - C_{ki}(n)] \quad (20b)$$

The $C_{ki}(.)$'s are the discrete aperiodic cross-correlation functions of the kth and ith spreading sequences given by [2]

$$C_{ki}(n) = \begin{cases} \sum_{m=0}^{N-1-n} a_m^{(k)} a_{m+n}^{(i)} & , \quad 0 \le n \le N-1 \\ \sum_{m=0}^{N-1+n} a_{m-n}^{(k)} a_m^{(i)} & , \quad -(N-1) \le n < 0 \\ 0 & , \quad |n| \ge N \end{cases} \quad (21)$$

Note that the definition for $I_{ii}(.,.)$ in (16) follows from (17) to (21) by substituting i for k.

2.5.3.1.1 Coherent Detection

For a receiver that locks on to the jth received signal replica from user i, coherent detection of the transmitted symbol requires two assumptions. First, the receiver is time-synchronized to the jth path, which implies that the jth path delay, τ_{ji}, usually determined in practice by symbol timing, is assumed in the simulation to be known and taken as reference for the delays of all the other arriving paths at the receiver input. Second, the receiver can acquire perfect knowledge of the phase of path j, ϕ_{ji} , which is also taken as reference for the phase of all the other paths. Under these assumptions, (16) becomes:

$$\mathrm{Re}[\tilde{Z}(T)] = \eta + [\beta_{ji} b_0^{(i)} + \sum_{\substack{l=1 \\ l \ne j}}^{L_i} \beta_{li} I_{ii}(\vec{b_i}, \tau_{li}') \cos\phi_{li}' + \sum_{\substack{k=1 \\ k \ne i}}^{K} \sum_{l=1}^{L_k} \beta_{lk} I_{ki}(\vec{b_k}, \tau_{lk}') \cos\phi_{lk}'] \quad (22a)$$

and

$$\mathrm{Im}[\tilde{Z}(T)] = \nu + [\sum_{\substack{l=1 \\ l\neq j}}^{L_j} \beta_{li} I_{ii}(\vec{b_i}, \tau'_{li}) \sin\phi'_{li} + \sum_{\substack{k=1 \\ k\neq i}}^{K} \sum_{l=1}^{L_k} \beta_{lk} I_{ki}(\vec{b_k}, \tau'_{lk}) \sin\phi'_{lk}] \tag{22b}$$

where

$$\phi'_{lk} = \phi_{lk} - \phi_{ji} \tag{23a}$$

$$\tau'_{lk} = \tau_{lk} - \tau_{ji} \tag{23b}$$

ϕ'_{li} and τ'_{li} follow from (23) by substituting i for k.

The decision statistic for a coherent matched filter receiver is defined by [6]

$$\zeta = \mathrm{Re}[\tilde{Z}(T)] \tag{24}$$

which is given by (22a) if $b_0^{(i)}$ is transmitted over a frequency selective fading channel. Finally, an estimate of $b_0^{(i)}$, denoted by $\widehat{b_0^{(i)}}$ is determined by comparing the decision statistic with a zero threshold. The decision rule is stated as follows:

$$\text{If } \zeta < 0, \text{ then } \widehat{b_0^{(i)}} = -1$$

$$\text{else} \qquad \widehat{b_0^{(i)}} = +1$$

For the special case where $b_0^{(i)}$ is sent over a frequency nonselective (flat) fading channel, i.e. $L_i = L_k = 1$, $k \neq i$, then the first summation term in (22a) and (22b) vanishes, and for notational convenience, denote τ'_{lk} by $\tau'_k = \tau_k - \tau_i$, ϕ'_{lk} by $\phi'_k = \phi_k - \phi_i$, and also let $\beta_{ji} = \beta_i$. Using these definitions, (22) reduces to

$$\mathrm{Re}[\tilde{Z}(T)] = \eta + [\beta_i b_0^{(i)} + \sum_{\substack{k=1 \\ k\neq i}}^{K} \beta_k I_{ki}(\vec{b_k}, \tau'_k) \cos\phi'_k] \tag{25a}$$

and

$$\mathrm{Im}[\tilde{Z}(T)] = \nu + [\sum_{\substack{k=1 \\ k\neq i}}^{K} \beta_k I_{ki}(\vec{b_k}, \tau'_k)\sin\phi'_k] \qquad (25b)$$

The decision statistic for the frequency nonselective fading channel case is then given by (25a).

2.5.3.1.2 Differential Detection

As in the case of coherent detection, it is assumed for differential detection that the receiver is time-synchronized to the jth signal replica from user i. Assuming τ_{ji} is known, it then serves as reference for the delay of each of the other paths. However, unlike coherent detection, exact knowledge of ϕ_{ji} is not required, but should ideally remain constant over the duration of two consecutive data bits for differential detection. In practice, ϕ_{ji} will vary very slowly depending on the amount of Doppler spreading of the channel. Under the above assumptions, and for frequency selective fading channel, (16) becomes

$$\mathrm{Re}[\tilde{Z}(T)] = \eta + [\beta_{ji} b_0^{(i)} \cos\phi_{ji} + \sum_{\substack{l=1 \\ l\neq j}}^{L_i} \beta_{li} I_{ii}(\vec{b_i}, \tau'_{li})\cos\phi_{li} + \sum_{\substack{k=1 \\ k\neq i}}^{K} \sum_{l=1}^{L_k} \beta_{lk} I_{ki}(\vec{b_k}, \tau'_{lk})\cos\phi_{lk}] \qquad (26a)$$

and

$$\mathrm{Im}[\tilde{Z}(T)] = \nu + [\beta_{ji} b_0^{(i)} \sin\phi_{ji} + \sum_{\substack{l=1 \\ l\neq j}}^{L_i} \beta_{li} I_{ii}(\vec{b_i}, \tau'_{li})\sin\phi_{li} + \sum_{\substack{k=1 \\ k\neq i}}^{K} \sum_{l=1}^{L_k} \beta_{lk} I_{ki}(\vec{b_k}, \tau'_{lk})\sin\phi_{lk}] \qquad (26b)$$

where τ'_{lk} is as defined in (23b).

The decision statistic ζ for the differential matched filter receiver is defined by [6]

$$\zeta = \mathrm{Re}[\tilde{Z}(T)\tilde{Z}^{*}_{-1}(T)] \qquad (27)$$

Fig. 8a Rayleigh Flat Fading Channel

(1 user, DPSK, Avg. Path Power = 0 dB,
Zero Doppler, Single Path Receiver)

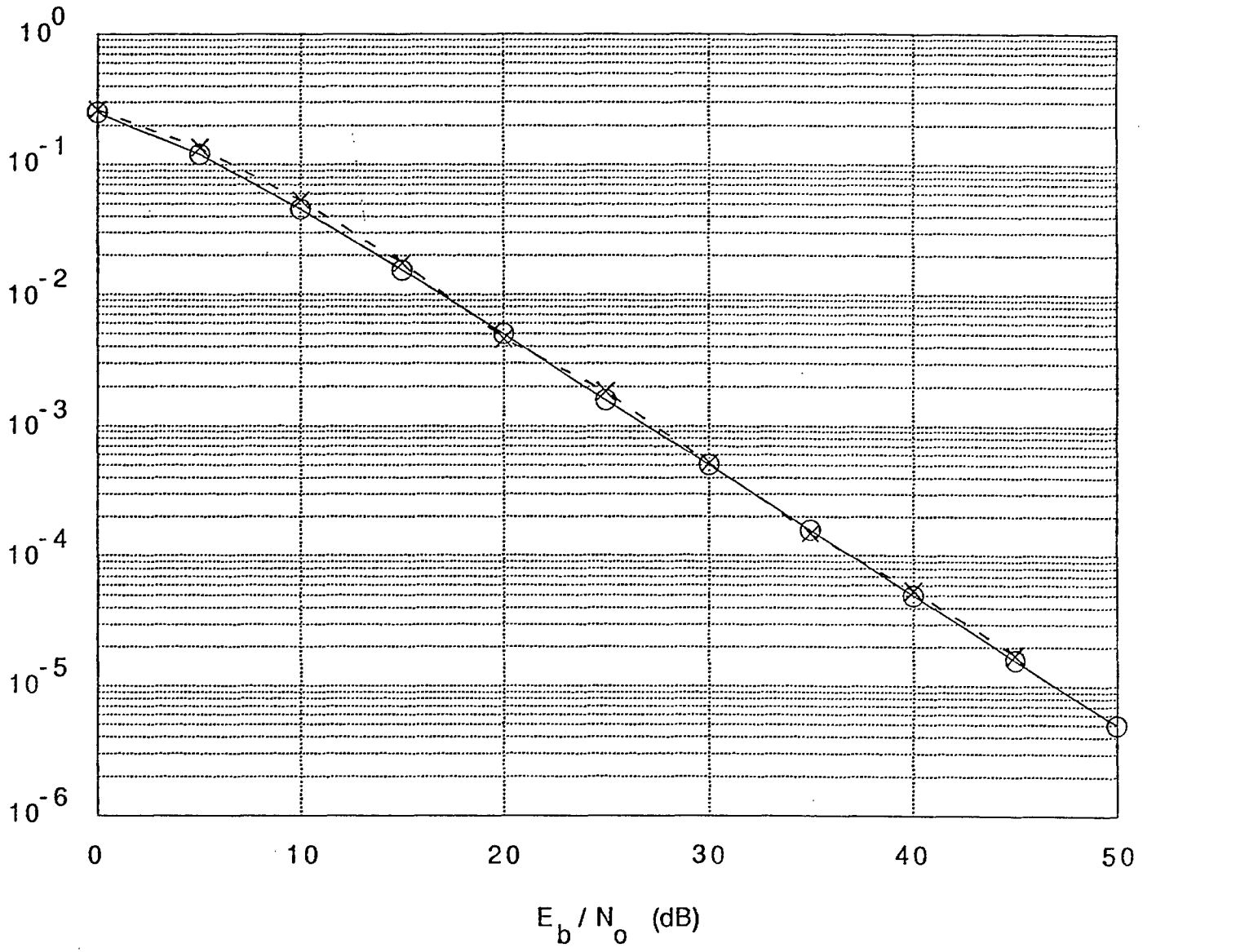

$\tilde{Z}^{*}_{-1}(T)$ is calculated using (26) assuming $b^{(i)}_{-1}$ is transmitted, and the data bit vector $\vec{b}_k$ is now defined as $(b^{(k)}_{-2}, b^{(k)}_{-1}, b^{(k)}_{0})$. Finally, substituting i for k gives $\vec{b}_i$. For the frequency nonselective fading channel case, (26) reduces to

$$\mathrm{Re}[\tilde{Z}(T)] = \eta + [\beta_i b^{(i)}_0 \cos\phi_i + \sum_{\substack{k=1 \\ k\neq i}}^{K} \beta_k I_{ki}(\vec{b}_k, \tau'_k)\cos\phi_k] \qquad (28a)$$

and

$$\mathrm{Im}[\tilde{Z}(T)] = \nu + [\beta_i b^{(i)}_0 \sin\phi_i + \sum_{\substack{k=1 \\ k\neq i}}^{K} \beta_k I_{ki}(\vec{b}_k, \tau'_k)\sin\phi_k] \qquad (28b)$$

where β_i, τ'_k and ϕ'_k are as defined previously.

2.5.3.2 Differential RAKE Receiver

The rationale of a multipath combining receiver, such as the RAKE considered in this study, is that the decision statistic is based on the contribution from all the signal replicas of the transmitted symbol (by user i) whose delays fall within the RAKE window such that the multipath becomes an advantage.

The block diagram of the differential RAKE receiver structure implemented in the simulation is shown in Fig. 4a, which is similar to that first proposed by Turin [7]. In Fig. 4a, there are L parallel matched filter/differential detector branches and the lth branch is assumed to lock on to the lth path. The output of the differential detector for branch l is sampled at time $T + \tau_l$ and denoted by $\zeta_l(\tau_l)$. Assuming the path gains and delays are known exactly at the receiver and for a given RAKE window, Δ_w (defined as the product of a specified number of taps and chip duration), then the differential detector outputs for those paths whose delays fall within the RAKE window are non-coherently combined (at time $(T + \Delta_w)$) to form the decision statistic for determining an estimate of the transmitted symbol. Turin has postulated that under the above assumption, the decision rule is given

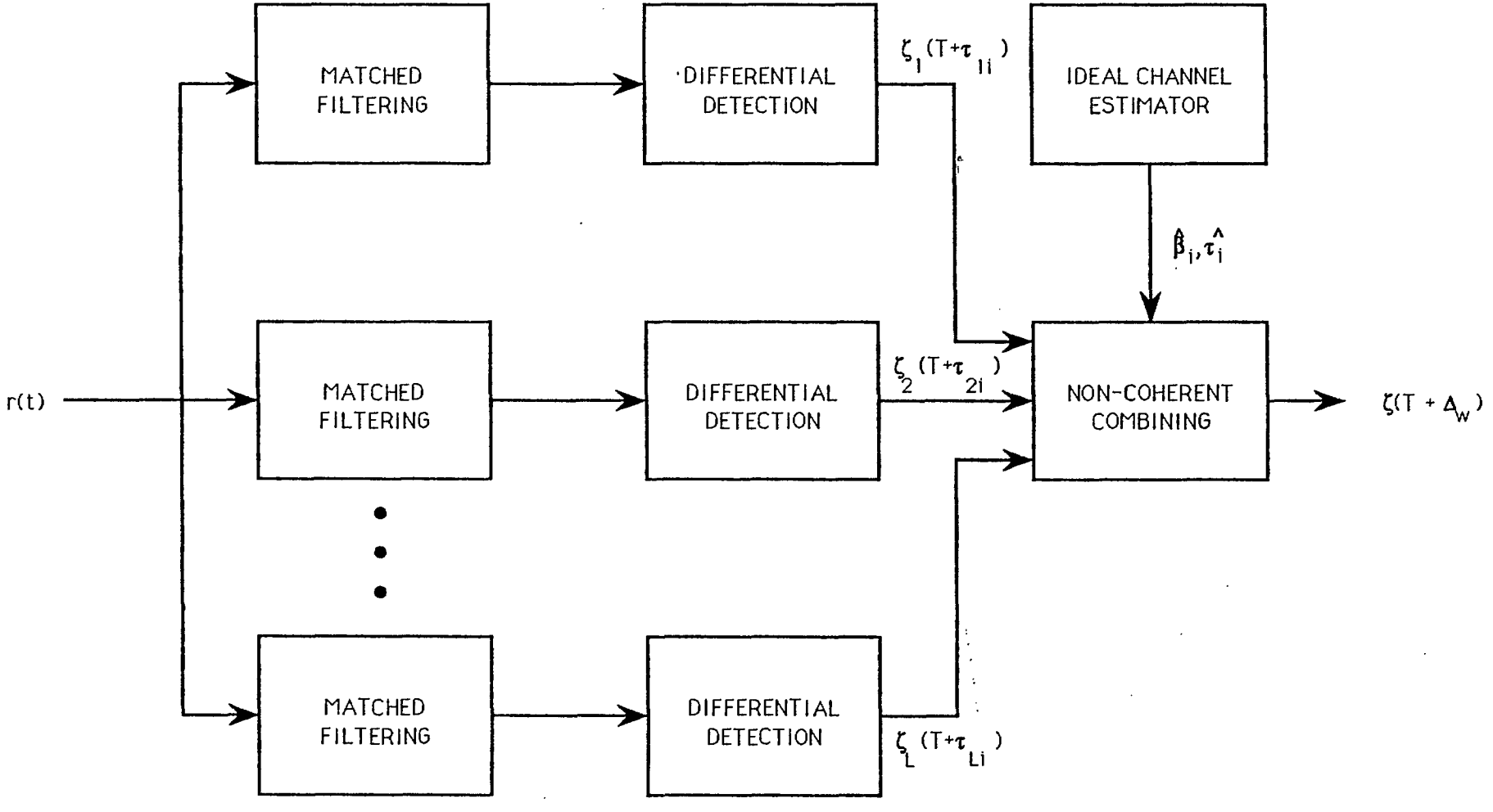

Fig. 4a Block Diagram of the Simulated Differential RAKE receiver

by [7, Eqn. (27)]

$$\zeta = \sum_{l} \ln[I_o(\frac{2\,\hat{\beta}_{li}\,\zeta_l(\hat{\tau}_{li})}{N_o})] \qquad (29a)$$

where the l's are the path indices whose $\hat{\tau}_{li}$'s lie within the RAKE window. Mathematically, $\ln[I_0(x)]$ is approximated by x for large x so that for large argument of $I_0(.)$ in (29a), the decision rule then becomes, to within a positive constant

$$\zeta \approx \sum_{l} \hat{\beta}_{li}\,\zeta_l(\hat{\tau}_{li}) \qquad (29b)$$

The approximation in (29b) is valid provided the path gains and delays are estimated very accurately, this is possible for example when the path powers are much stronger than the background noise.

Equation (29b) suggests that the non-coherent combining block in Fig. 4a can be realized by a tapped delay line filter as illustrated in Fig. 4b. The taps, numbered from right to left and starting from 1 to tot are placed T_c seconds apart - this ensures that the tap positions correspond to the estimated path delays (the correspondence is exact if the path delays are integral multiples of T_c but approximate otherwise). Note that the total number of taps, "tot", may be a design specification which then defines the RAKE window Δ_w; alternatively, the maximum number of taps can be determined from knowledge of the maximum delay spread for the radio environment in which the receiver will operate. Finally in Fig. 4b, the weight for tap i is denoted by w_i, $1 \le i \le$ tot.

Under the assumption that the path gains and delays are estimated very accurately (using an ideal channel estimator for example), the decision rule for estimating a transmitted symbol is formed in the simulation using a three step procedure. First, the #1 tap position is assumed to correspond to the shortest of the estimated path delays and then chosen as time reference for the RAKE window; this choice of time reference ensures there is at least one path within the RAKE window so that the RAKE receiver becomes a single path receiver when the

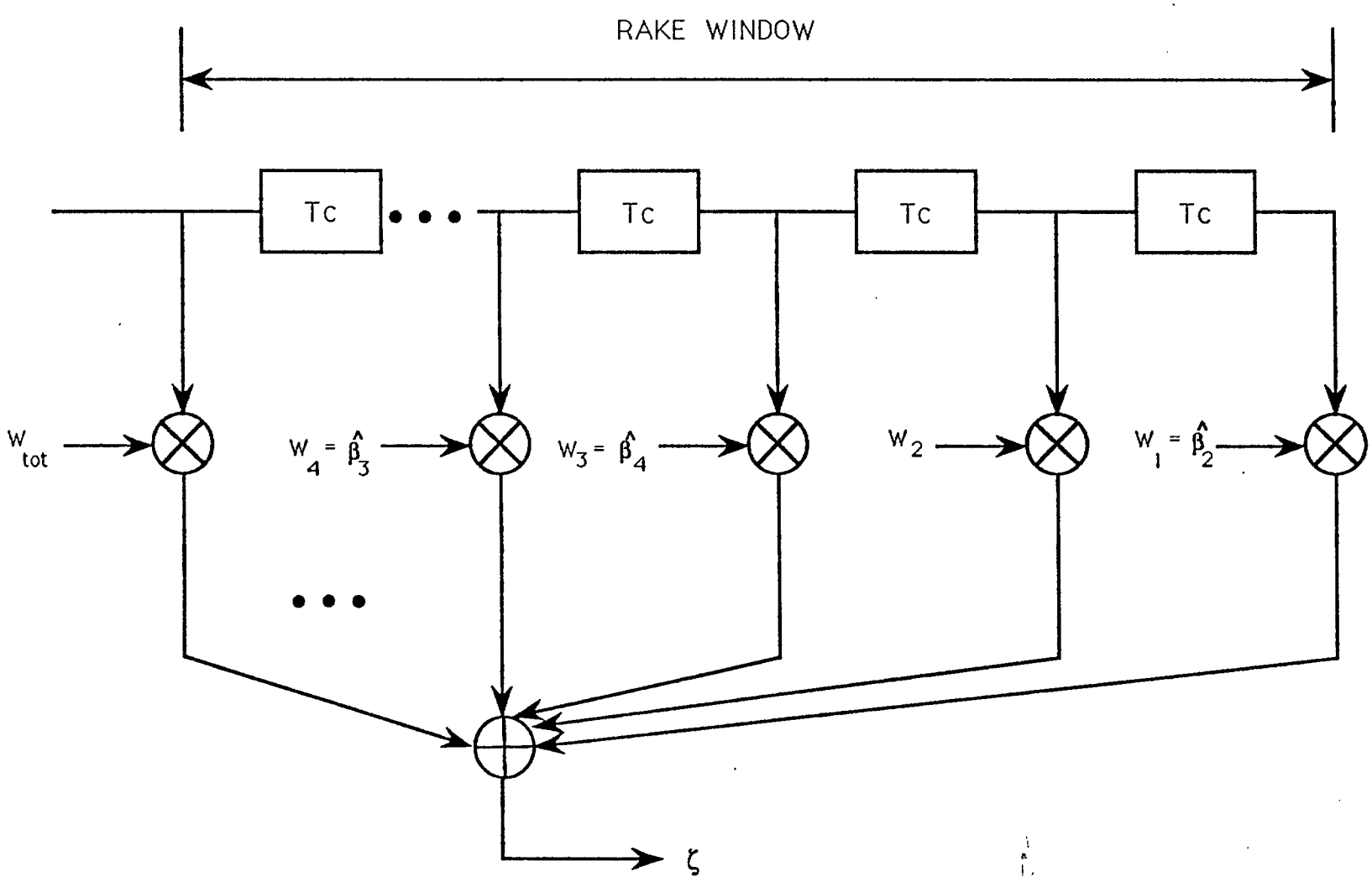

Fig. 4b Tapped Delay Line Implementation of Non-Coherent Combining

window is determined by only one tap. Also, w_1 is always tuned to the estimated gain of the path having the shortest (estimated) delay. Second, for the other paths whose estimated delays fall within the RAKE window, the tap weight at a position corresponding to each estimated delay is tuned to the estimated path gain for that delay. In case an estimated path delay is not an integral multiple of T_c, then the weight of the tap at a position closest to the delay is tuned to the gain for that delay. Third, the overall decision statistic ζ is calculated at time $T + \Delta_w$ using (29b), where $\zeta_l(\hat{\tau}_{li})$ for each l is computed by (27).

The preceding procedure is best illustrated by an example. Suppose there are five paths and assume that the estimated path parameters $(\hat{\beta}_1, \hat{\tau}_1)$, $(\hat{\beta}_2, \hat{\tau}_2)$, $(\hat{\beta}_3, \hat{\tau}_3)$, $(\hat{\beta}_4, \hat{\tau}_4)$ and $(\hat{\beta}_5, \hat{\tau}_5)$ are known exactly at the receiver. Further, suppose that $\min(\hat{\tau}_1, \hat{\tau}_2, \hat{\tau}_3, \hat{\tau}_4, \hat{\tau}_5)$ is $\hat{\tau}_2$. Hence, by step 1, the reference time for the RAKE window is set at $\hat{\tau}_2$ and w_1 is tuned to $\hat{\beta}_2$. To implement the second step, suppose there are only two other paths (say paths 3 and 4) whose delays fall within a specified RAKE window Δ_w (Fig. 4b) and assume that $\hat{\tau}_2 < \hat{\tau}_4 < \hat{\tau}_3$. If #3 tap position corresponds to $\hat{\tau}_4$, then w_3 is tuned to $\hat{\beta}_4$; also if #4 tap position corresponds to $\hat{\tau}_3$, then w_4 is tuned to $\hat{\beta}_3$. Finally, the decision statistic (obtained at time $(T + \Delta_w)$) is given by $\hat{\beta}_2\, \zeta_2(\hat{\tau}_2) + \hat{\beta}_4\, \zeta_4(\hat{\tau}_4) + \hat{\beta}_3\, \zeta_3(\hat{\tau}_3)$. From the above, it is seen that only the three paths whose delays fall within the RAKE window contribute to the decision rule and more paths contribute to the decision rule by increasing the RAKE window, that is, increase the number of taps. The limiting case when all the five paths contribute to the decision rule occurs if the RAKE window is equal to the maximum delay spread.

It is observed that the RAKE receiver structure of Fig. 4 differs from the conventional RAKE receiver structure [8, Section 7.5]. In the conventional structure, the differential detector input is weighted by the estimated channel parameters whereas in Fig. 4, it is the output of the differential detector that is weighted by the estimated channel parameters. An explanation for post-detection weighting in the structure of Fig. 4 is due to the specified relationship for calculating the decision rule which, as defined by (29), depends on the detector

output. This difference in the weighting point between the structure of Fig. 4 and that in [8] may result in dissimilar performance. However, if all the tap weights in each structure are identically set to unity, one expects the performance of either structure to be the same. Fig. 4 is adopted in this study because of the resulting simplicity in its simulation.

3.0 System Simulation

3.1 Simulation Assumptions

S1) The number of users remains constant, with every user transmitting over the duration of the simulation. This is a worst case scenario for a practical system.

S2) The unit of time in the simulation is the data symbol (bit) duration and all the users are time-synchronized at the bit level. This implies that a data bit is generated for all users at the beginning of every symbol period. However, in practice this is not necessarily so, hence, this assumption is made for convenience in the simulation. In any case, user asynchronism is accounted for at the receiver through the random path delays. Chip synchronization of users is not considered so as to ease the computation demand in the simulation.

S3) The spreading code for each user is pre-assigned and remains unchanged over the duration of the simulation. This implies that the discrete auto- and cross-correlation functions of the spreading sequences are computed once at the beginning of the simulation, and then serve as inputs for the calculation of the continuous-time partial correlation functions. This assumption may be restrictive with respect to a practical CDMA system in which handoff is implemented by the assignment of a new spreading code to a mobile that has moved into another cell.

S4) To facilitate signal processing during a simulation run, symbols are processed in blocks where for each user one block comprises S successive symbols. A good value for S that satisfies the computation speed and

memory requirements is found to be 10.

S5) Interferers maintain different relative delays throughout a simulation run. Hence, the total number of bits received in error at the end of a simulation run is a number that is averaged over different relative delays. For ease of computation load, the relative delays are updated at the beginning of every block (of S symbols) during a simulation run.

S6) The resultant phase of path l for symbol n ($1 \le n \le S$), ϕ_l, is determined solely by $\gamma_l(n)$ (where $\gamma_l(n)$ is calculated by (4b)) and the effect of $(\theta - \omega_c\tau_l)$ in (12b) is neglected. Clearly, neglecting $(\theta - \omega_c\tau_l)$ does not affect the result for coherent detection because of the perfect knowledge of phase assumption. In the case of differential detection, if $(\theta - \omega_c\tau_l)$ is assumed to be constant over the S symbols of one block but chosen randomly over $[0, 2\pi]$ at the beginning of each block, then neglecting $(\theta - \omega_c\tau_l)$ also does not significantly affect the final result at low E_b/N_0 and is immaterial at large E_b/N_0, i.e. error floor region. Assumption S6 is therefore made so that the variations in ϕ_l is caused primarily by the changes in $\gamma_l(n)$ as well as to reduce the computation burden in the simulation.

S7) Coherent detection of a symbol transmitted on a Rician fading channel assumes that the receiver locks on to the combined phase of the nonfading subpath plus the fading subpaths. A justification for this assumption is given as follows: For a Rician fading path comprising a nonfading subpath and many fading subpaths whose differential delays with respect to the nonfading subpath are much less than the chip duration, then by assumption C6, the nonfading subpath is not resolvable as a separate path without including the fading subpaths. Note however that locking on to the combined phase presumes that the phase of the fading subpaths does not change very fast to prevent loss of phase synchronization during the detection process.

3.2 Simulation Structure

Direct implementation of the system block diagram shown in Fig. 1 entails processing the input/output signals for each block from the transmitter to the receiver for each user in the system. This approach is not computationally efficient, and to ease the computational load a different approach has been adopted in the current simulation. The starting point of the revised approach is the expression for the decision statistic (section 2.5.3), which suggests that the signals of all the users can be processed simultaneously at one point, rather than at several points using direct block - to - block signal processing. It is seen that for a given set of transmitted bit and channel parameters, calculation of the decision statistic involves only multiplication and addition operations.

The simulation program, named CDMAsim consists of three main parts (Fig. 5):

Transmitter Generates a sequence of data symbols for the desired user and its interferers. Differential encoding of data symbols is performed if required.

Channel Generates the radio channel parameters.

Receiver Calculates the decision statistic used for detecting an estimate of a transmitted symbol.

The transmitter, channel and receiver are further broken down into modules and a detailed description of the modules is provided in Appendix I, the Software Design Document. Appendix II contains the user guide and the software for the simulation.

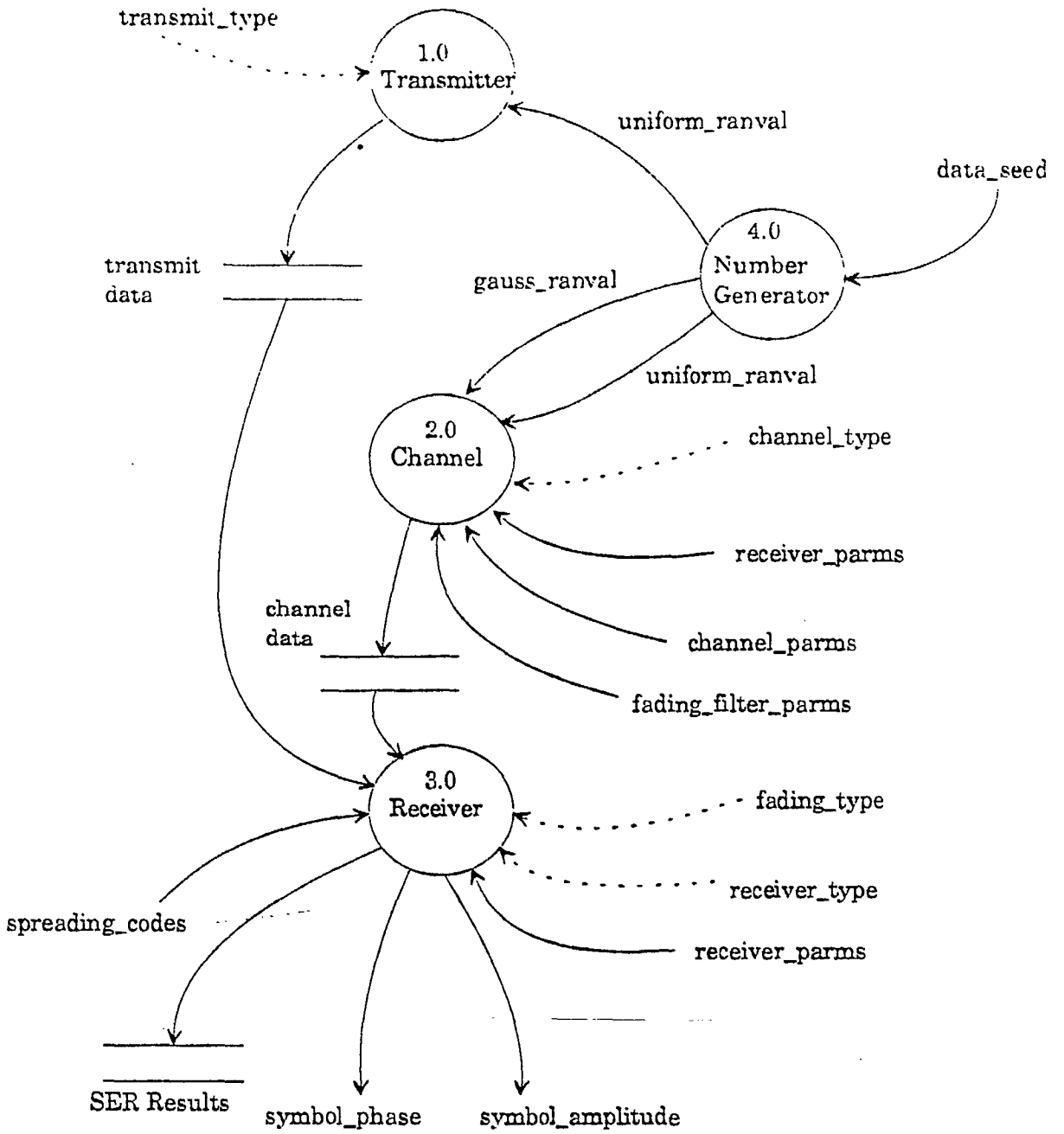

Fig. 5 Data flow diagram

4.0 Simulation Results and System Design Considerations

4.1 Simulation Results

The main measure of system performance is the bit error rate (BER), which is calculated in the simulation by

$$BER = \lim_{M->\infty} \frac{1}{M} \sum_{j=1}^{M} U(\widehat{b_j^{(i)}}) \tag{30}$$

where the indicator random variable U(.) is defined by

$$U(\widehat{b_j^{(i)}}) = \begin{cases} 1, & \widehat{b_j^{(i)}} \neq b_j^{(i)} \\ 0, & \text{otherwise} \end{cases} \tag{31}$$

Before presenting the main results, it is worthwhile to first show the autocorrelation functions of Gold and Kasami sequences used in the simulation, after which the accuracy of the outputs from the simulation are demonstrated and finally the format for presenting the results are described.

4.1.1 Autocorrelation Functions of Gold and Kasami Sequences

Gold sequences of length 31 and Kasami sequences of length 255 used in the simulation have been selected according to the auto-optimal/least sidelobe energy criteria [9]. Figures 6a and 6b show the discrete aperiodic autocorrelation functions for a 31-chip Gold sequence and a 255-chip Kasami sequence respectively. For the 31-chip Gold sequence, the peak mainlobe to (absolute) peak sidelobe ratio is found to be 7.75 (Fig. 6a) compared to a ratio of 19.62 (Fig. 6b) for the 255-chip Kasami sequence. Therefore, the 255-chip Kasami sequence exhibits a better autocorrelation property (and subsequently introduces less self interference) than the 31-chip Gold sequence.

4.1.2 Validation of Simulation Results

The validity of the simulation results is demonstrated through a comparison of the bit error rate predicted by theory and numerical approximation to that calculated using the simulation software. First, the performance of a single user

Fig. 6a Discrete Aperiodic Autocorrelation Function of Gold Code #0

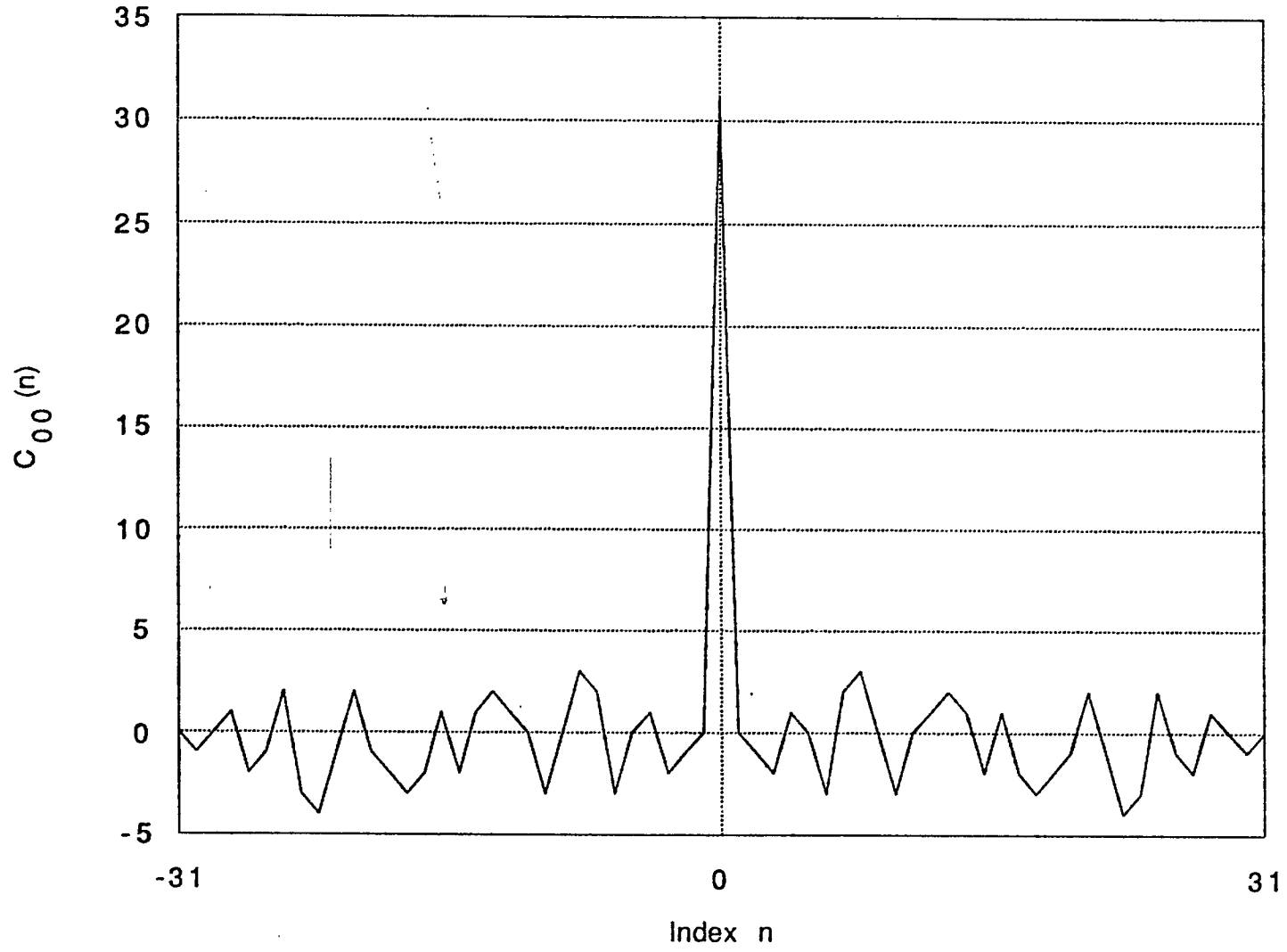

Fig. 6b Discrete Aperiodic Autocorrelation Function of Kasami Code #0

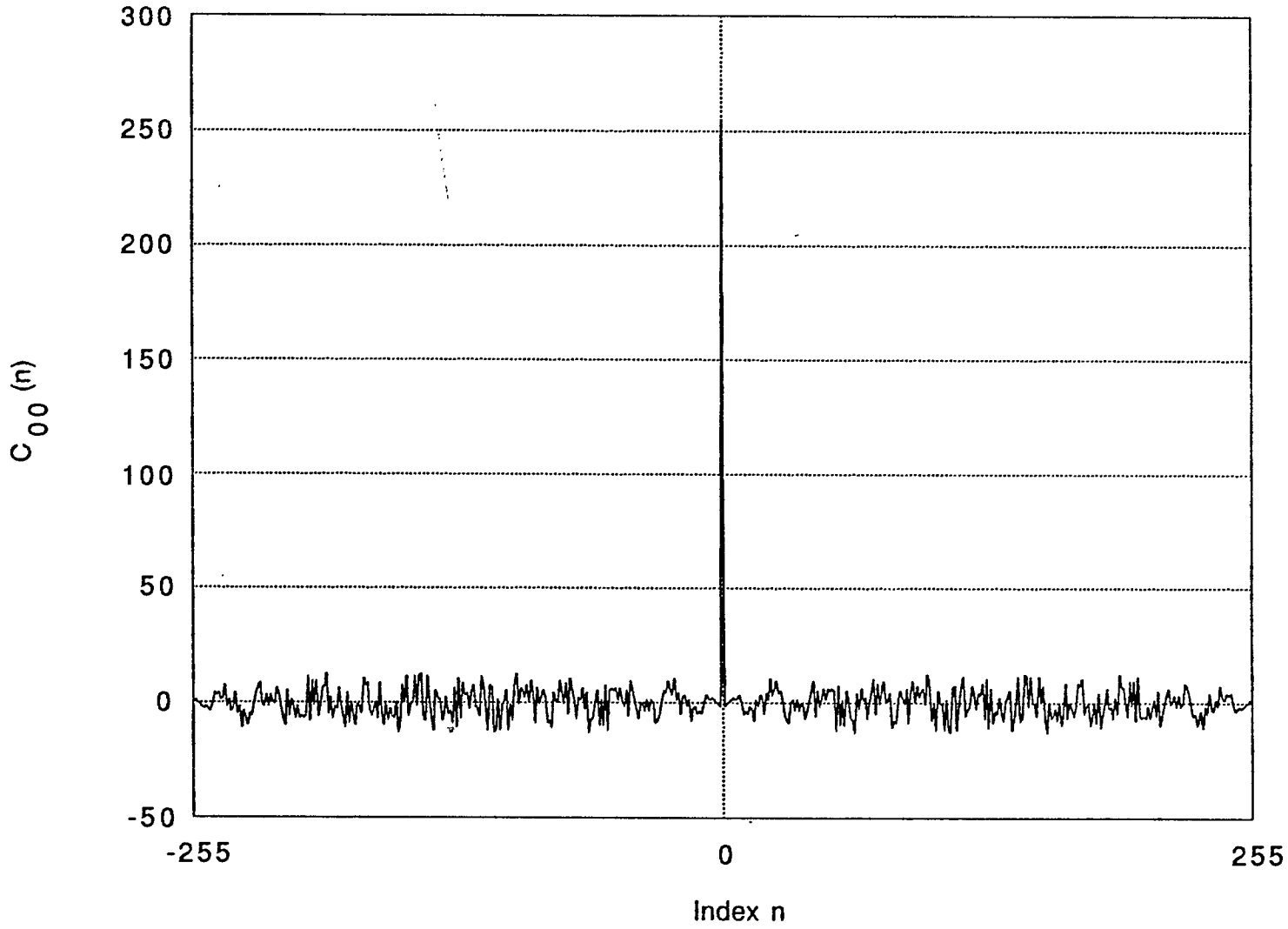

system operating over three different channel scenarios (for which closed form theoretical results are available) is investigated by simulation. The simulated scenarios are itemized below:

i) Pure AWGN channel only: DPSK (Fig. 7a)
Coherent BPSK (Fig. 7b)

ii) Rayleigh flat fading channel (no Doppler) + AWGN:
DPSK (Fig. 8a)
Coherent BPSK (Fig. 8b)

iii) Correlated Rayleigh flat fading channel + AWGN:
DPSK, Norm. Doppler BW = 0.1 (Fig. 9a)
DPSK, Norm. Doppler BW = 0.01 (Fig. 9b)
DPSK, Norm. Doppler BW = 0.001 (Fig. 9c)

Figs. 7 to 9 are plots of the BER versus E_b/N_0, the energy per bit to noise power spectral density ratio. The benchmark results in Figs. 7 and 8 are extracted from [8] while those in Fig. 9 are taken from [10]. Note that in Fig. 7, the E_b in E_b/N_0 is the nonfaded energy per transmitted bit and in Figs. 8 and 9 the E_b represents the average received energy per bit per path since in the simulation the average power in the fading path is assumed to be unity. The simulation results shown in Fig. 8a (zero Doppler frequency and DPSK detection) assume that the path gains for symbols 2, 3, ..., S-1 are the same as the gain for the first symbol in each block comprising S symbols - this assumption is necessary to obtain meaningful results for zero Doppler frequency and differential detection; however, the path phase varies from symbol to symbol. It is seen from Figs. 7 to 9 that the simulated bit error rates agree very well to the predicted BER using closed form theoretical results. This excellent agreement provides some confidence level in the simulation software.

The single user, single path system just simulated is simplistic - in fact as seen from (16), the mutual and self interference terms do not contribute to the decision statistic for generating the simulation results shown in Figs. 7 to 9. Clearly, a practical spread spectrum multiple access system consists of more than one user and, as a land mobile radio system, must operate in a multipath fading

Fig. 7a Performance of BPSK with Coherent Detection on AWGN Channel

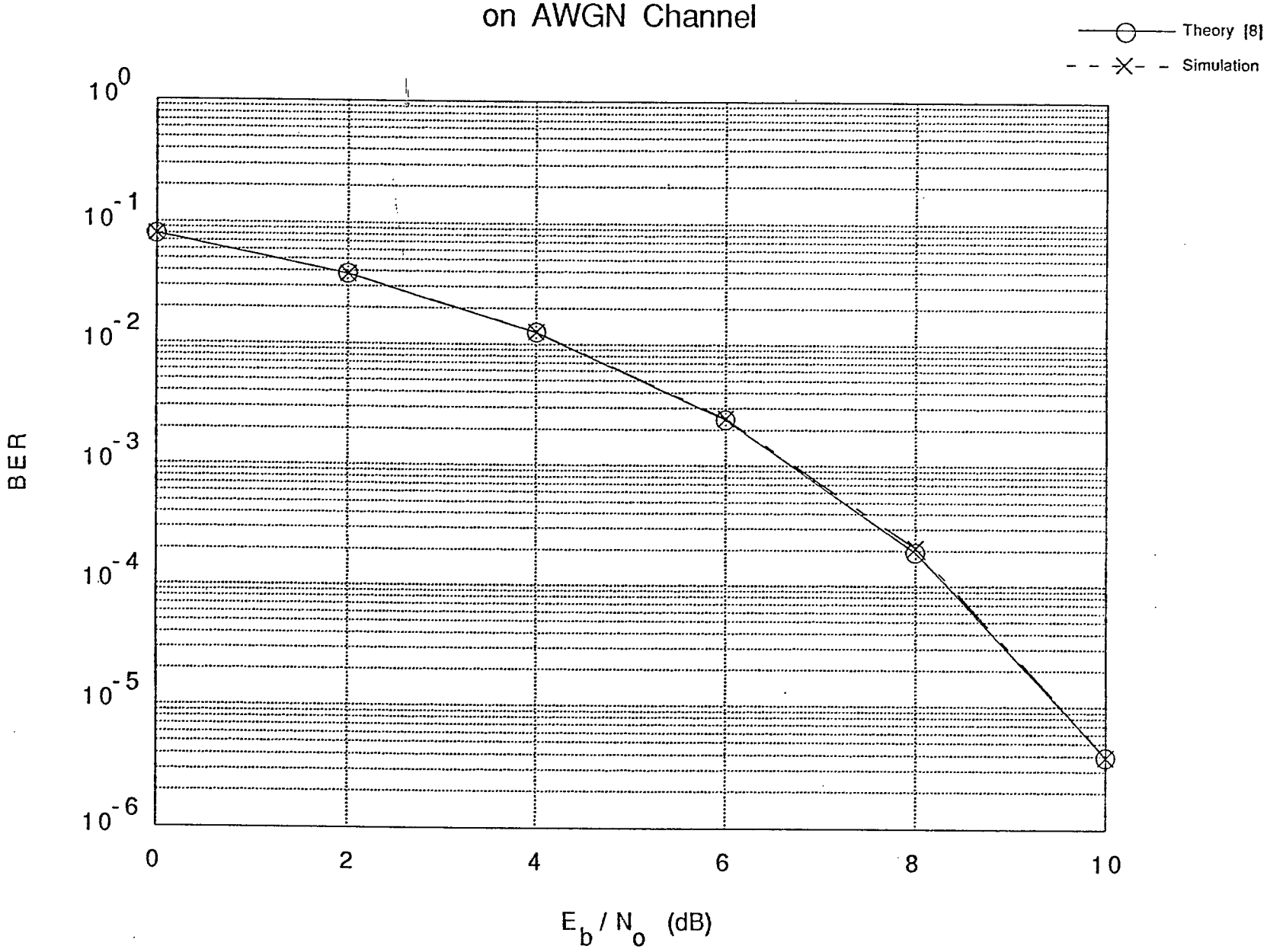

Fig. 7b Performance of DPSK on AWGN Channel

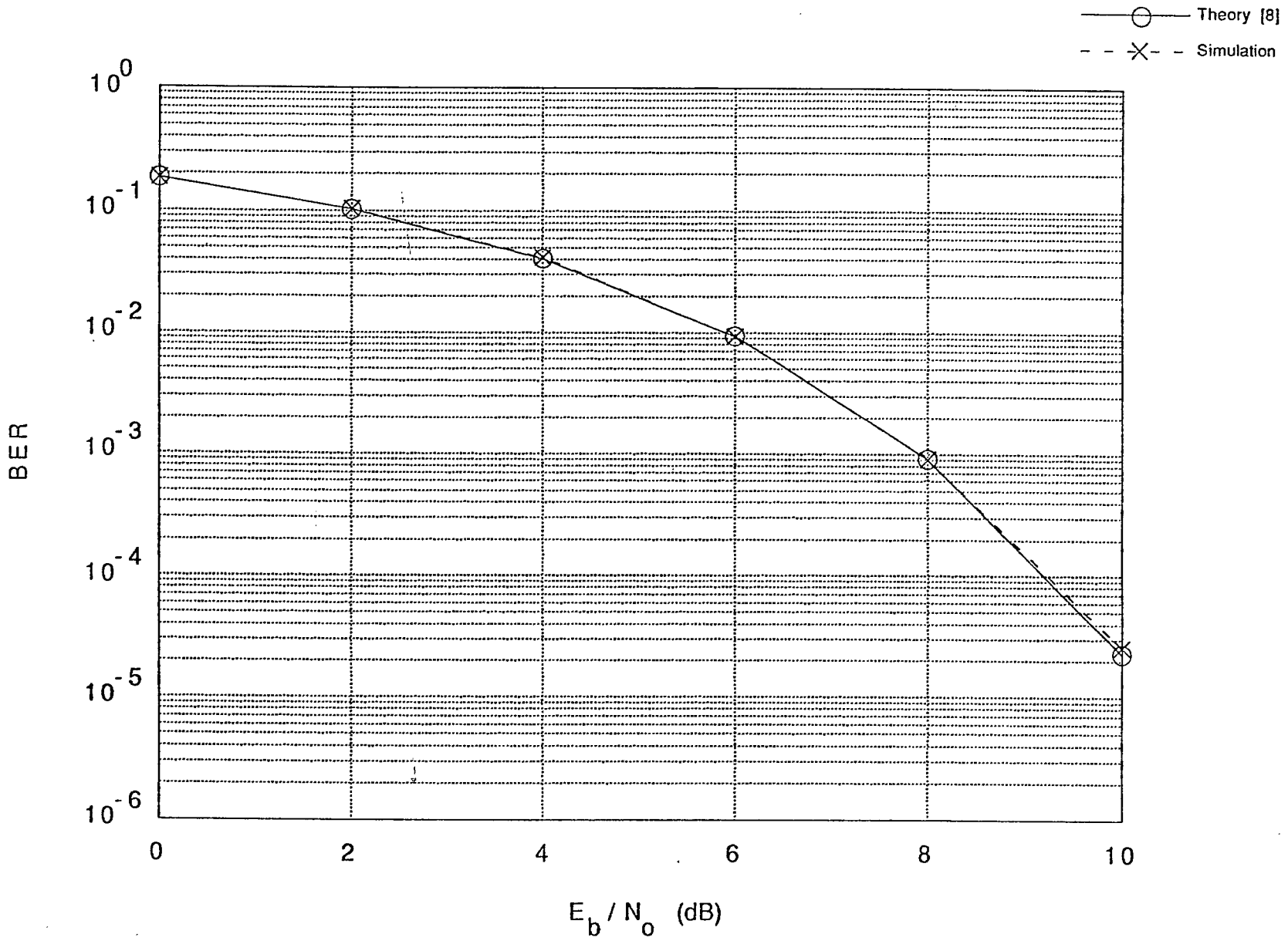

Fig. 8b Rayleigh Flat Fading Channel

(1 user, Coherent BPSK, Avg. Path Power = 0 dB,
Zero Doppler, Single Path Receiver)

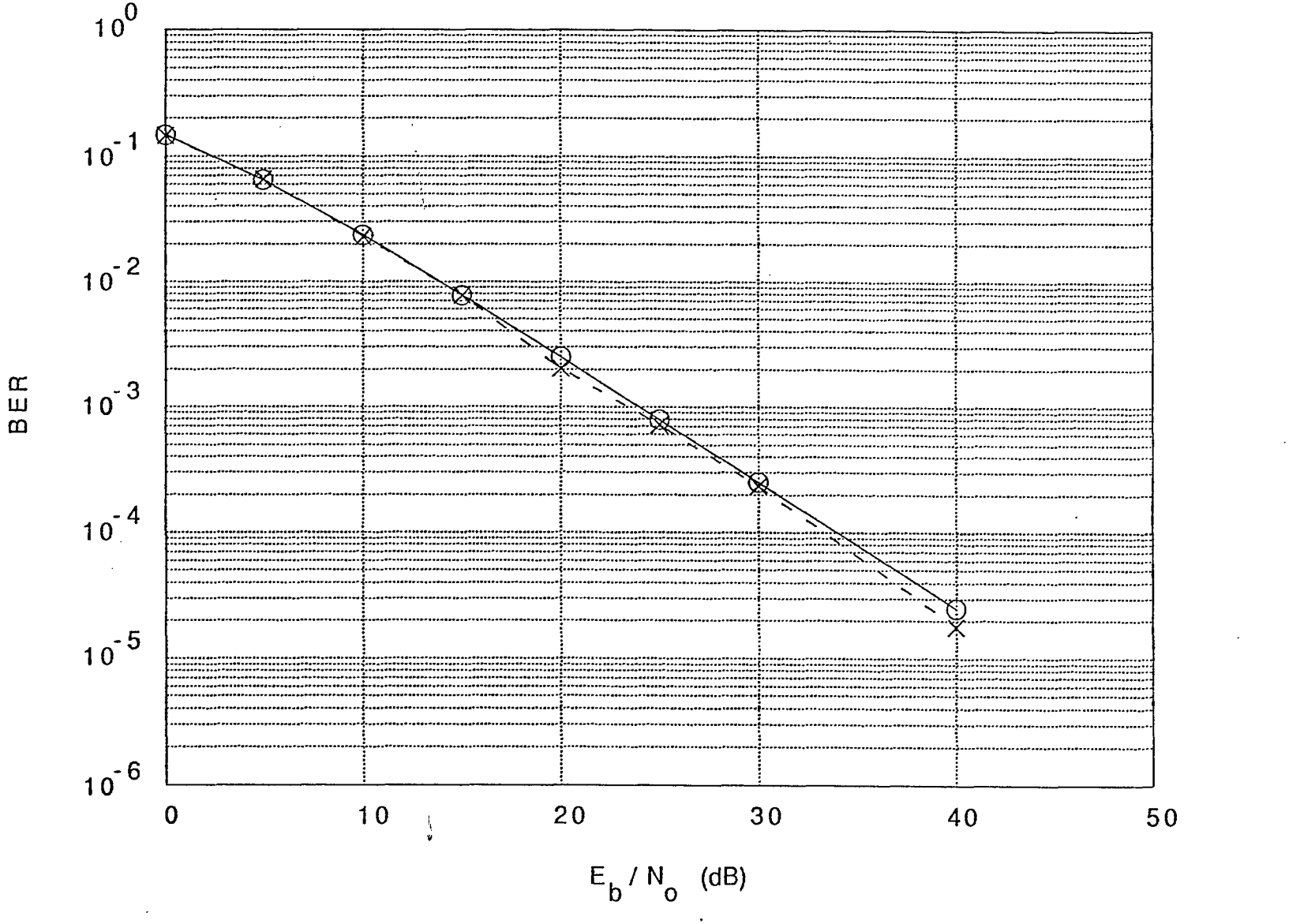

Fig. 9a Rayleigh Flat Fading Channel

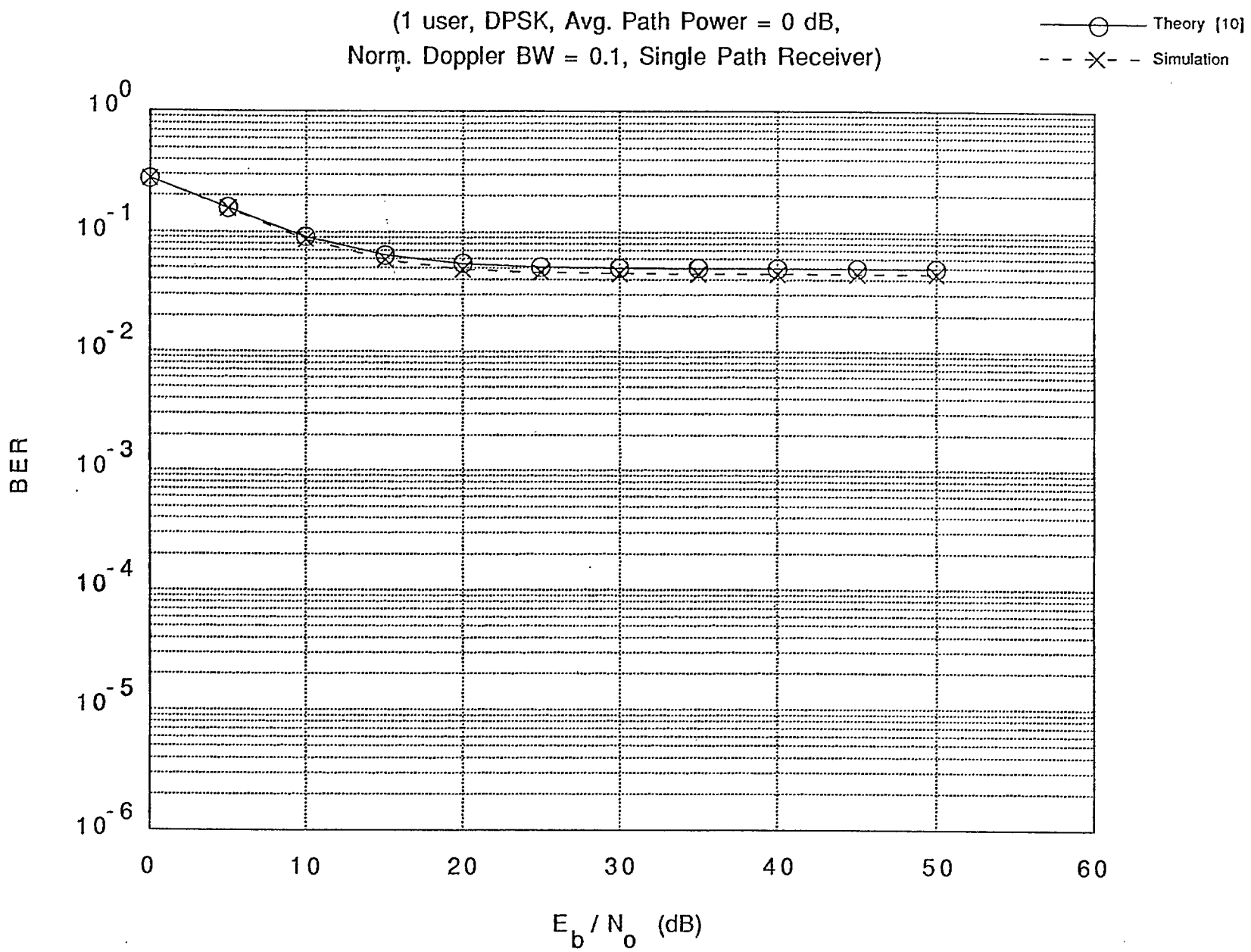

Fig. 9b Rayleigh Flat Fading Channel

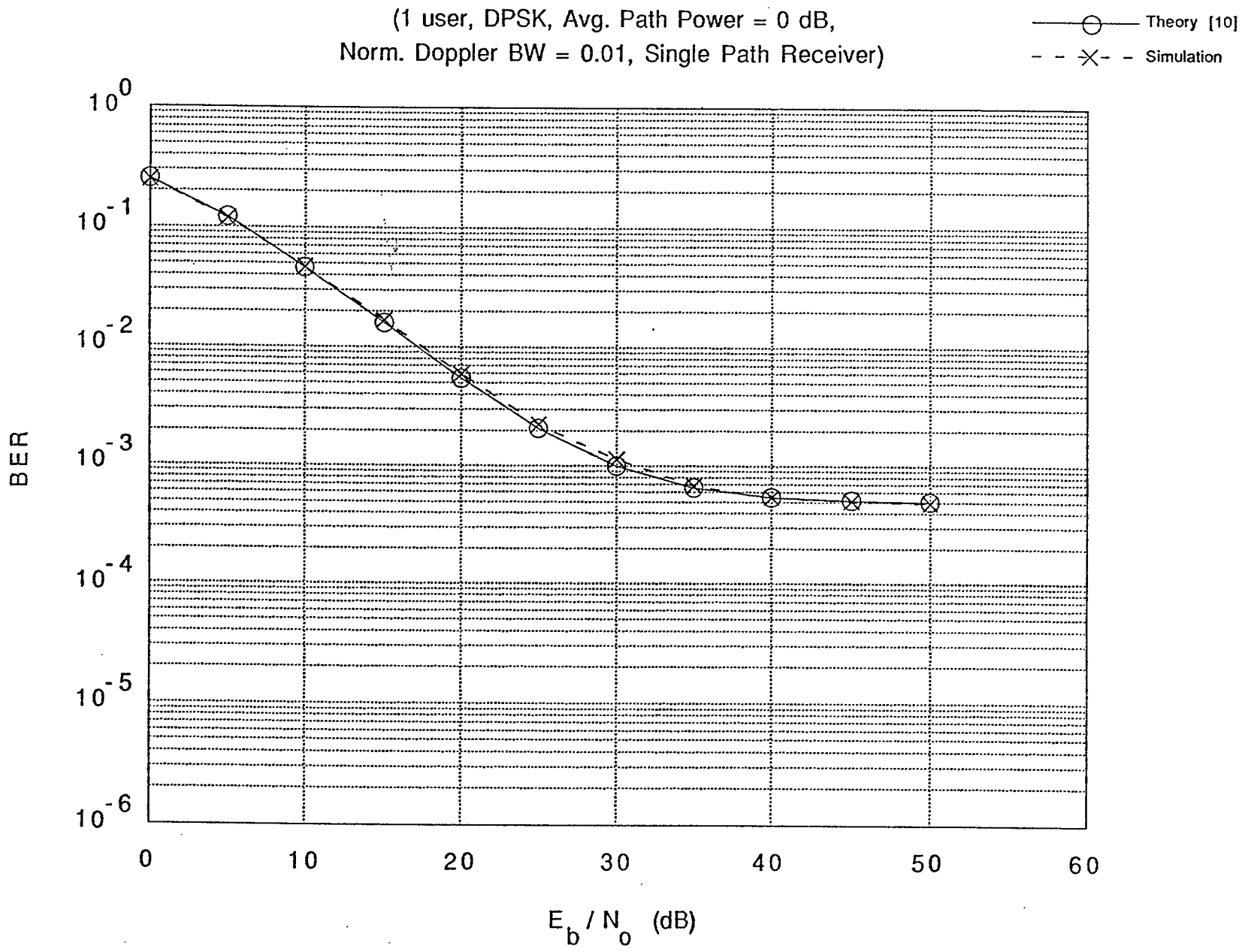

Fig. 9c Rayleigh Flat Fading Channel

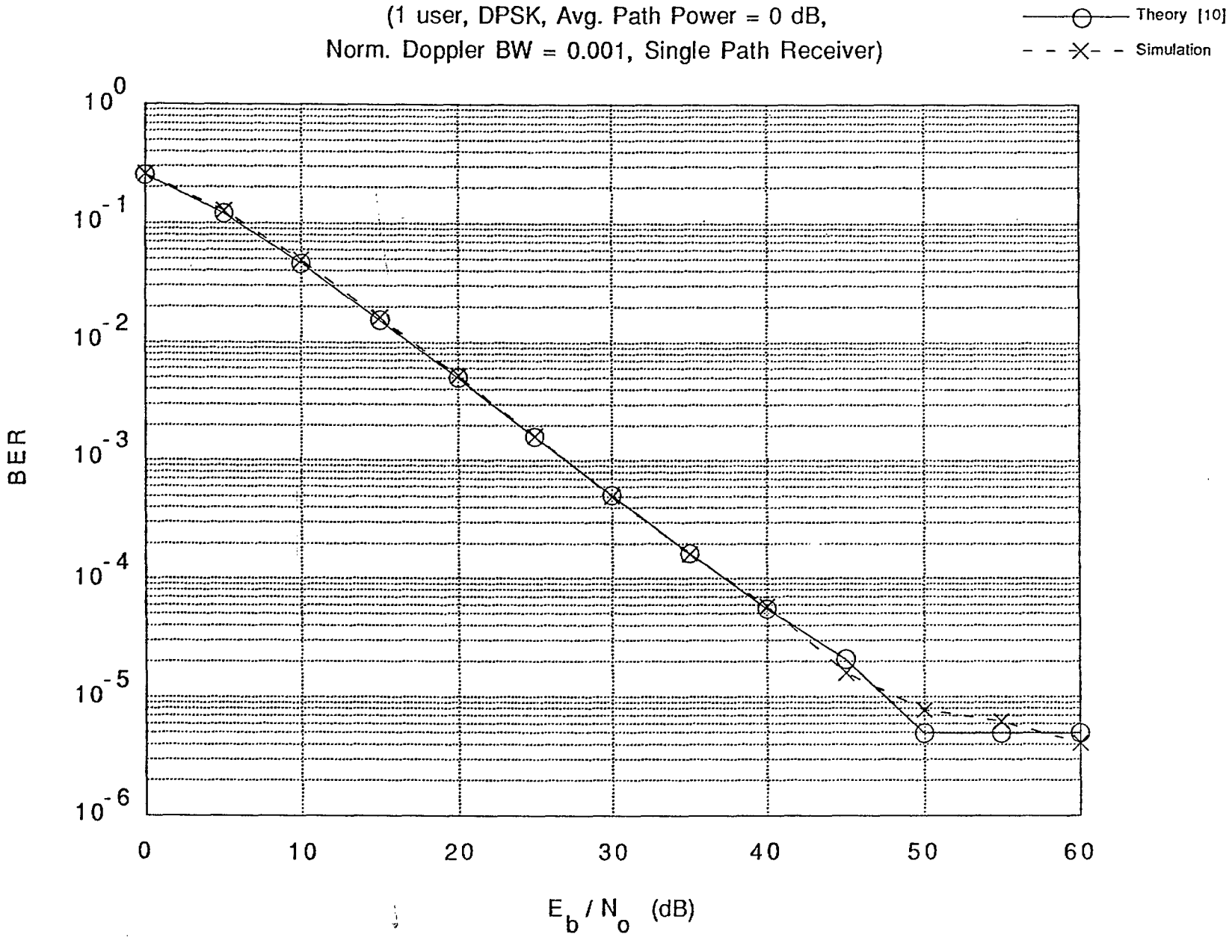

environment. It is therefore of interest to compare the simulation results of such a system with theoretical results in order to properly assess the correctness of the simulation software outputs. Unfortunately, the derivation of closed form theoretical results for the BER of a multi-user spread spectrum system in a multipath fading environment is a formidable problem. As such, previous efforts at finding a solution to this problem have resorted to theoretical bounds or numerical approximations. In Fig. 10 the simulated BER of a practical spread spectrum system is compared with some of the previously published results (based on numerical approximations) under identical system input parameters. For a Rayleigh frequency selective fading channel, Fig. 10a compares the BER calculated using Gauss Quadrature Rule (GQR) approximation [11] with the simulated BER. The E_b in E_b/N_0 in Fig. 10a assumes the same meaning as stated above for Figs. 8 and 9. Notice the very good agreement between the two results when E_b/N_0 is below 20 dB, and there is only a small difference between the error floors. As stated in [11], the selected Gold sequences are not optimized, this explains why the error floor predicted by the GQR approximation is worse than that obtained from the current simulation which uses optimized Gold sequences. In the case of a Rician frequency selective fading channel, the bit error rate calculated using the characteristic function approximation [12] is compared with the simulated BER in Fig. 10b. Here, the E_b in E_b/N_0 represents the energy in the nonfading subpath of the received signal and from [12], the power in the nonfading subpath is assumed to be unity. It is seen in Fig. 10b that at a given BER, the difference in E_b/N_0 between the predicted and simulated values is within 0.5 dB, which is not too large. Fig. 10 therefore demonstrates that the simulation results are comparable to those based on numerical approximations - the output of the simulator is therefore accepted with a high confidence level.

4.1.3 Bit Error Rate Result Summary

Simulation results have been obtained for the four channel scenarios specified in section 2.2. By assumption C4, all the channel paths have unity average path power except where otherwise stated. Other major input parameters to the simulator are as indicated on each graph shown on the following pages. The user guide (Appendix II) provides more detail on the input parameter specification to CDMAsim.

Fig. 10a Rayleigh Frequency Selective Fading Channel

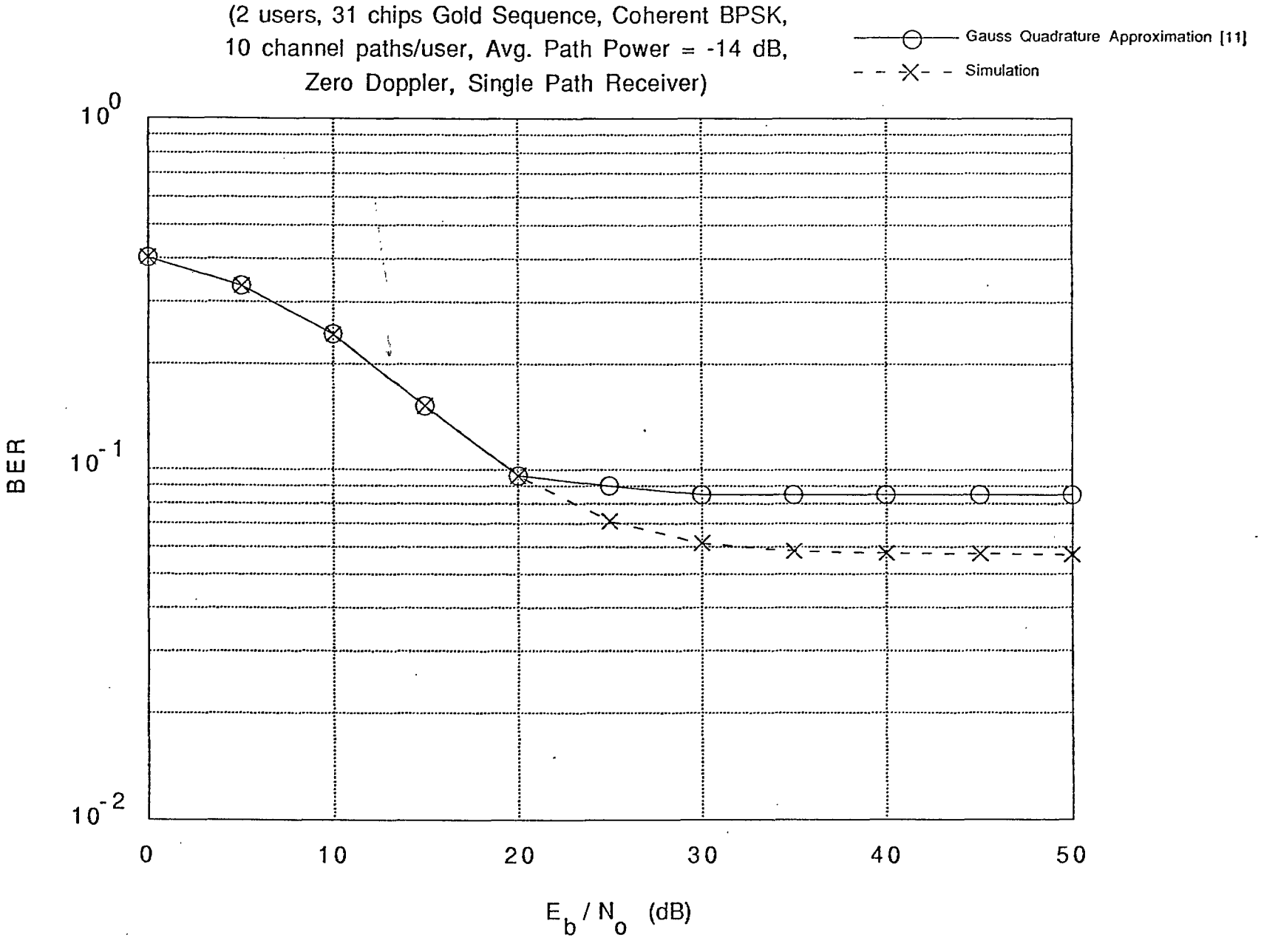

Fig. 10b Rician Frequency Selective Fading Channel

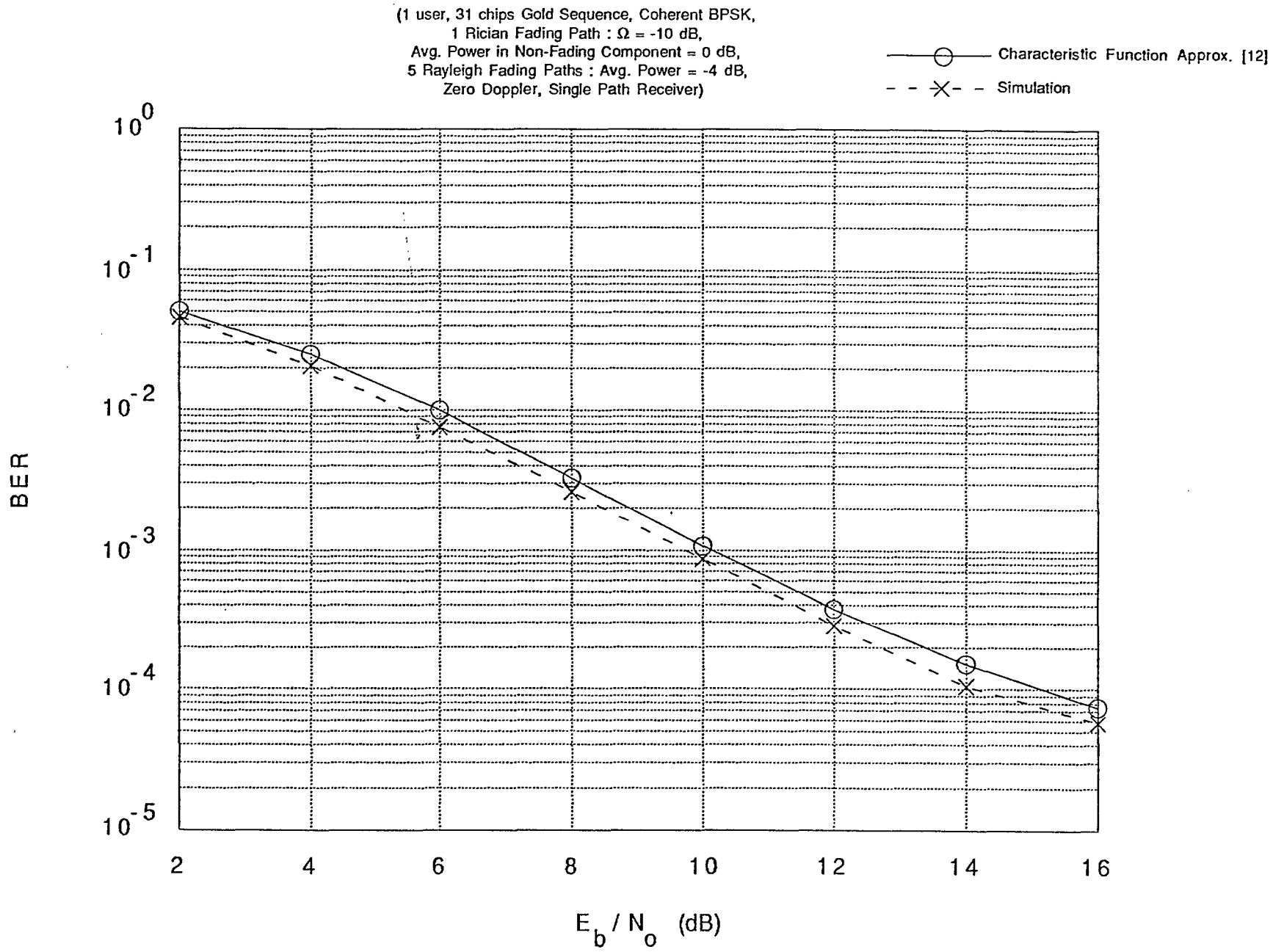

The format for all the results presented below is a plot of the simulated BER versus E_b/N_0. For consistency with the normalization imposed in Section 2.5.2, the E_b in E_b/N_0 on each of the following graphs represents the energy per bit per path. As such, for a Rician fading path, the E_b refers to the total average path power. Figs. 11 to 14 present the effect of the fading bandwidth and multipath interference on the BER performance, Figs. 15 to 18 depict the effect of multi-user interference, and Figs. 19 to 24 show the combined effects of multipath and multi-user interference as well as the performance of different receiver structures.

4.2 System Design Considerations

The issues pertaining to the design of a spread spectrum system for a mobile environment are discussed in the following under appropriate subheadings - the discussions are based on the simulation results shown in Figs. 11 to 24.

4.2.1 Effect of Doppler Bandwidth

It is important to first observe that at a data rate of 10 kbps and an operating frequency of 900 MHz, the specified normalized Doppler bandwidths (B_dT) of 0.001, 0.01, and 0.1 [1] translate to mobile speeds of 12 km/hr, 120 km/hr and 1200 km/hr respectively. Clearly, a land mobile speed of 1200 km/hr is not practical, as such, the performance discussion given below concentrate largely on normalized Doppler bandwidths of 0.001 and 0.01.

Figure 11a shows that for a single-user system operating in a Rayleigh flat fading channel with a Doppler bandwidth of 0.1, the BER falls from 0.28 at E_b/N_0 of 0 dB to a constant value of 4.4×10^{-2}. This limiting BER value is referred to as "error floor", which for the single-user system in a flat fading channel is caused primarily by the random FM noise (random phase fluctuations). Reducing the Doppler bandwidth by an order of magnitude causes the BER curve to approximate that for zero Doppler bandwidth over $0 \leq E_b/N_0 \leq 15$ dB. At E_b/N_0 of 45 dB, an error floor of 5×10^{-4} is obtained which is approximately two orders of magnitude smaller than that at a fading bandwidth of 0.1. Clearly, the preceding observation agrees with standard BER performance trend for a system employing differential detection in a fading channel: there is an improved BER performance

Fig. 11a Effect of Doppler Bandwidth on Rayleigh Flat Fading Channel

(1 user, DPSK, Avg. Path Power = 0 dB, Single Path Receiver)

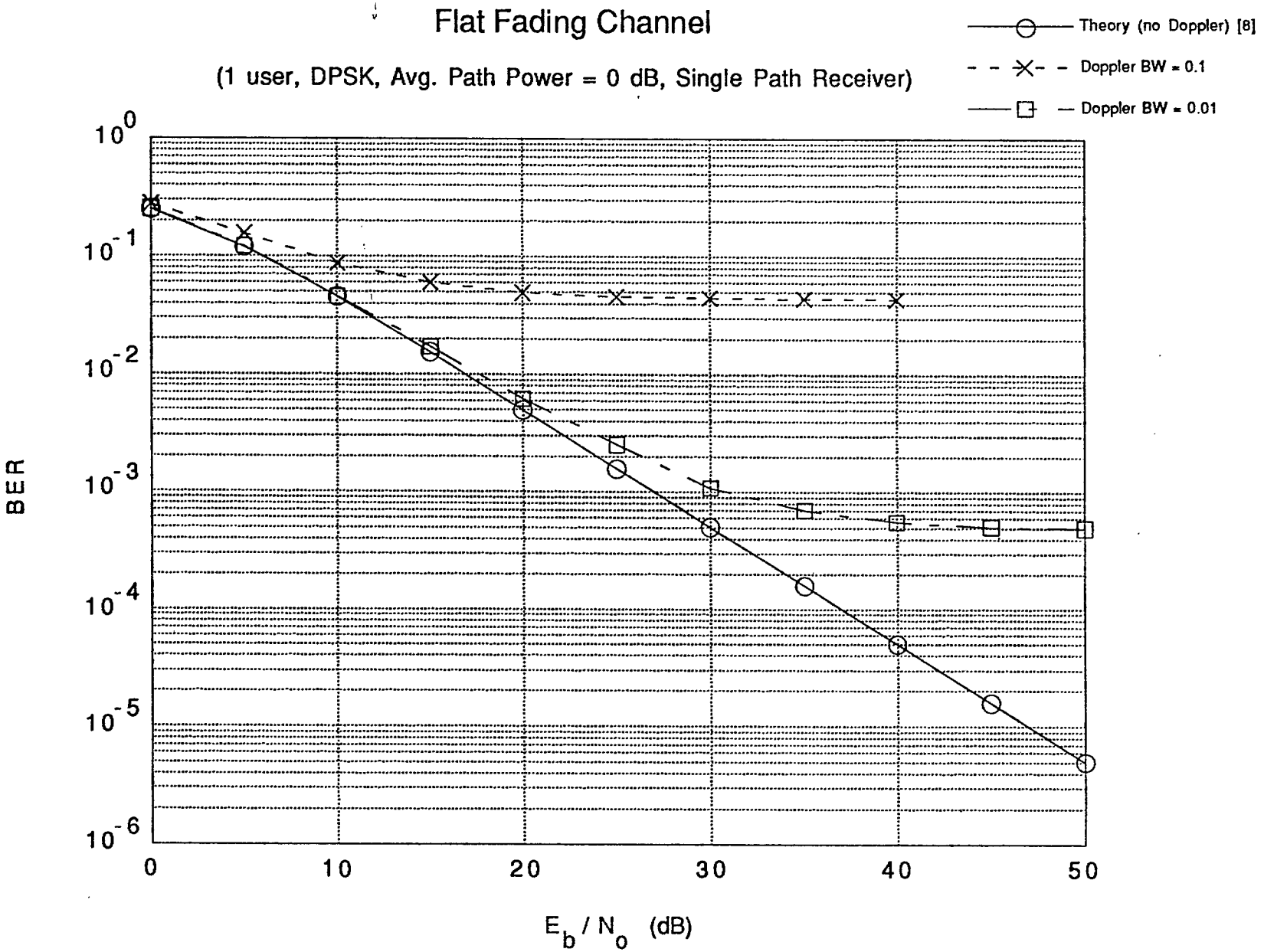

Fig. 11b Effect of Doppler Bandwidth on Rayleigh Frequency Selective Fading Channel

(1 user, 31 chips Gold Code, DPSK, 5 paths, Avg. Path Power = 0 dB, Rake Receiver, Equal Gain Combining)

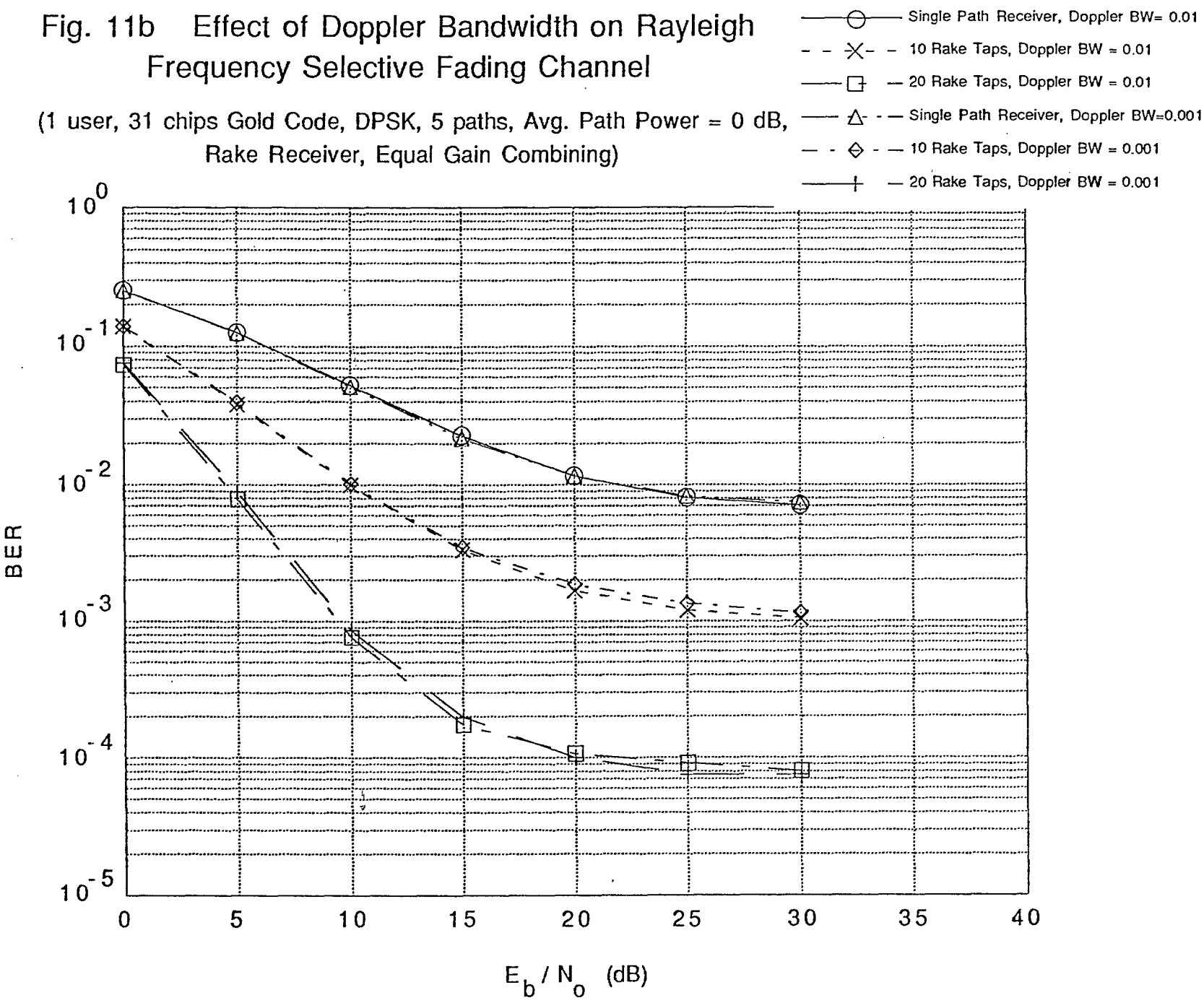

Fig. 11c Effects of Combining Method and Number of Rake Taps on Rayleigh Frequency Selective Fading Channel

(1 user, 31 chips Gold Code, DPSK, 5 paths, Avg. Path Power = 0 dB, norm. Doppler BW = 0.01, Rake Receiver)

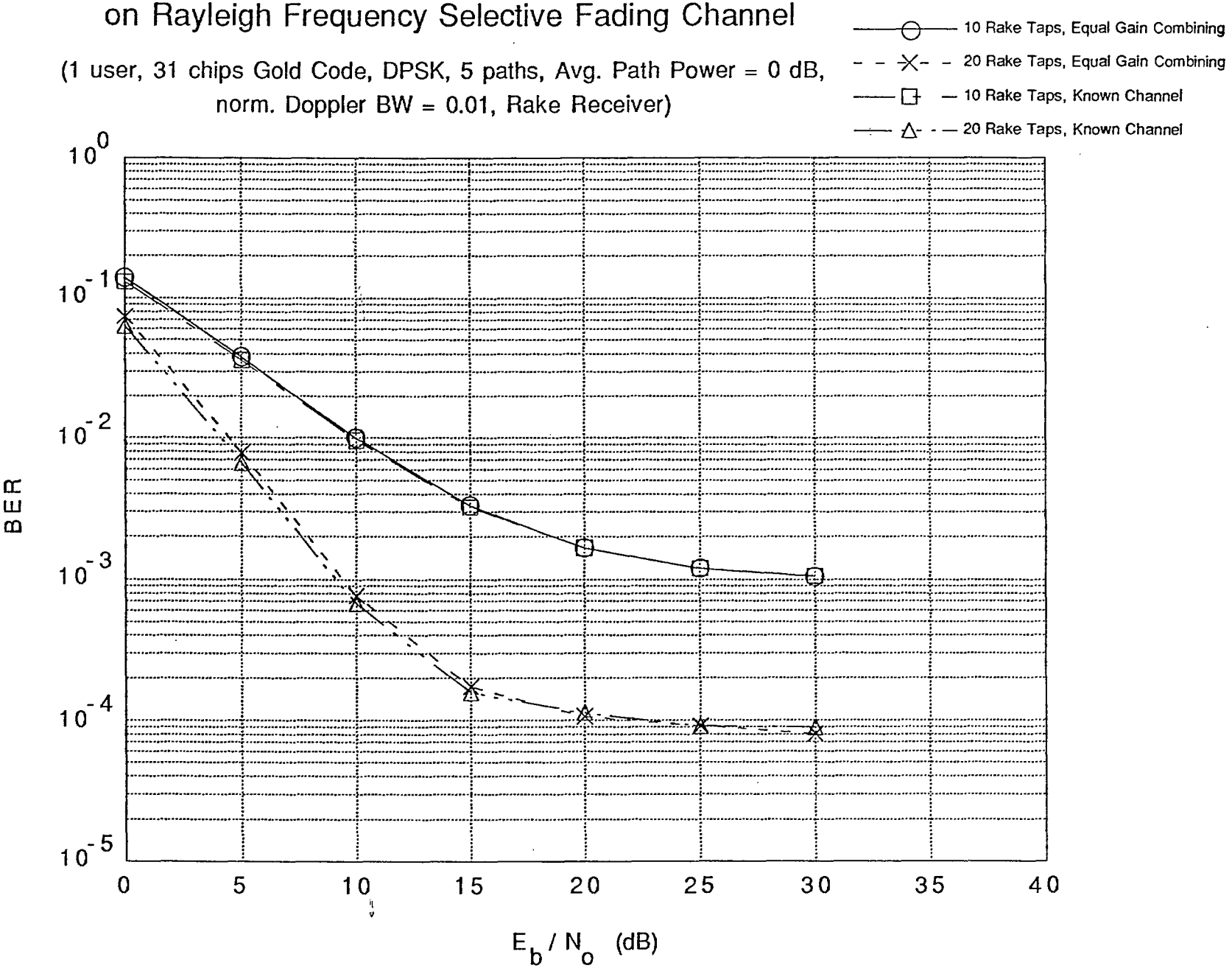

Fig. 12a Effects of Doppler Bandwidth and Rice Factor on Rician Flat Fading Channel

(1 user, Coherent BPSK, Avg. Path Power = 0 dB, Single Path Receiver)

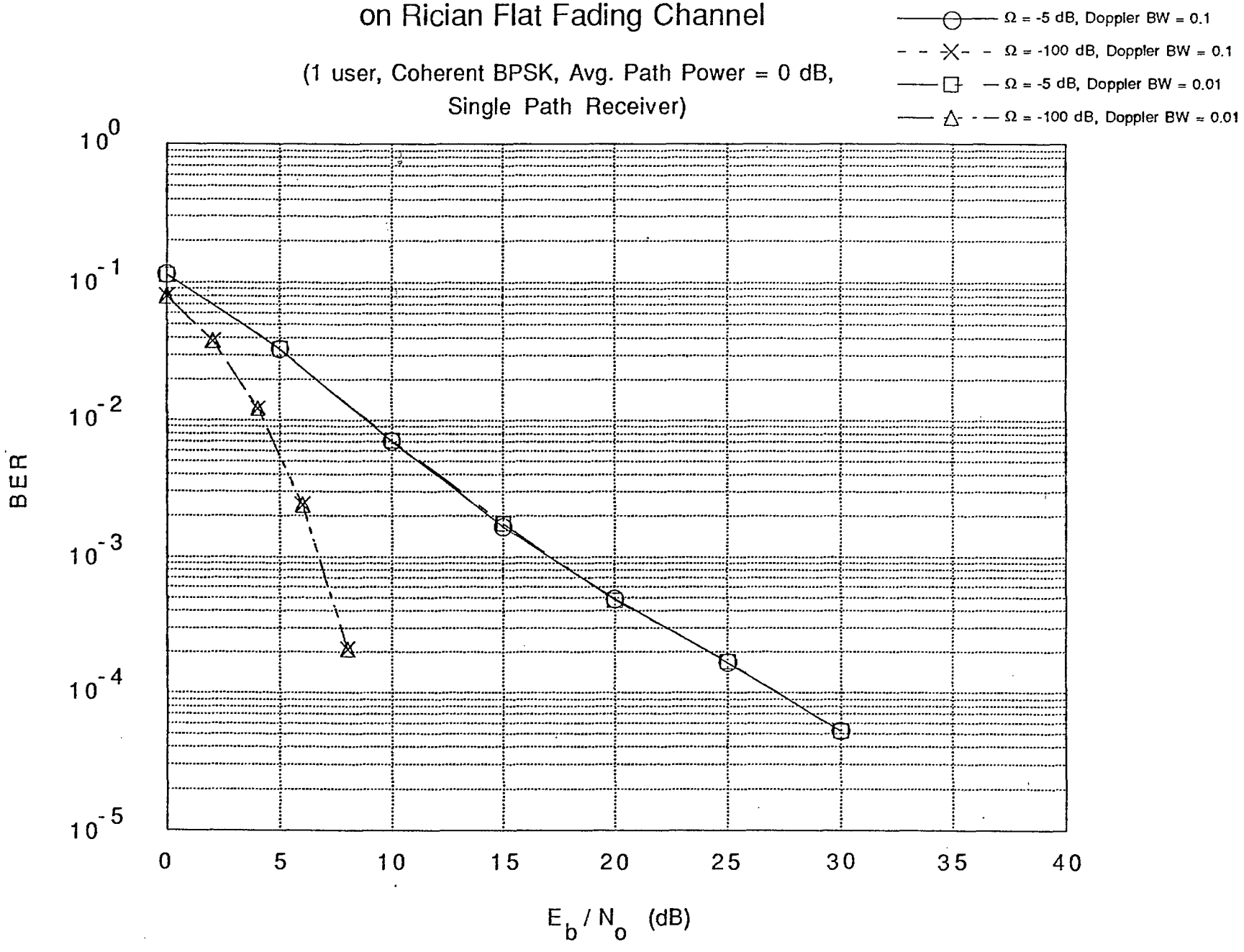

Fig. 12b Effects of Doppler Bandwidth and Rice Factor on Rician Frequency Selective Fading Channel

(1 user, 31 chips Gold Code, Coherent BPSK, 5 paths, Avg. Path Power = 0 dB, Single Path Receiver)

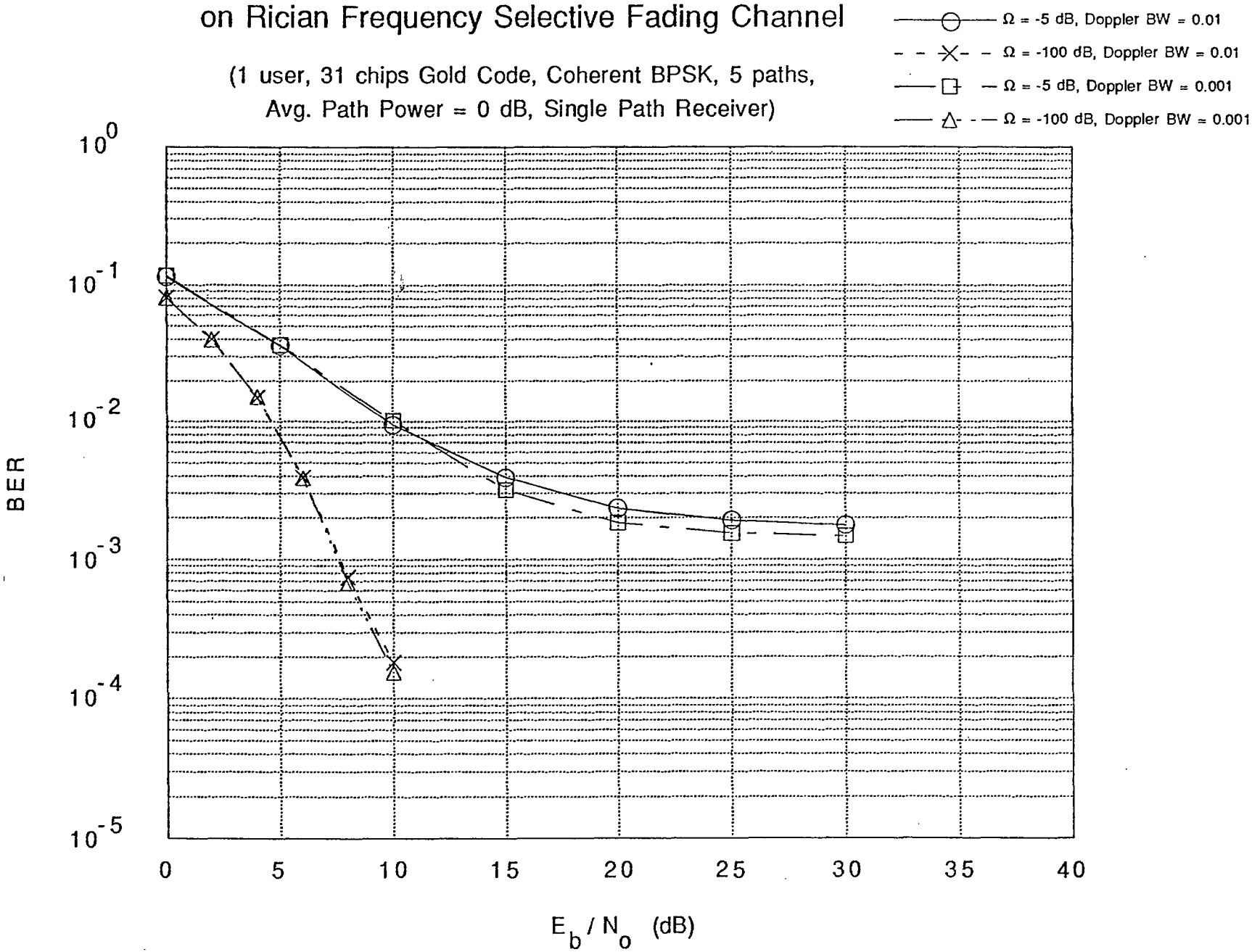

for smaller fading bandwidths because the slow fading process causes strong correlation between adjacent symbols.

Fig. 12a shows the corresponding performance over a Rician flat fading channel with Rice factor, Ω of -5 dB and -100 dB. When Ω equals -100 dB (and also -5 dB) there is no difference between the BER curves at fading bandwidths of 0.1 and 0.01 as evident in Fig. 11a for a Rayleigh fading channel. This is partly due to the coherent detection scheme that is adopted for the Rician fading channel compared to differential detection for Rayleigh fading channel. Also, the phase variation in the Rician fading channel is over a narrower range compared to the $[0, 2\pi]$ range for Rayleigh fading. The preceding statements explain why there is no occurrence of an error floor over the range of E_b/N_0 shown in Fig. 12a. It is also observed that for the Rician fading channel, the BER performance for Ω = -100 dB (i.e. average path power is almost dominated by the average power of the nonfading component) is better than that for Ω = -5 dB when the average power of the fading component is 31% of total average power of the Rician fading path.

By comparing Figs. 11a with 12a, it is clear that at a given fading bandwidth, the BER performance of a single-user system is better in a Rician than in a Rayleigh flat fading channel. For example, at a fading bandwidth of 0.01 and a performance quality specification of 10^{-3} BER, it is seen from Figs. 11a and 12a that a single-user system in a Rician flat fading channel requires an E_b/N_0 which is 14 dB (Ω = -5 dB) and 24 dB (Ω = -100 dB) less than that required in a Rayleigh flat fading channel to achieve the same BER. The difference in performance over Rayleigh and Rician fading channels is attributed to the variation of the instantaneous path power about the mean power. A Rayleigh fading channel generally exhibits a large variation about the mean path power, whereas in a Rician fading channel, the variation depends on the value of Ω. For example, Ω equals -100 dB means an almost zero variation about the mean path power.
For a single user system in a Rayleigh frequency selective fading channel with differential single path receiver or differential 10/20 - tap RAKE receiver, it is also seen (Fig. 11b) that there is not much difference in the BER performance at fading bandwidths of 0.01 and 0.001.

Examination of Figs. 15a and 15b seems to indicate that the BER performance of a spread spectrum system consisting of 5 users (31-chip Gold sequence) in a

Rayleigh flat fading channel is independent of mobile speed, this is in contrast to the distinct performance displayed in Fig. 11a for the single-user system. This non-dependence of error floor on the fading bandwidth is attributed to the dominance of multi-user interference over random FM noise in a multi-user system so that the impact of random FM noise becomes minimal leading to the small difference in performance. When 255-chip Kasami sequence is used, the multi-user interference is minimized (Fig. 17) and there now exists a distinction in the BER performance at fading bandwidths of 0.1 and 0.01.

Figs. 16a and 16b show that for a single- and multiple-user spread spectrum system (31-chip Gold sequence) in a Rician fading channel (Ω = -100 dB and -5 dB), there is no difference in BER performance at fading bandwidths of 0.1 and 0.01. Even when 255-chip Kasami sequence is used, the BER performance (shown in Figs. 18a and 18b) at the two fading bandwidths are almost identical to those for the 31-chip Gold sequence. One explanation for this behavior is the fact that for the Rice factors of -100 dB and -5 dB considered, the average total Rician fading path power is dominated by the average power of the nonfading component: a Rice factor of -100 dB implies an almost zero power from the fading component and Ω = -5 dB means that 69% of the total power is contributed by the nonfading component. The zero (or 31%) contribution of the fading component therefore results in identical performance at fading bandwidths of 0.1 and 0.01.

Finally, notice from Figs. 19a and 19b (as well as in Figs. 23a and 23b, and in Figs. 24a and 24b) that there is very little difference in performance at fading bandwidths of 0.01 and 0.001, this is due to the dominance of the multipath and multi-user interference over the random FM noise.

4.2.2) Effect of Multipath Interference

In a non-multiple access spread spectrum system, where the transmitted signal arrives at the receiver via several paths, multipath interference is caused by the nonzero partial autocorrelation of the spreading code, which in turn is due to the nonzero path delays.

Fig. 13a Effect of Doppler Bandwidth on Rayleigh Frequency Selective Fading Channel

(1 user, 255 chips Kasami Code, DPSK, 5 paths,
Avg. Path Power = 0 dB, Rake Receiver, Equal Gain Combining)

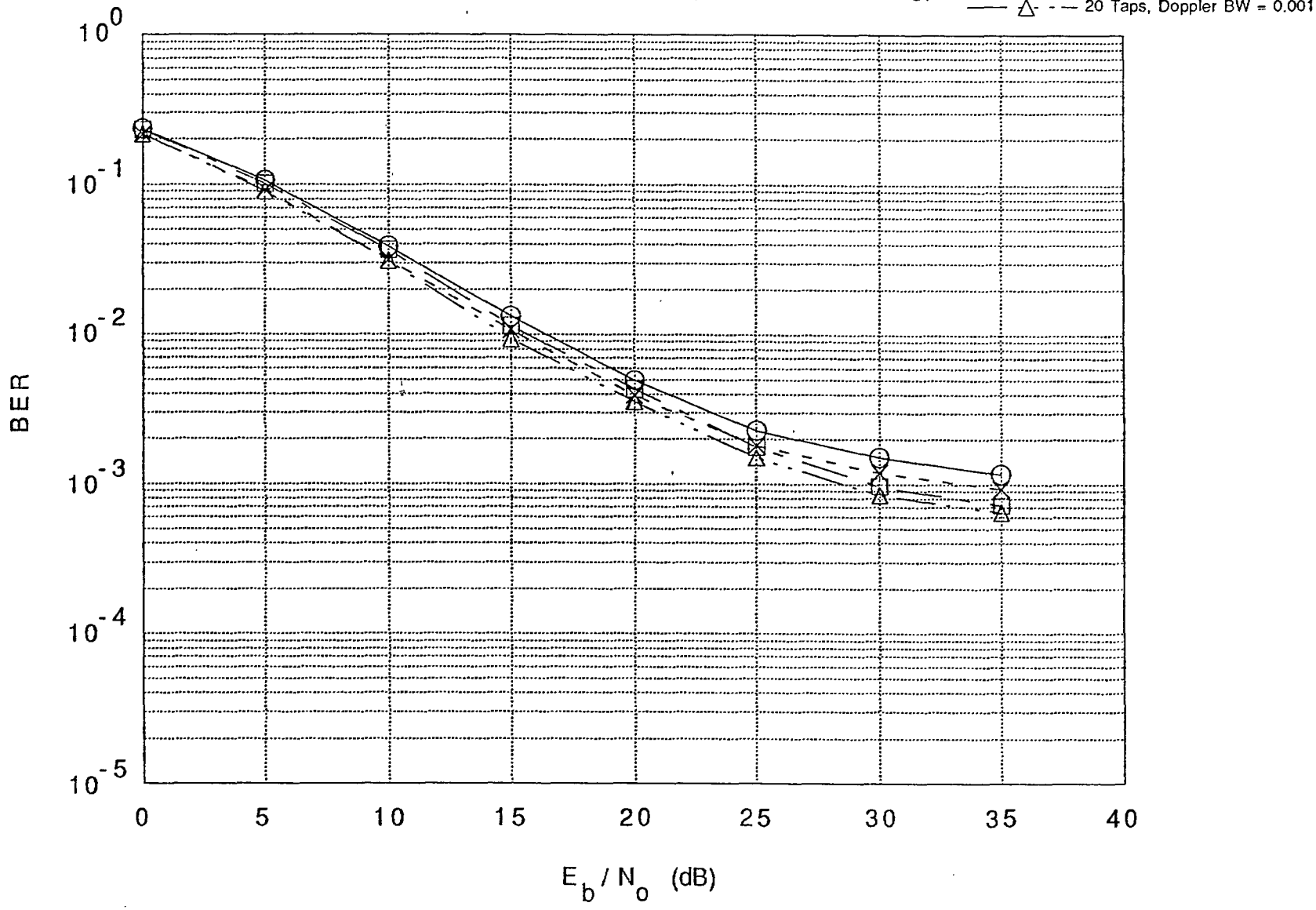

Fig. 13b BER Performance Comparison on Rayleigh Frequency Selective Fading Channel

(1 user, DPSK, 5 paths, Avg. Path Power = 0 dB, Single Path Receiver)

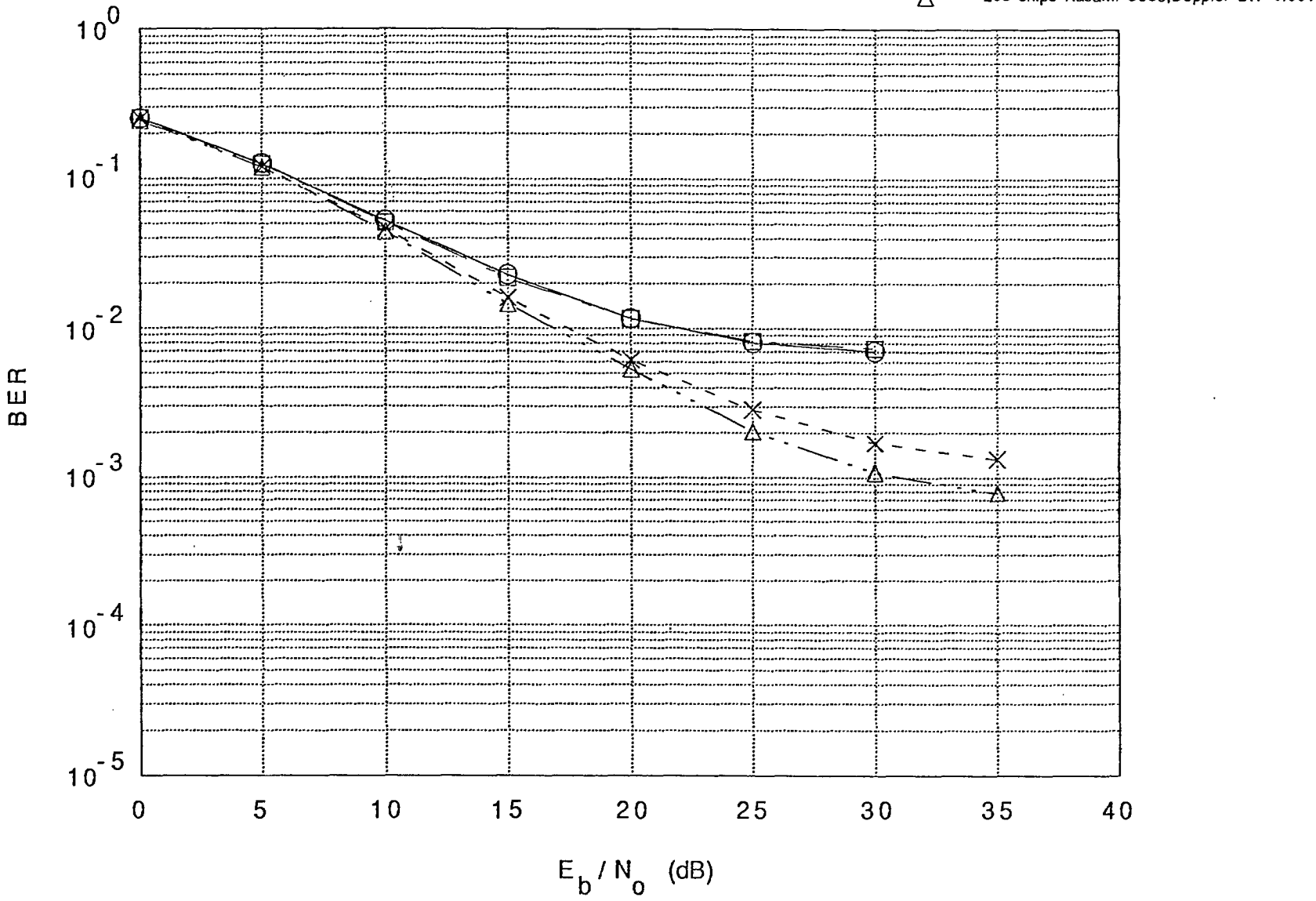

Intuitively, it is expected that this additional self interference will cause degradation in BER performance compared to the results in Figs. 11a and 12a. A challenge therefore is to design a spread spectrum system that will operate in a frequency selective fading channel such that the BER is minimized. For simplicity reasons, preliminary system design incorporates the single path receiver structure analyzed in Section 2.5.3.1. Fig. 11b shows the BER performance over a Rayleigh frequency selective fading channel at normalized fading bandwidths of 0.01 and 0.001 and assuming 31-chip Gold sequence. As expected, at a Doppler bandwidth of 0.01, the BER performance of the single path receiver in Fig. 11b is worse (due to the added self interference) compared to that of Fig. 11a. In fact, the error floor shown in Fig. 11b (single path receiver) is 7×10^{-3} compared to a corresponding value of 5×10^{-4} in Fig. 11a. Notice that in Fig. 11b, the error floor is due largely to multipath interference which now limits the system performance. One way to improve the BER and the error floor is to combine the multiple signal replicas (of the desired user) available at the receiver input, this is realized by the RAKE receiver structure described in Section 2.5.3.2. The BER results shown in Figs. 11b and 13a assume that only the path delays are estimated perfectly and the tap weight at a position corresponding to each path delay that falls within the RAKE window is tuned to unity - referred to as equal gain combining. It is observed from Fig. 11b that at a given value of E_b/N_0, smaller bit error rates are obtained using a RAKE receiver structure compared to those for a single path receiver. For example, at a Doppler bandwidth of 0.01 and E_b/N_0 of 10 dB, the bit error rates are found to be 5.2×10^{-2}, 10^{-2} and 7.7×10^{-4} for single path receiver, 10-tap RAKE receiver and 20-tap RAKE receiver respectively. Notice also that the error floor decreases with increasing number of RAKE taps.

The results for a 255-chip Kasami sequence are shown in Fig. 13a which corresponds to Fig. 11b. A direct comparison of Fig. 11b with Fig. 13a at first glance may indicate some inconsistencies in the BER results: Why is the BER performance for the 10-tap and 20-tap RAKE receivers in Fig. 13a worse than their corresponding performance in Fig. 11b despite the assertion in Section 4.1.1 that a 255-chip Kasami sequence exhibits better autocorrelation property than a 31-chip Gold sequence? An answer to this question begins by first noting that a comparison between Figs. 11b and 13a based on the number of RAKE taps is not fair. This is because for the same code period (in units of time), the chip duration

Fig. 14 Effects of Doppler Bandwidth and Rice Factor on Rician Frequency Selective Fading Channel

(1 user, 255 chips Kasami Code, Coherent BPSK, 5 paths, Avg. Path Power = 0 dB, Single Path Receiver)

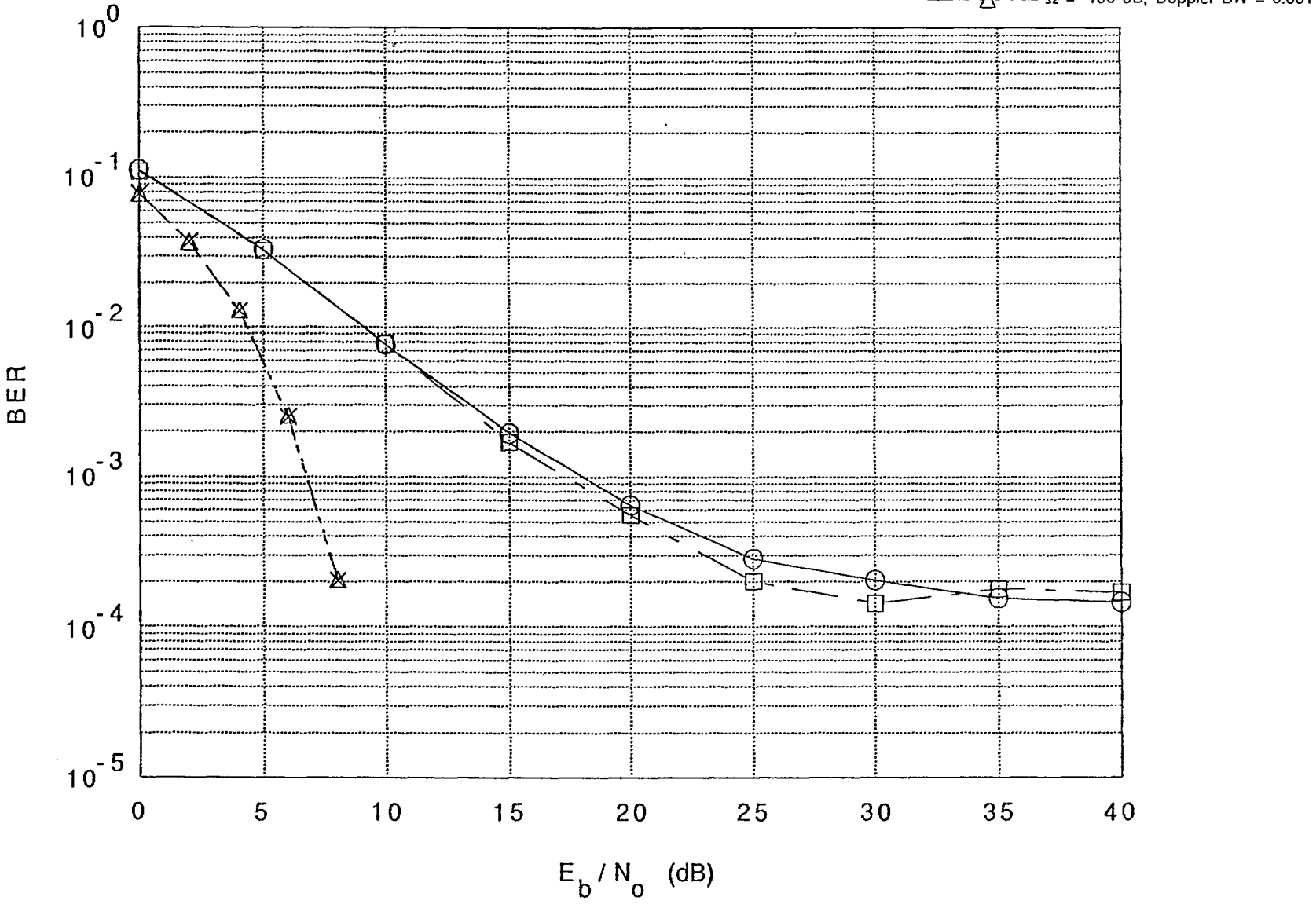

will be different because of the different spreading code lengths. As such, for the same number of RAKE taps, the RAKE window is also different and this makes a direct comparison of the BER results on the basis of only the number of RAKE taps meaningless. If the comparison is based on the same RAKE window, then the improvement of the 255-chip Kasami sequence over the 31-chip Gold sequence will become apparent. The preceding claim is verified by the results for the single path receiver where as seen from Fig. 13b, the 255-chip Kasami sequence exhibits better performance than 31-chip Gold sequence. Another important observation from Fig. 13a is the little improvement in the BER performance between a 20-tap and a 10-tap RAKE receiver. An explanation for this behavior is based on the likelihood that a given path delay falls within the RAKE window. Recall that path delays are selected according to a uniform distribution over [0, T]. It then follows from simple probability arguments that for the 255-chip Kasami sequence, a path delay falls within a RAKE window corresponding to 10 taps and 20 taps with probability 0.04 and 0.08 respectively - the very small difference between the probabilities explains the little performance improvement. For the 31-chip sequence, the corresponding probabilities are found to be 0.32 and 0.64 and this explains the distinct performance shown in Fig. 11b.

In a Rician frequency selective channel (31-chip Gold sequence), Fig. 12b does not employ any form of spread spectrum diversity because the single path receiver always locks on to the dominant path. At a Rice factor of -5 dB, notice the appearance of an error floor (due to multipath interference), which is not seen in Fig. 12a (flat fading case). The performance in the absence of fading subpaths (i.e. Ω = -100 dB) is seen to be better than that at a Rice factor of -5 dB. For example, at a fading bandwidth of 0.01 and Ω equals -100 dB, a BER of 10^{-3} is achieved at an E_b/N_0 of 7.5 dB, this performance quality cannot be achieved when Ω equals -5 dB at any value of E_b/N_0 because the error floor is 1.8×10^{-3}. Comparison of Fig. 14 with Fig. 12b shows a better BER performance for the 255-chip Kasami sequence than that of the 31-chip Gold sequence.

4.2.3) Effects of Multi-user Interference

Multi-user interference results in a degradation of the bit error rate and error floor. By comparing Fig. 17a with Fig. 15a (and also Fig. 17b with Fig. 15b) it is

Fig. 15a Effect of Multiuser Interference on Rayleigh Flat Fading Channel

(31 chips Gold Code, DPSK, 1 path, Avg. Path Power = 0 dB, norm. Doppler BW = 0.1, Single Path Receiver)

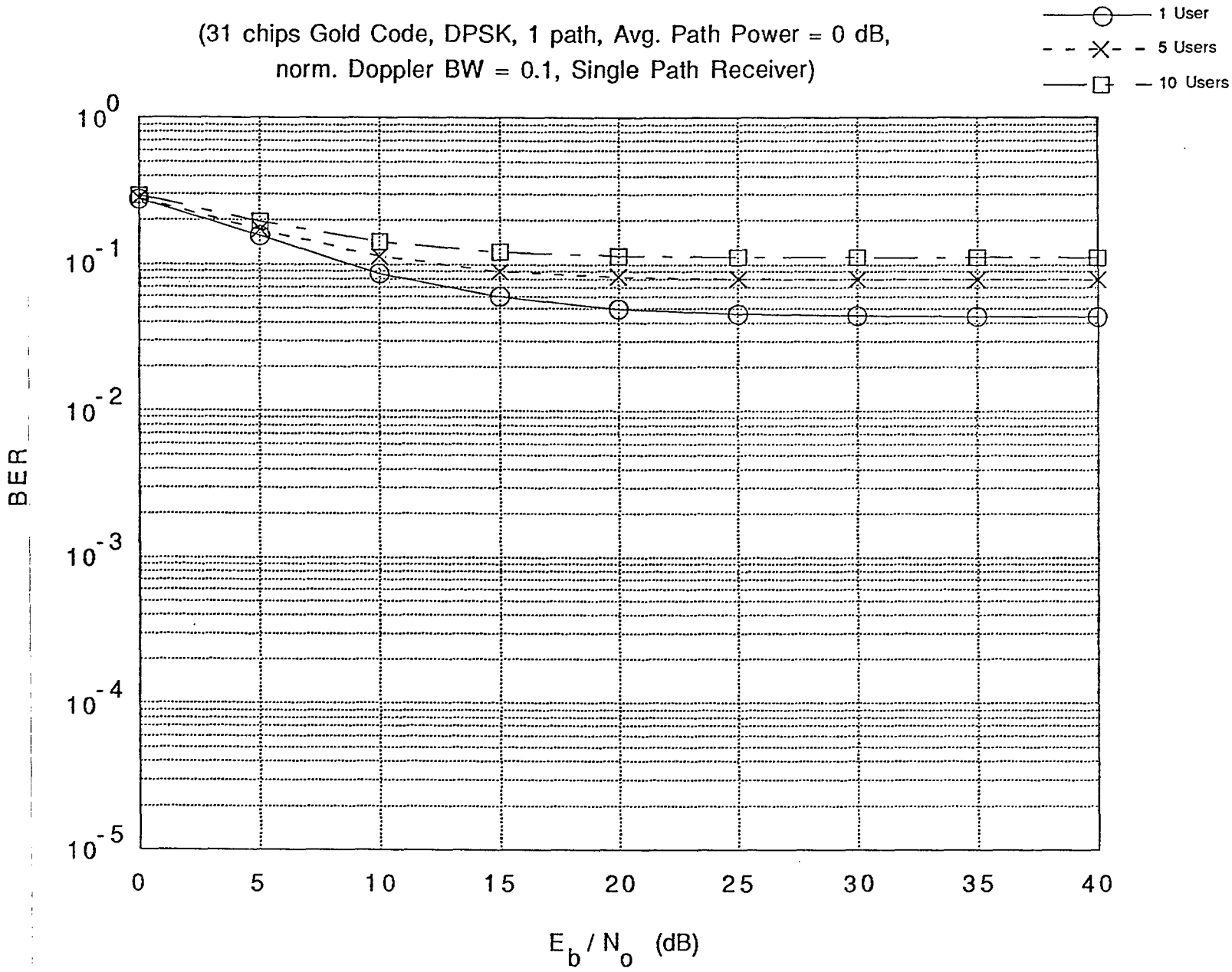

Fig. 15b Effect of Multiuser Interference on Rayleigh Flat Fading Channel

(31 chips Gold Code, DPSK, 1 path, Avg. Path Power = 0 dB, norm. Doppler BW = 0.01, Single Path Receiver)

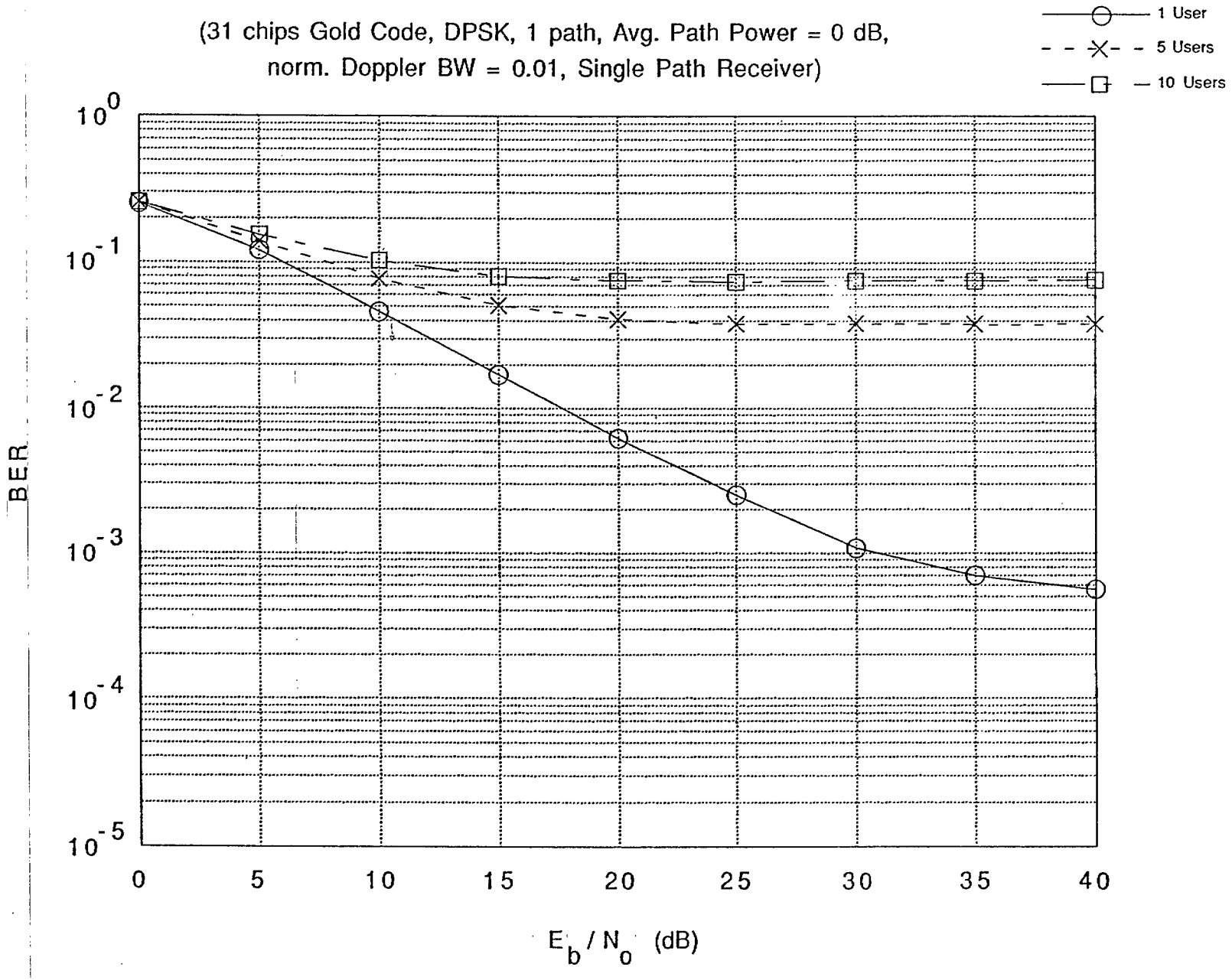

Fig. 16a Effect of Multiuser Interference on Rician Flat Fading Channel

(31 chips Gold Code, Coherent BPSK, 1 path, Avg. Path Power = 0 dB, norm. Doppler BW = 0.1, Single Path Receiver)

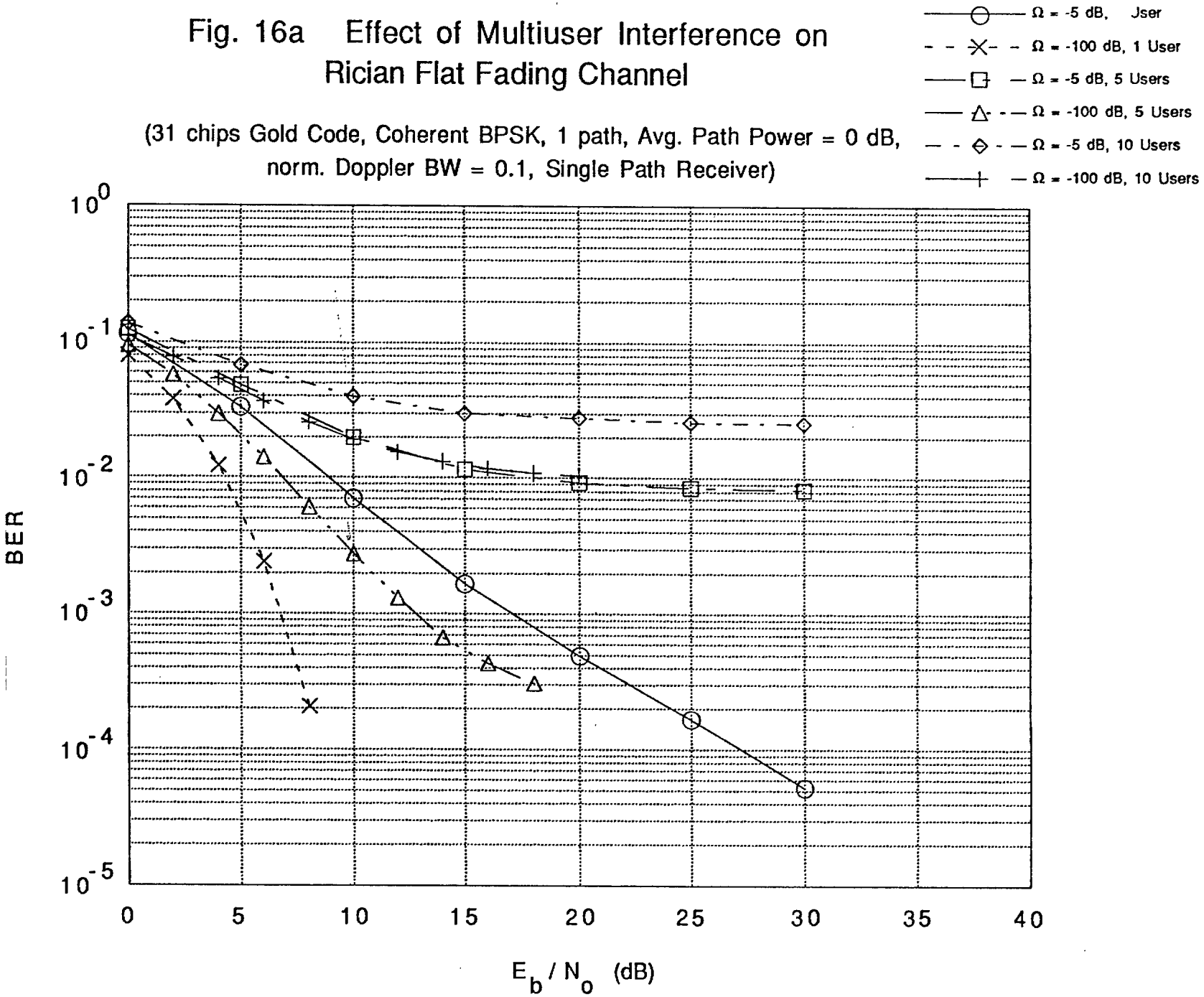

Fig. 16b Effect of Multiuser Interference on Rician Flat Fading Channel

(31 chips Gold Code, Coherent BPSK, 1 path, Avg. Path Power = 0 dB, norm. Doppler BW = 0.01, Single Path Receiver)

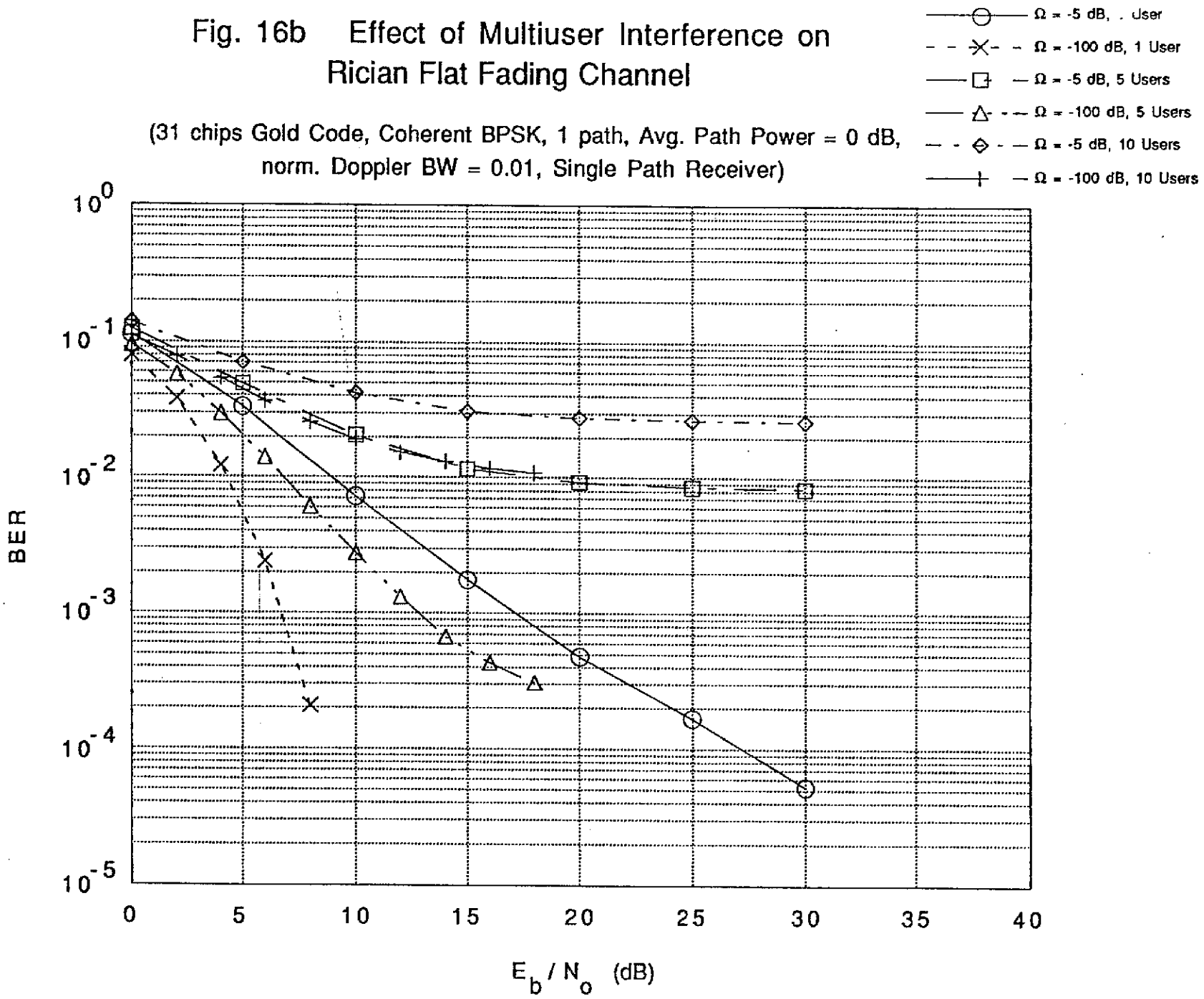

Fig. 17a Effect of Multiuser Interference on Rayleigh Flat Fading Channel

(255 chips Kasami Code, DPSK, 1 path, Avg. Path Power = 0 dB, norm. Doppler BW = 0.1, Single Path Receiver)

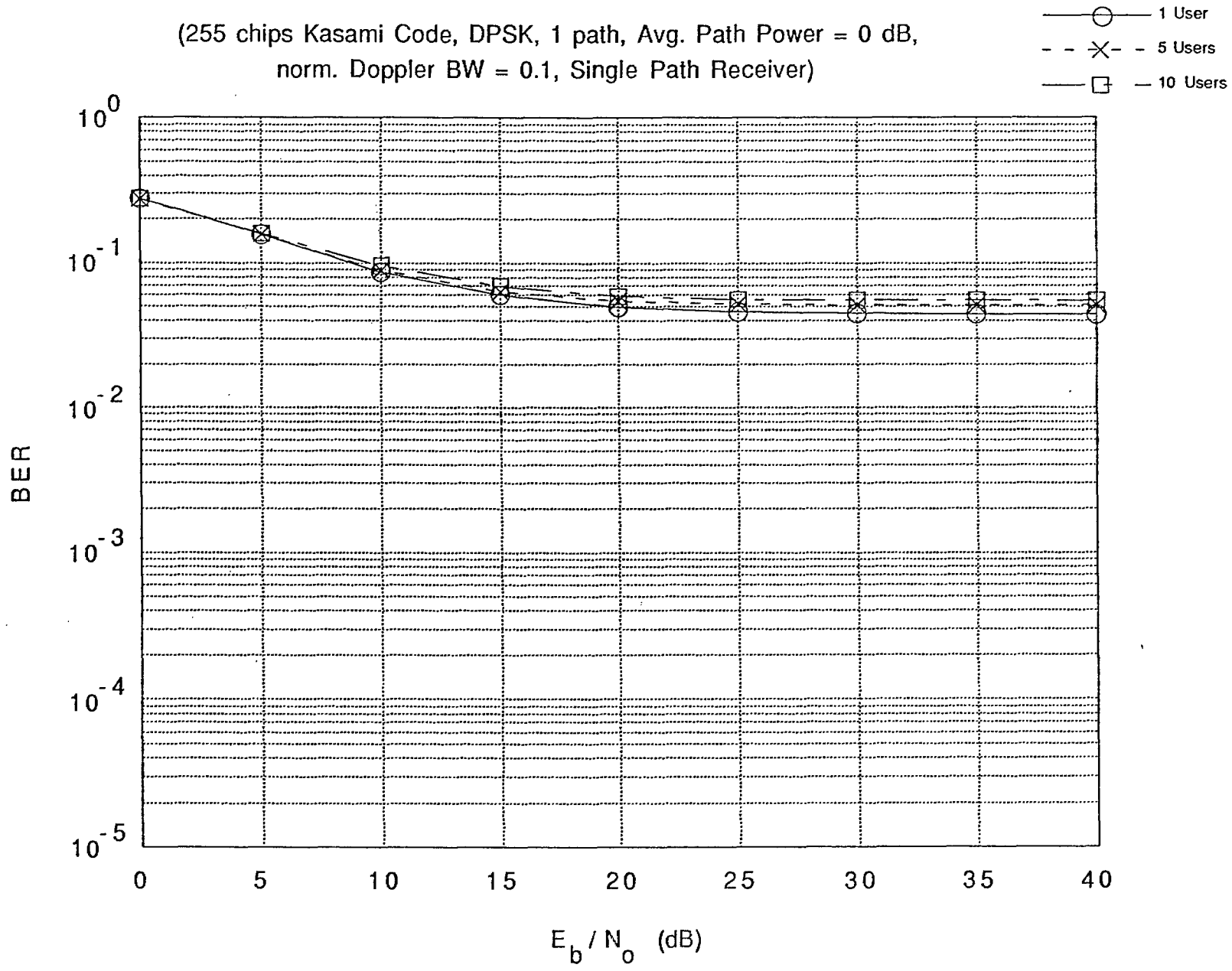

Fig. 17b Effect of Multiuser Interference on Rayleigh Flat Fading Channel

(255 chips Kasami Code, DPSK, 1 path, Avg. Path Power = 0 dB, norm. Doppler BW = 0.01, Single Path Receiver)

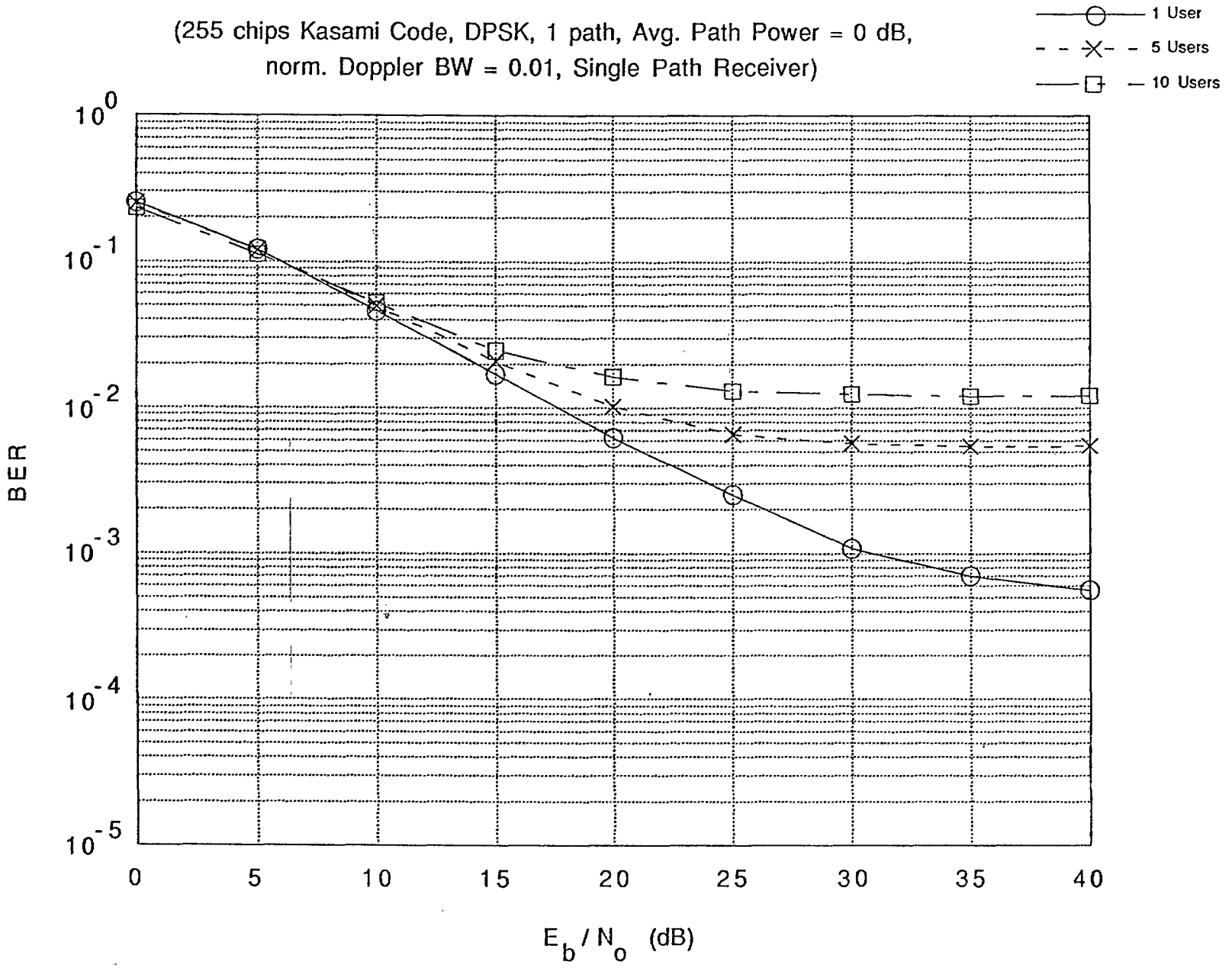

Fig. 18a Effect of Multiuser Interference on Rician Flat Fading Channel

(255 chips Kasami Code, Coherent BPSK, 1 path, Avg. Path Power = 0 dB, norm. Doppler BW = 0.1, Single Path Receiver)

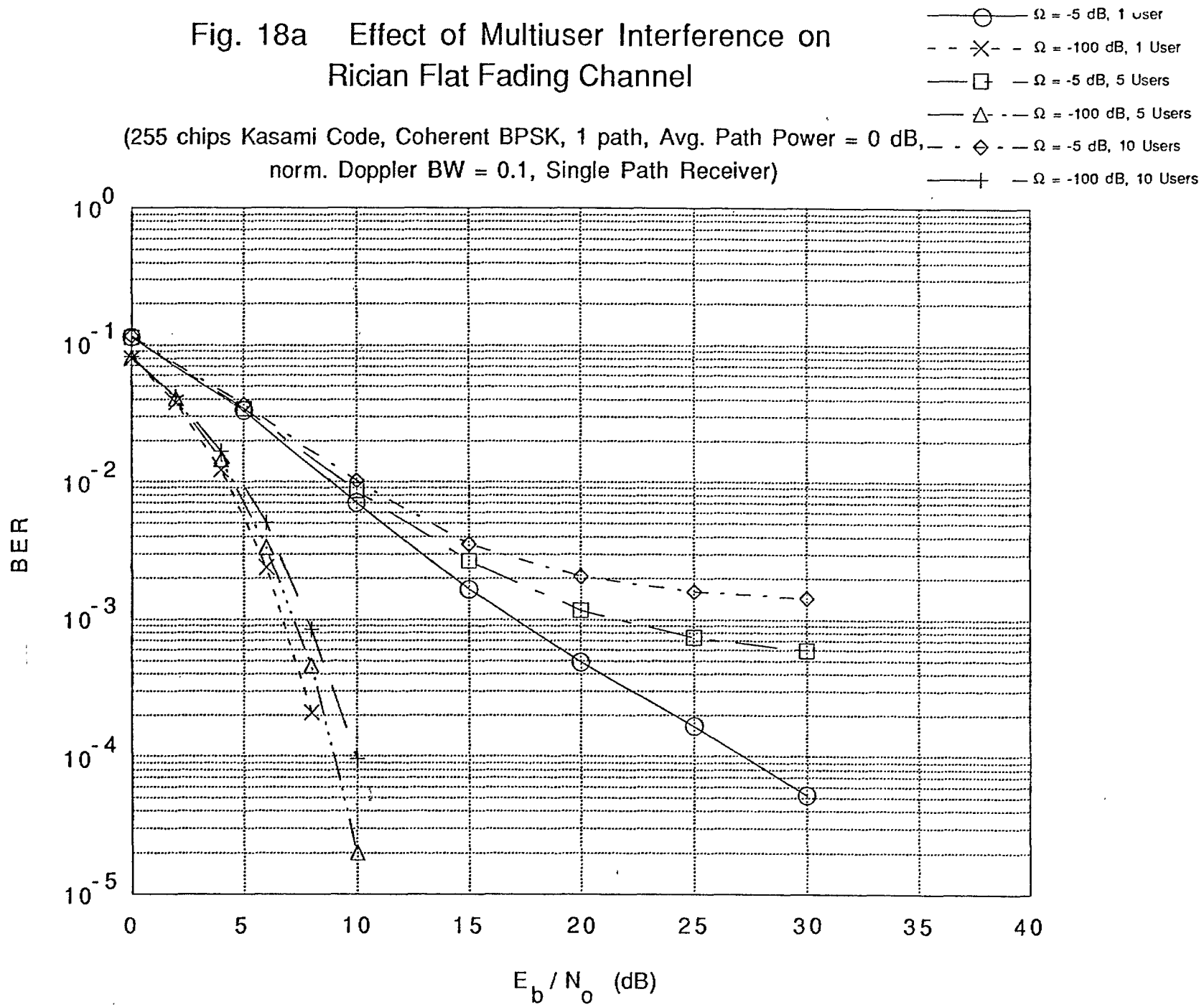

Fig. 18b Effect of Multiuser Interference on Rician Flat Fading Channel

(255 chips Kasami Code, Coherent BPSK, 1 path, Avg. Path Power = 0 dB, norm. Doppler BW = 0.01, Single Path Receiver)

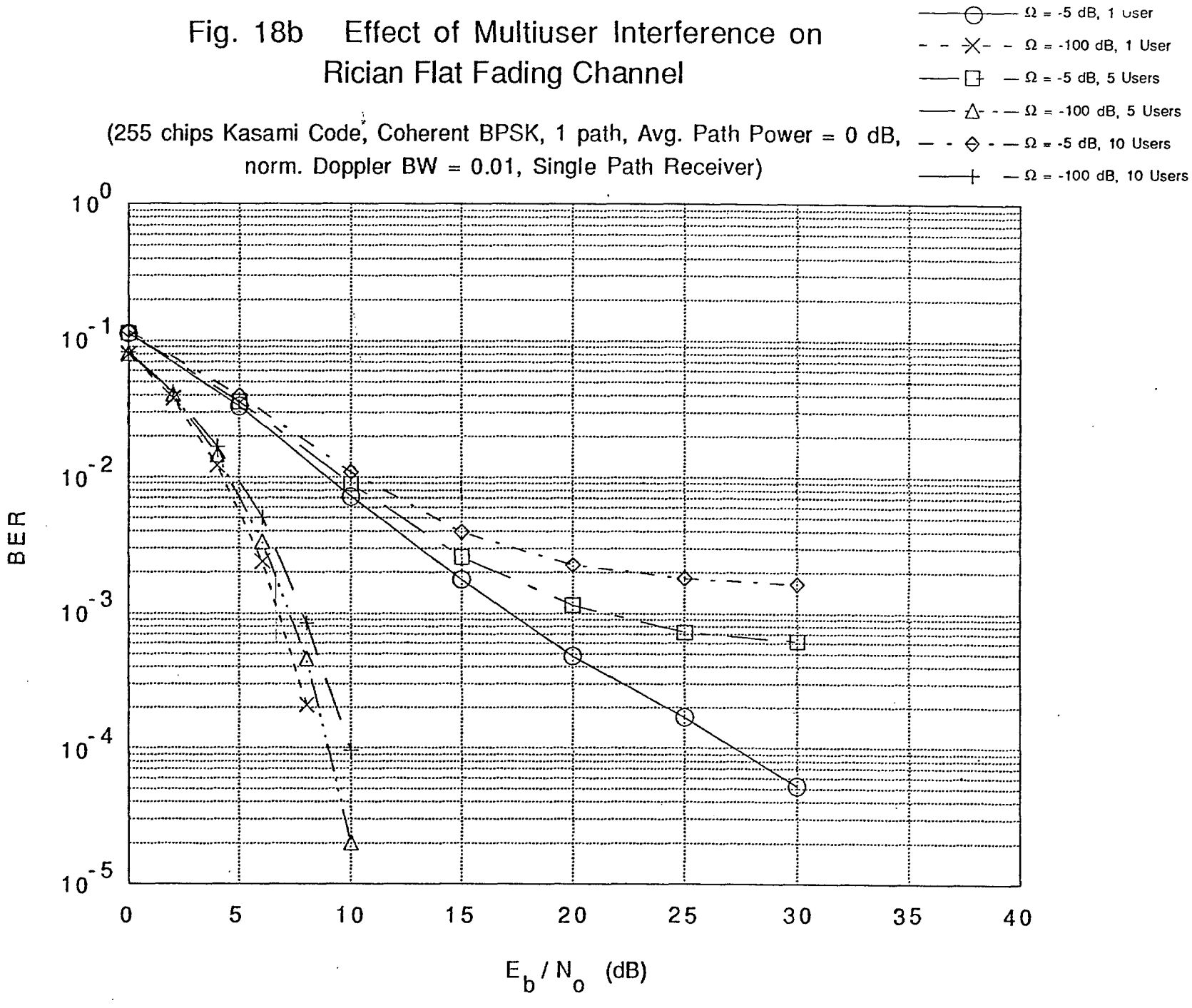

observed that a multiple-access system experiences less degradation in BER performance with 255-chip Kasami sequence than with 31-chip Gold sequence - this is true due to a conclusion drawn in Section 4.1.1 that 255-chip Kasami sequence has greater interference suppression capability than 31-chip Gold sequence.

It is also observed from Fig. 16a that the BER performance of a system consisting of several users (31-chip Gold codes) and operating in a Rician fading channel attains an error floor even in the absence of fading (that is Ω = -100 dB) and multipath interference. The error floor is caused by multi-user interference (contrast with Fig. 13a where multipath interference causes the error floor). Using 255-chip Kasami sequence, the effect of the multi-user interference is reduced which then results in an improved BER and error floor (Figs. 18a and 18b) compared to those shown in Figs. 16a and 16b. For example, for a system consisting of 5 users in Rician fading (Ω = -100 dB) there is a 6 dB gain in E_b/N_0 (at BER of 10^{-3}) when 255-chip Kasami sequence is used instead of 31-chip Gold sequence.

Figs. 15 to 18 are useful for system design because they provide answers to important questions on system capacity, for example: how many users can be supported by a spread spectrum system in a flat fading channel without exceeding a desired performance quality criterion?

At a typical BER of 10^{-3} for acceptable voice quality, Table I summarizes the E_b/N_0 requirements (extracted from Figs. 15 to 18) of a simulated spread spectrum system consisting of 5 mobile transmitters in a flat fading channel. From Table I, the following comments are drawn:

i) In Rayleigh fading (at a fading bandwidth of 0.01) a spread spectrum system does not support 5 or more users even with 255-chip Kasami sequence because the error floor attained is 5.5×10^{-3}

ii) In Rician fading (Rice factor equals -100 dB for example), 5 users are supported at the specified performance criterion but requires E_b/N_0 of 13 dB and 7.2 dB with 31-chip Gold sequence and 255-chip Kasami sequence respectively.

iii) To maintain the specified BER of 10^{-3} as more users join the system necessitates an increase in E_b/N_0 requirement, the increase is less for 255-chip Kasami sequence than that for 31-chip Gold sequence. For example, increasing

Table I

E_b/N_o Requirements at a BER of 10^{-3}

a) 31 chips Gold sequence

	Rician Flat Fading, Doppler BW = 0.1, 0.01		Rayleigh Flat Fading	
# of Users	Ω = -100 dB	Ω = -5 dB	Doppler BW = 0.1	Doppler BW = 0.01
1	6.6 dB	17.3 dB	Error floor at $4.4 * 10^{-2}$	31 dB
5	13 dB	Error floor at $8.0 * 10^{-3}$	Error floor at $8.0 * 10^{-2}$	Error floor at $3.8 * 10^{-2}$
10	Error floor at 10^{-2}	Error floor at $2.5 * 10^{-2}$	Error floor at 0.11	error floor at $7.5 * 10^{-2}$

b) 255 chips Kasami sequence

	Rician Flat Fading, Doppler BW = 0.1, 0.01		Rayleigh Flat Fading	
# of Users	Ω = -100 dB	Ω = -5 dB	Doppler BW = 0.1	Doppler BW = 0.01
1	6.6 dB	17.3 dB	Error floor at $4.4 * 10^{-2}$	31 dB
5	7.2 dB	22 dB	Error floor at $5.1 * 10^{-2}$	Error floor at $5.5 * 10^{-3}$
10	7.7 dB	Error floor at $1.4 * 10^{-3}$	Error floor at $5.5 * 10^{-2}$	error floor at $1.2 * 10^{-2}$

the number of users from 1 to 5 in a Rician fading channel (Ω equals -100 dB) requires an increase in E_b/N_0 of 6.4 dB if 31-chip Gold sequence is used compared to only 0.6 dB increase for 255-chip Kasami sequence.

iv) For a Rician fading channel, increase in the severity of fading implies more E_b/N_0 requirement: increasing Ω from -100 dB to -5 dB requires an additional E_b/N_0 of 10.7 dB and 14.8 dB for 1 user and 5 users respectively with a 255-chip Kasami sequence.

v) Error floor increases with increasing number of users, decreases with decreasing fading bandwidth for a Rayleigh fading channel and increases with increasing Rice factor for a Rician fading channel.

4.2.4) Effect of Combined Multipath and Multi-user Interference

In a multiple access system where each user's transmitted signal arrives at the receiver input via several paths, there is an underlying multipath interference in the interference caused by each other transmitter in the system. The BER performance of a multiple-user spread spectrum system in frequency selective fading channels is shown in Figures 19 to 24. In these figures, the desired mobile's transmitted signal (as well as the transmitted signal of each interferer) reaches the receiver input via 5 paths. As stated before, the average power of each path is set to unity except where otherwise stated.

For a system consisting of 5 users (31-chip Gold code) in a Rayleigh frequency selective fading channel, it is seen from Fig. 19a that the BER performance is bad, in fact the BER assuming a differential single path receiver saturates at 0.15 which is not acceptable for a practical communication system. To improve the BER performance, the combined multi-user and multipath interference is compensated by combining the signal replicas of the desired user available at the receiver input. It is assumed that the simulated n-tap (n = 10 or 20) RAKE receiver has perfect knowledge of path delays and gains (referred to as known channel). The simulation results (Fig. 19a) show that a multipath combining receiver exhibits an improvement in BER performance over that of a single-path receiver structure: error floors of 5.4×10^{-2} and 1.7×10^{-2} are attained with 10-tap and 20-tap RAKE receiver structure respectively, which are very much lower than the corresponding value of 0.15 for the single path receiver. If each transmitted

Fig. 19a Combined Effects of Multipath and Multiuser Interference on Rayleigh Frequency Selective Fading Channel

(5 users, 31 chips Gold Code, DPSK, 5 paths, Avg. Path Power = 0 dB, norm. Doppler BW = 0.01, Rake Receiver, Known Channel)

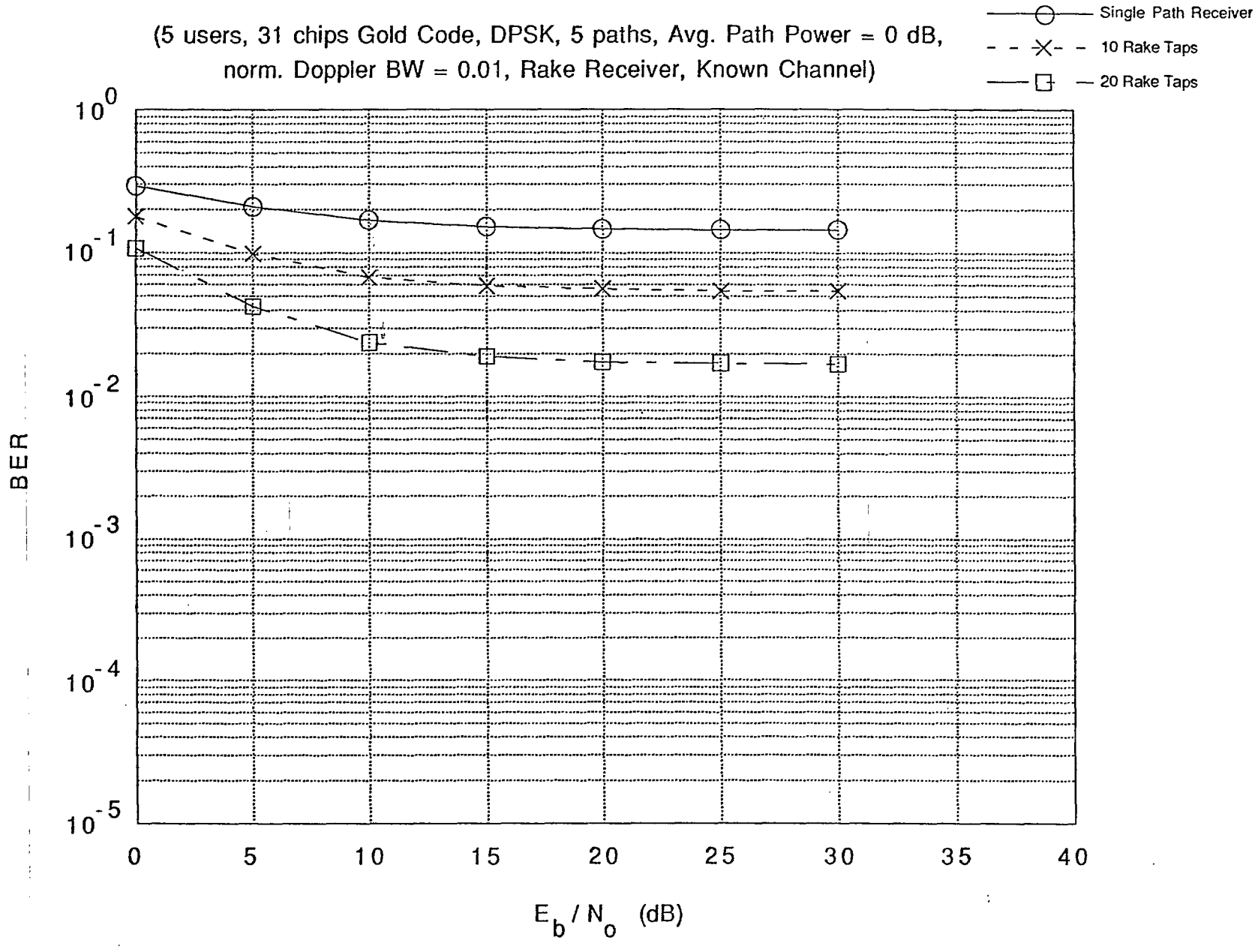

Fig. 19b Combined Effects of Multipath and Multiuser Interference on Rayleigh Frequency Selective Fading Channel

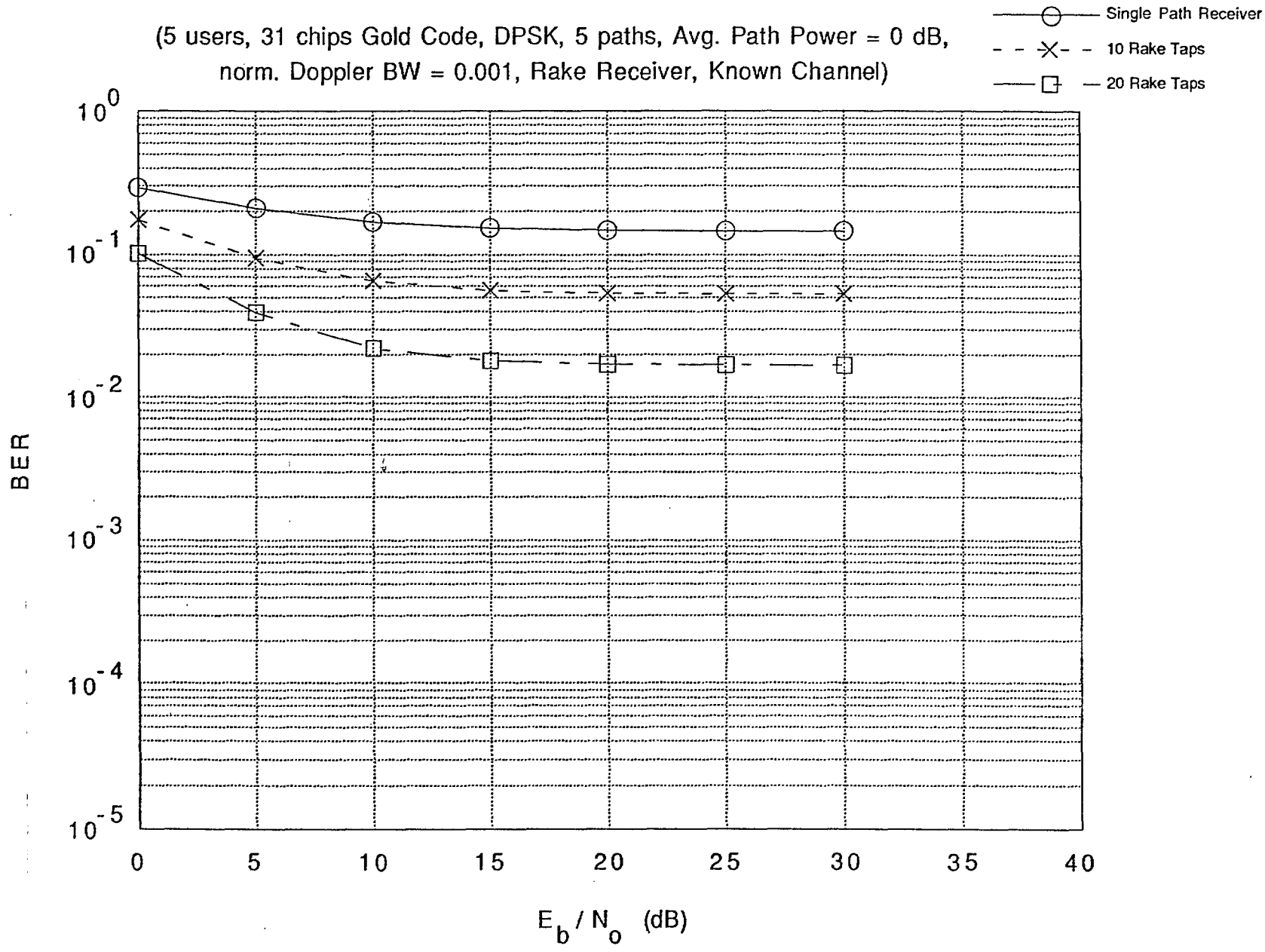

Fig. 20a Effects of Multipath and Multiuser Interference on Rician Frequency Selective Fading Channel

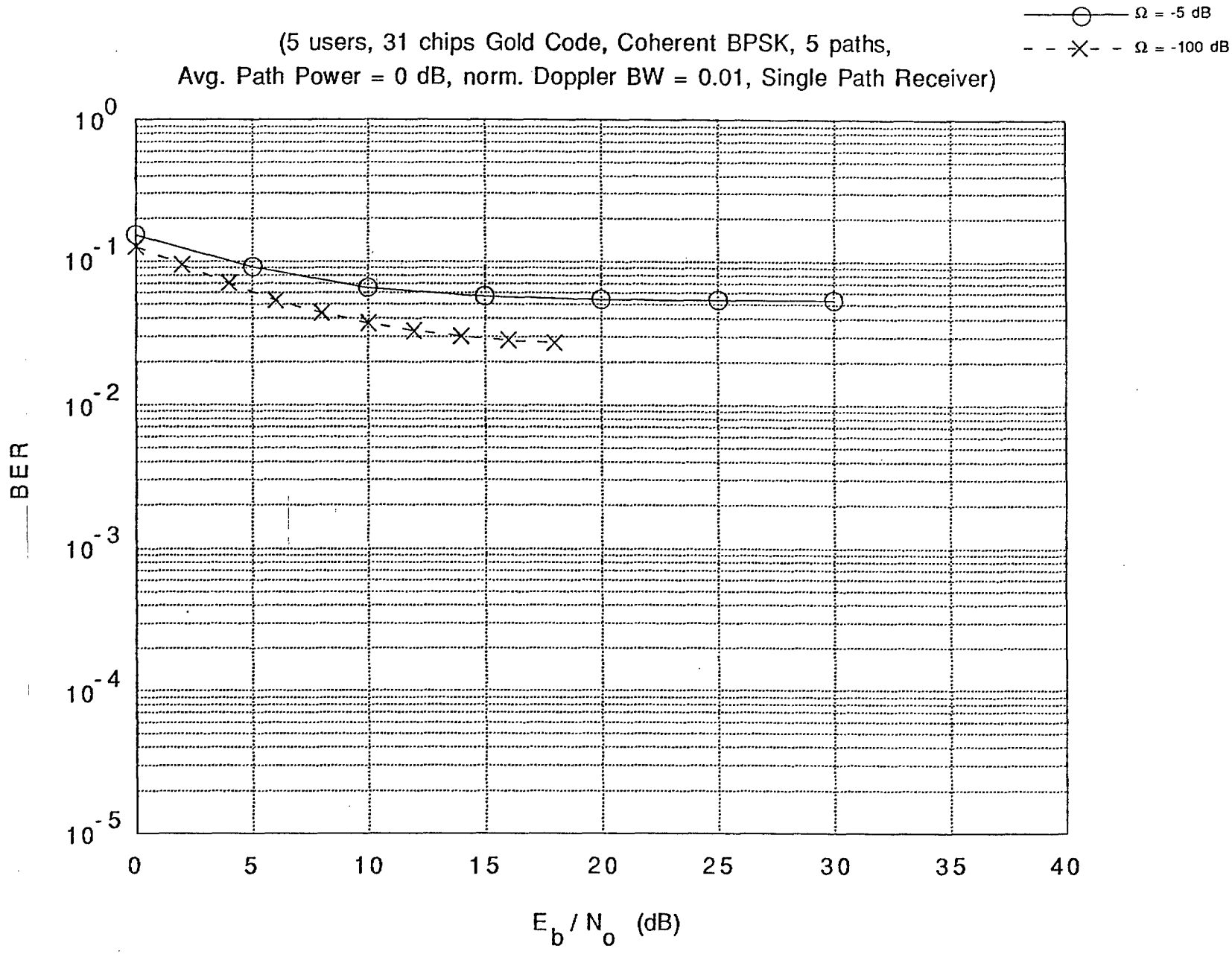

Fig. 20b Effects of Multipath and Multiuser Interference on Rician Frequency Selective Fading Channel

(31 chips Gold Code, Coherent BPSK, 5 paths, Avg. Path Power = 0 dB, Ω = -100 dB, norm. Doppler BW = 0.01, Single Path Receiver)

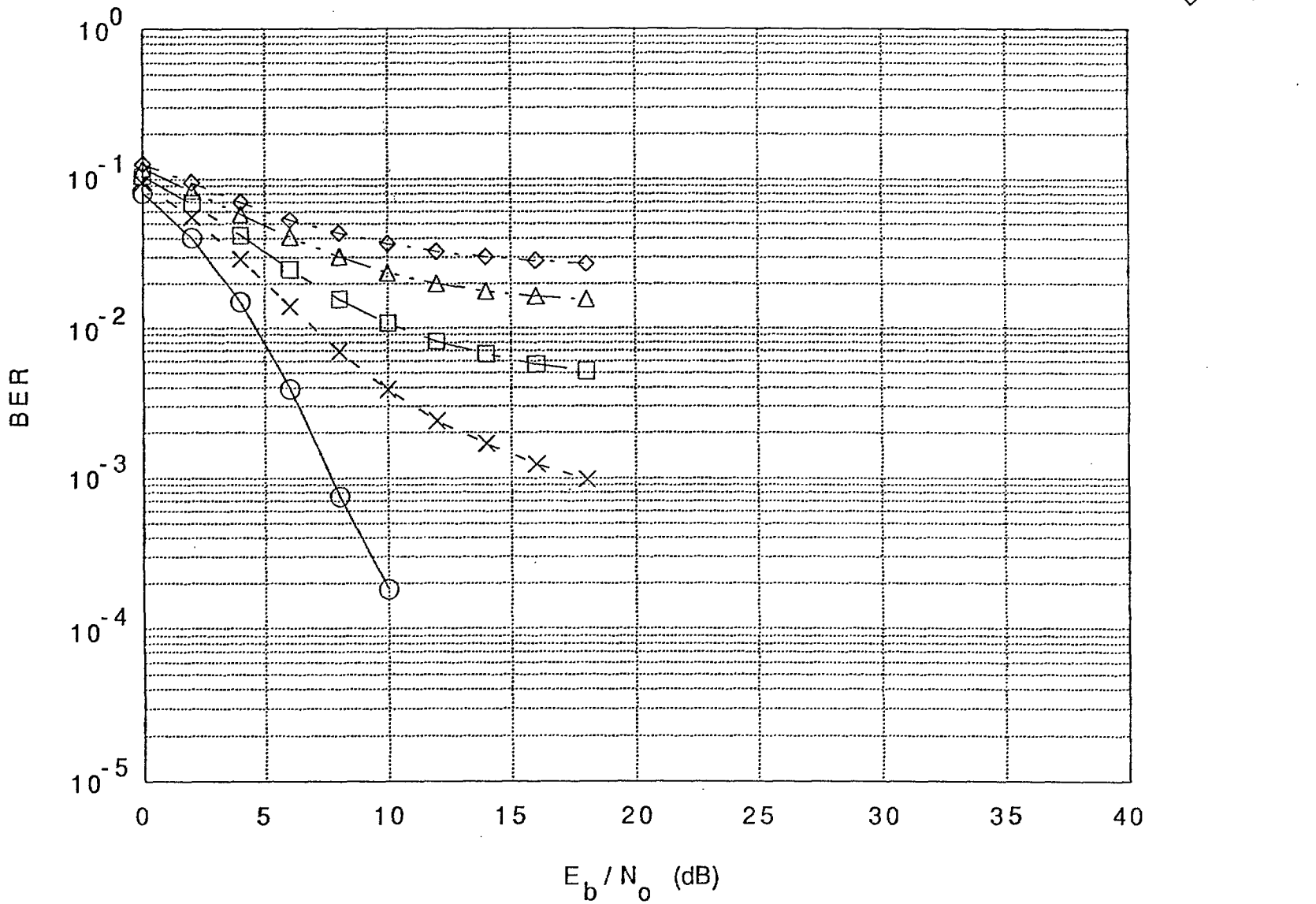

symbol is spread by 255-chip Kasami code (instead of 31-chip Gold code), the impact of the multipath and multi-user interference is also reduced which then leads to BER performance improvement. The preceding statement is confirmed by the results shown in Fig. 21a where for differential single path receiver, an error floor of 2.5×10^{-2} is obtained (compared to 0.15 from Fig. 19a for 31-chip Gold code). Also from Fig. 21a, the 10-tap and 20-tap differential RAKE receiver structures give error floors of 2.1×10^{-2} and 1.7×10^{-2} respectively, which are not too different from 2.5×10^{-2} - the error floor for differential single path receiver. An explanation for the small difference is the same as that given for a similar characteristic seen in Fig. 13. Notice also that it is not fair to directly compare, on the basis of number of RAKE taps, the results in Fig. 19 with those of Fig. 21 for the same reasons stated before.

A system consisting of 5 users (31-chip Gold code) in a Rician frequency selective fading channel with coherent single path receiver also exhibits bad BER performance (Fig. 20a) even when the average power of the fading components in the Rician fading path is almost zero, that is Ω = -100 dB. In the absence of fading, it is seen from Fig. 20a and Fig. 12b that the BER performance of the 5-user system becomes much worse than that of the single-user system. An explanation for the worse performance is given as follows. First note that the results in Fig. 20a are obtained under the assumption that one out of the 5 paths between each interfering transmitter and the receiver undergoes Rician fading while the rest are Rayleigh fading paths; a similar assumption is also made for the desired user. As such, the four Rician fading paths from the interfering transmitters contribute significant interference (especially at Ω = -100 dB) and this explains the worse performance in Fig. 20a. Fig. 20b shows how performance degrades as the number of interferers is increased by one at a time. It is expected that the degradation will of course be less if there is no Rician fading path among the 5 paths between each interfering transmitter and the receiver but only the desired user has one of its five paths being Rician faded while the remaining four are Rayleigh faded. By comparing Fig. 20a with Fig. 22, notice the improvement in BER performance for the 255-chip Kasami sequence over that of 31-chip sequence which is expected. It is interesting to observe from Figs. 19a and 20a that a 5-user system (31-chip Gold sequence) exhibits better performance in a Rayleigh frequency selective fading channel with 20-tap differential RAKE receiver than in a Rician frequency selective fading (Ω = -100 dB) with coherent

Fig. 21a Combined Effects of Multipath and Multiuser Interference on Rayleigh Frequency Selective Fading Channel

(5 users, 255 chips Kasami Code, DPSK, 5 paths, Avg. Path Power = 0 dB, norm. Doppler BW = 0.01, Rake Receiver, Known Channel)

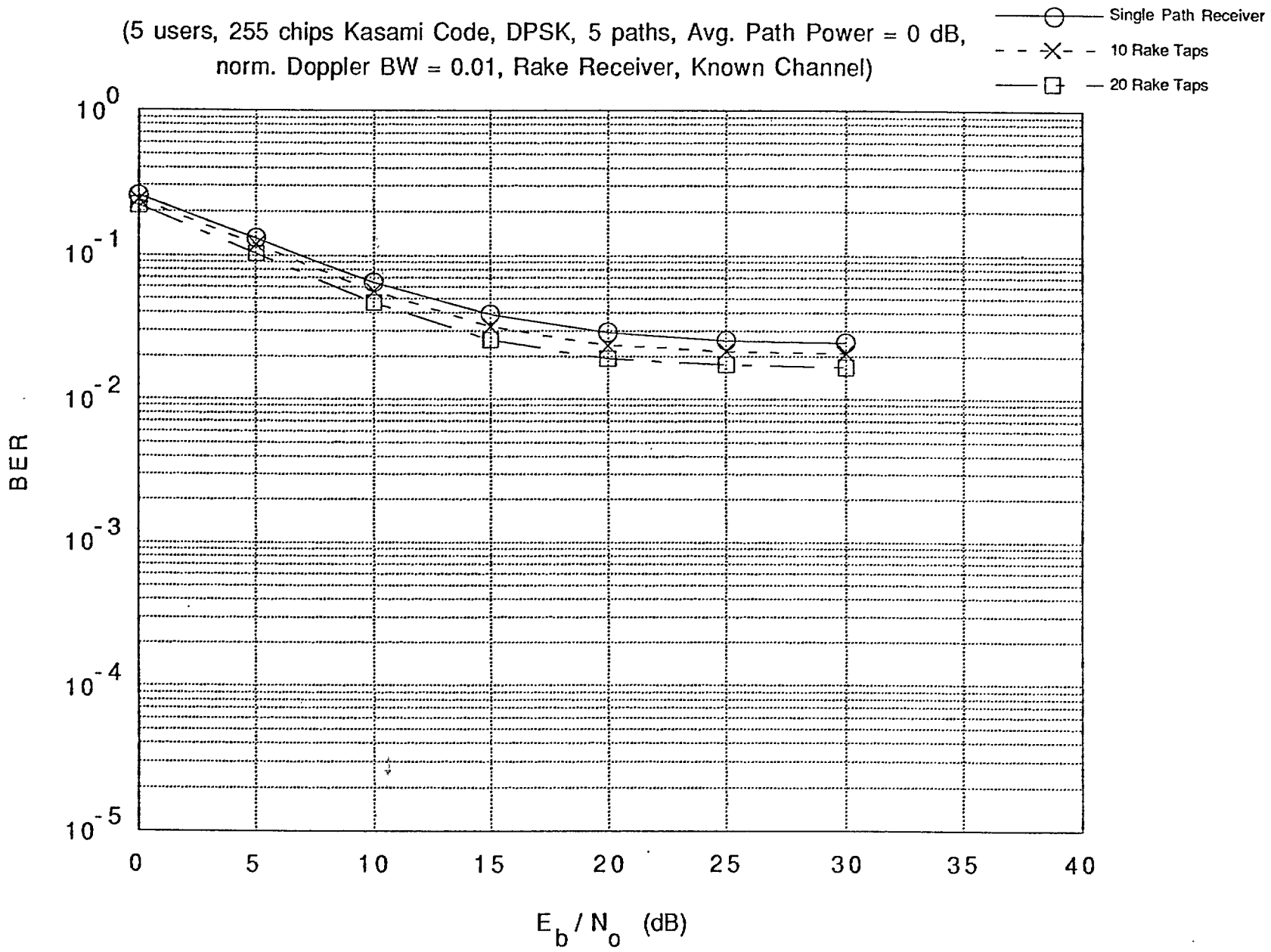

Fig. 21b Combined Effects of Multipath and Multiuser Interference on Rayleigh Frequency Selective Fading Channel

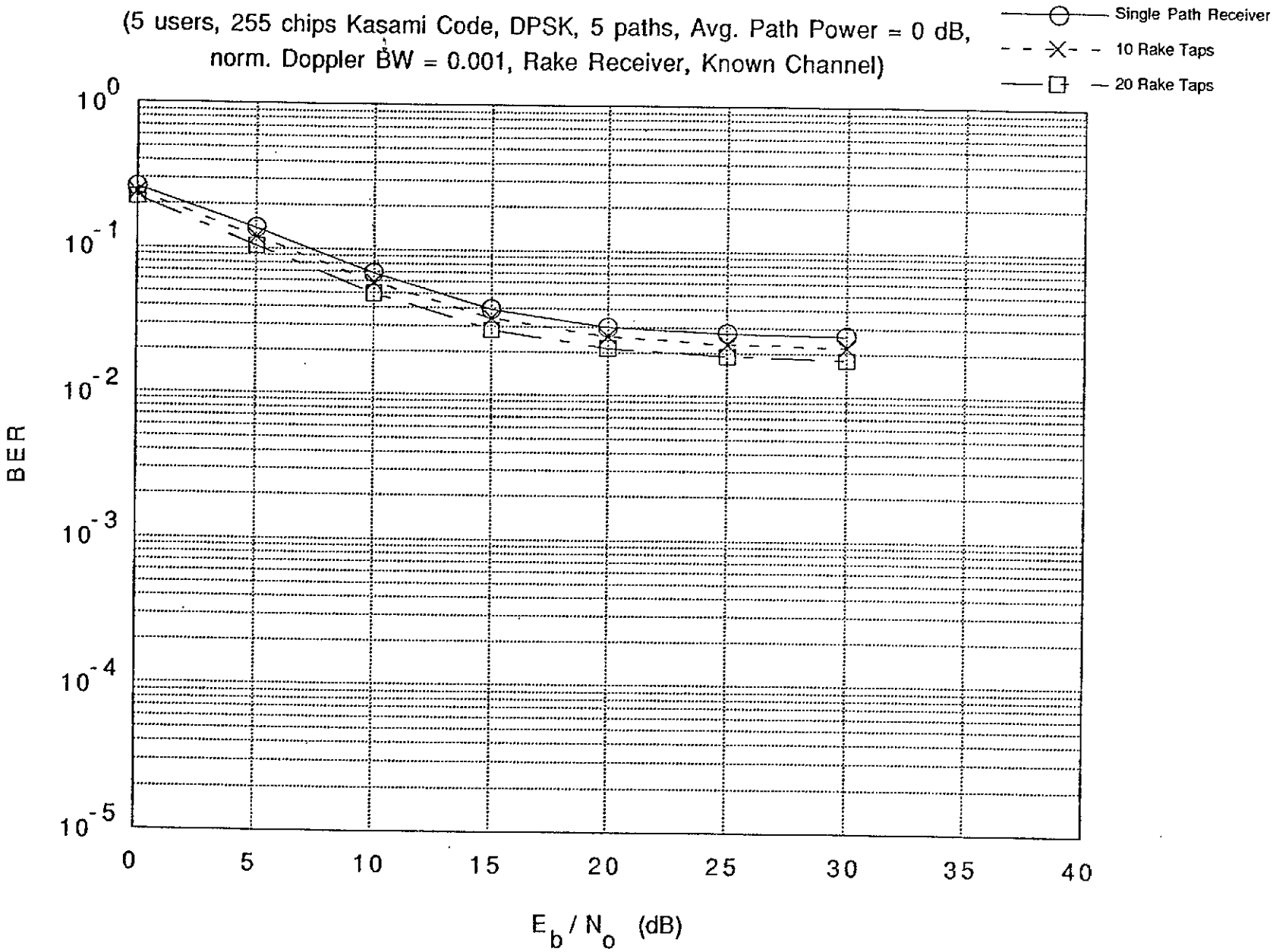

Fig. 22 Combined Effects of Multipath and Multiuser Interference on Rician Frequency Selective Fading Channel

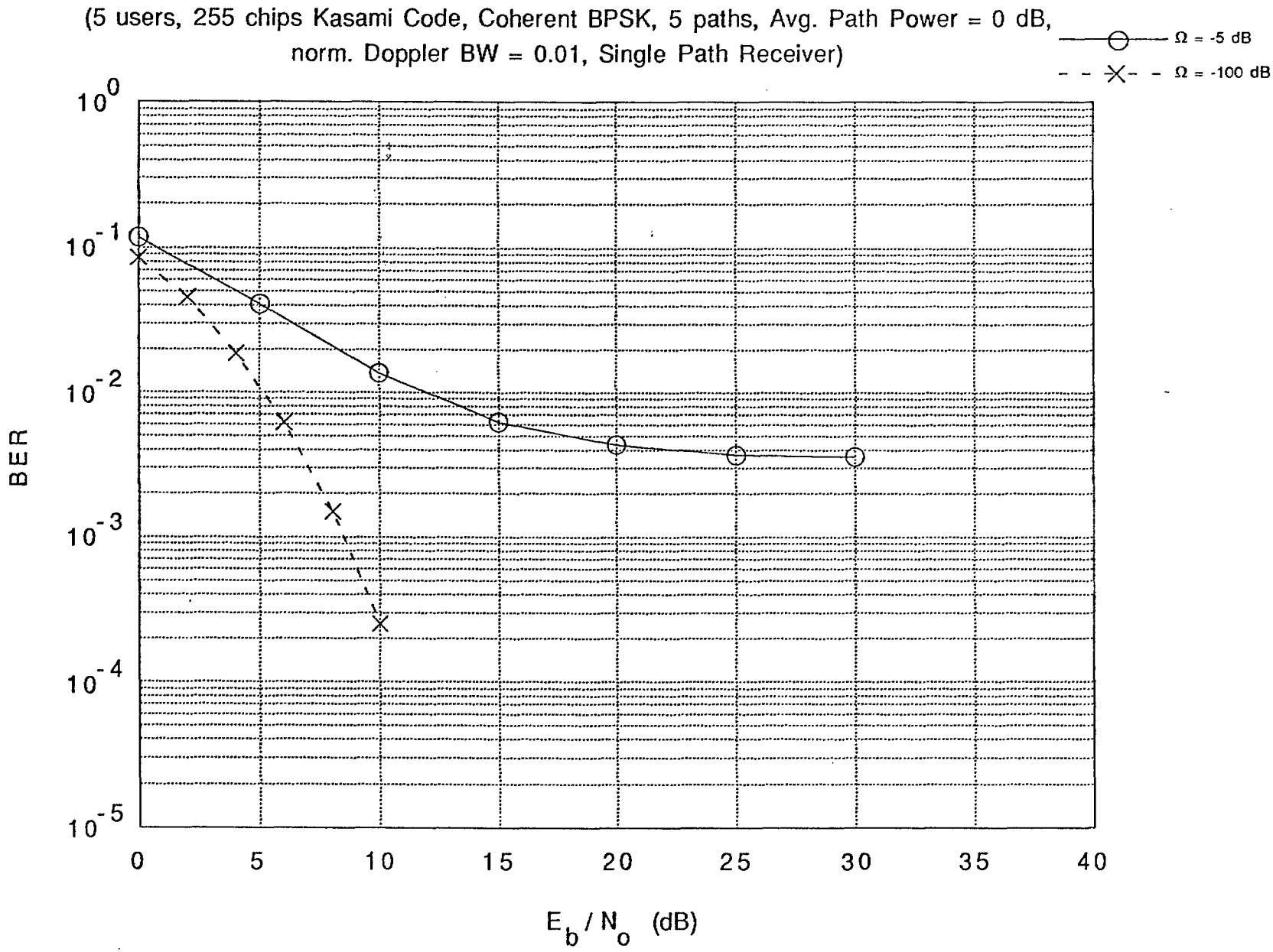

single path receiver. Such an observation is not apparent between Figs. 21a and 22 (255-chip sequence) because of the very small RAKE window corresponding to the 20 taps.

Figures 23 and 24 depict the BER performance of a spread spectrum system in a Rayleigh frequency selective fading channel using differential RAKE receiver with 3 taps. Unlike previous simulation experiments, the five paths over which signals of different transmitters reach the receiver input now have unequal average powers. Specifically, the average power of the paths are now set to 0 dB, -2 dB, -4 dB, -6 dB and -8 dB in the order of increasing path delay - that is, the average power of a path arriving with the shortest delay is set to 0 dB while the longest delay path has a power of -8 dB. The 3 taps in the differential RAKE receiver are dynamically tuned to the paths whose delays (assumed to be known exactly by the receiver) fall within the RAKE window. Furthermore, the tap weight at a position corresponding to each estimated path delay (within the RAKE window) is set to unity. Depending on the (estimated) path delays, it is possible for all the three taps to be activated in which case three out of the five paths have delays within the RAKE window or in the worst case scenario, only one of the five paths has its delay within the RAKE window, resulting in only one tap being activated. From Fig. 23 (31-chip Gold sequence) and Fig. 24 (255-chip Kasami sequence), it is observed that the BER performance becomes worse as the number of simultaneous users increases. Notice that the range over which thermal noise dominates the total interference decreases with increasing number of users - as evident from the large jump in error floor from 1 to 5 users compared to a lesser jump from 5 to 10 users. As expected, the BER performance of a system using 255-chip Kasami sequence (Fig. 24) is better than that of a system that uses 31-chip Gold sequence (Fig. 23). Clearly, unequal average powers of the signal replicas from the other users (other than the desired user) results in reduced interference to the desired user's signal at the receiver. With respect to the desired transmitter, unequal average path power at the receiver input also implies a reduction in the effectiveness of spread spectrum diversity. How do the results in Figs. 23 and 24 compare with the corresponding previous results that assume equal average path powers? Using 31-chip Gold sequence, it is seen from Figs. 23a and 11b that the BER performance of a single-user system in a Rayleigh frequency selective fading channel with unequal average path power and a RAKE receiver with 3 taps (Fig. 23a) is worse than with equal average path power and a

Fig. 23a Combined Effects of Multipath and Multiuser Interference on Rayleigh Frequency Selective Fading Channel

(31 chips Gold Code, DPSK, 5 paths, Avg. Path Power = 0, -2, -4, -6, -8 dB, norm. Doppler BW = 0.01, Rake Receiver with 3 Taps, Equal Gain Combining)

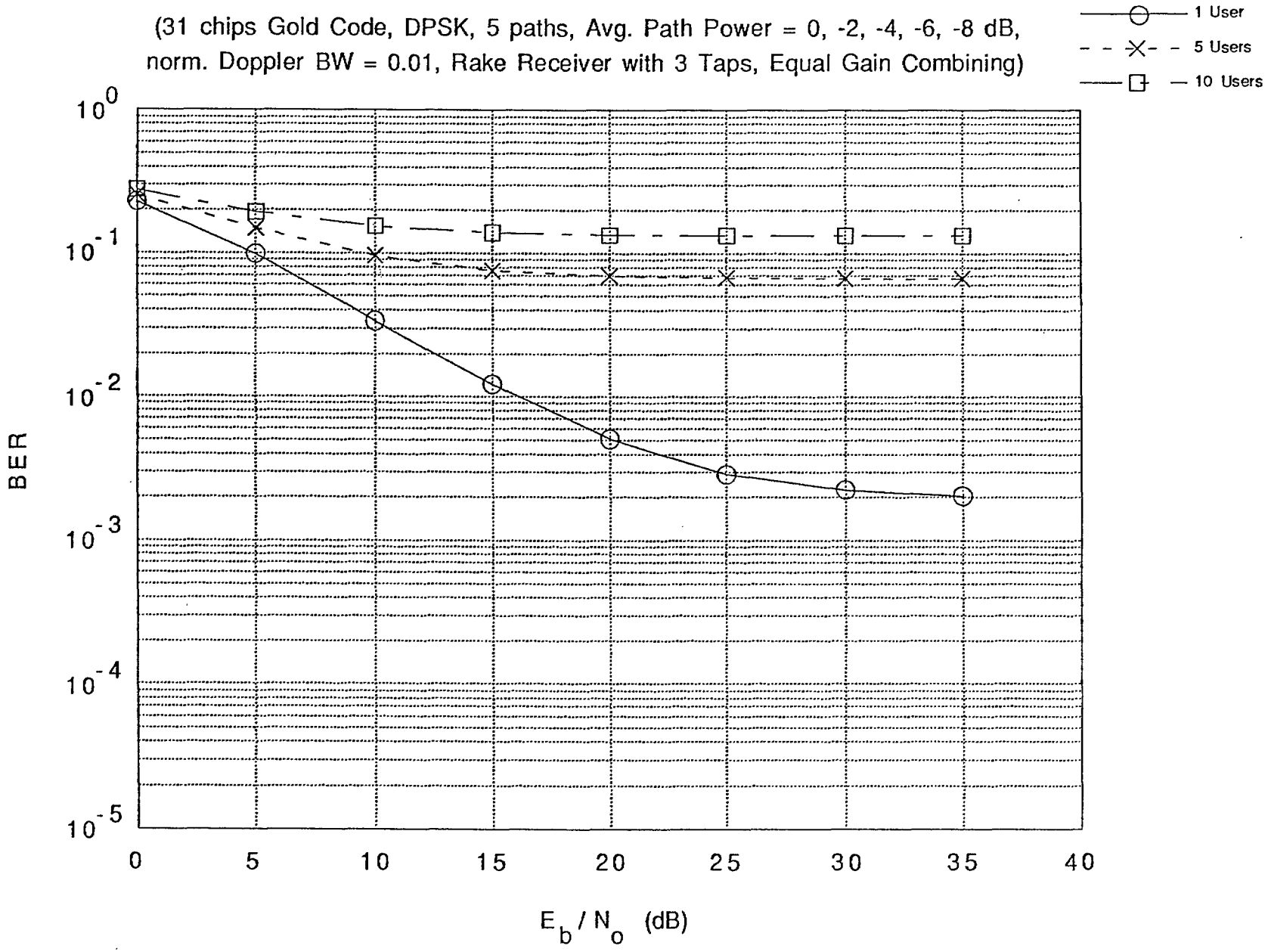

Fig. 23b Combined Effects of Multipath and Multiuser Interference on Rayleigh Frequency Selective Fading Channel

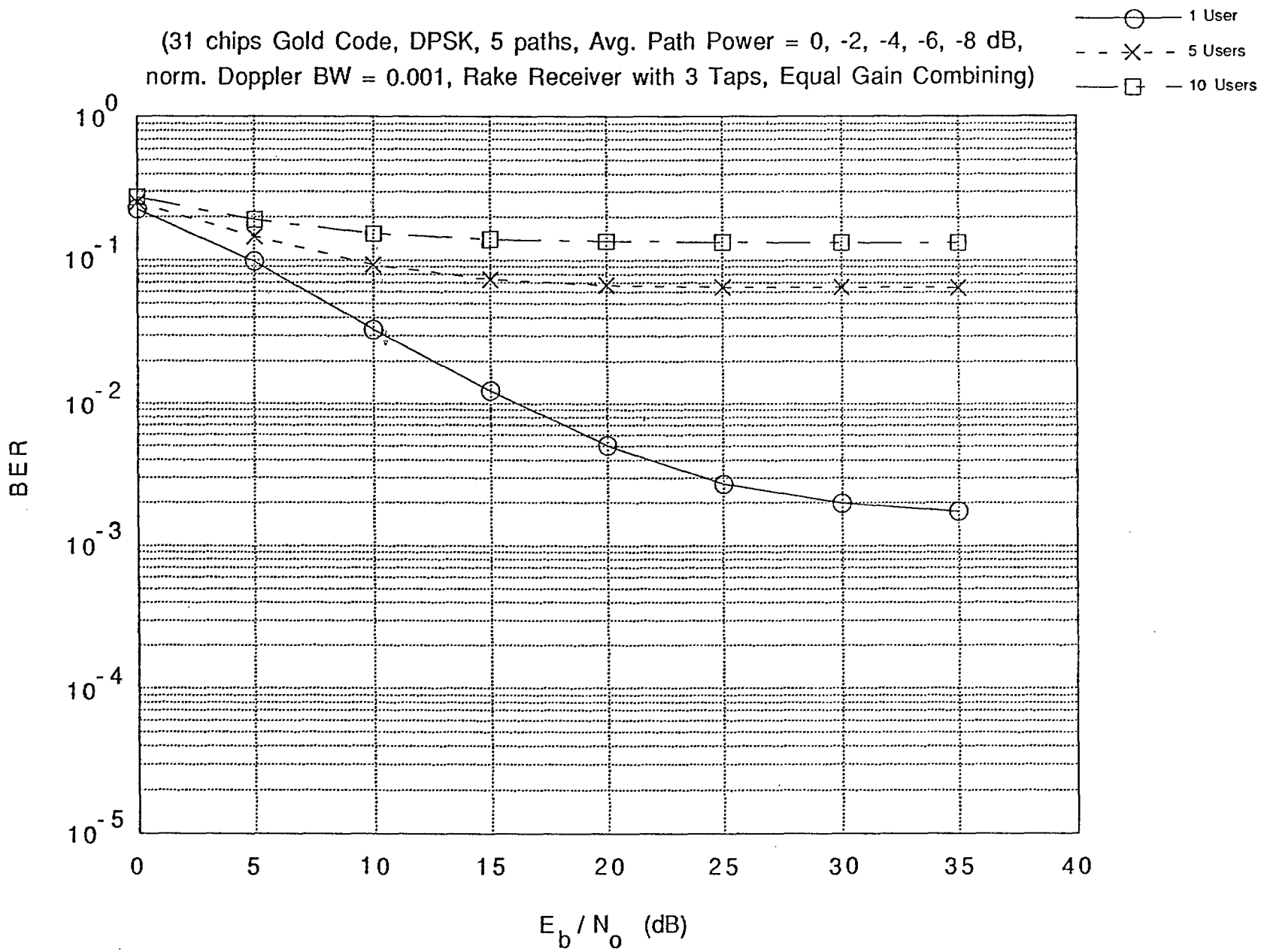

Fig. 24a Combined Effects of Multipath and Multiuser Interference on Rayleigh Frequency Selective Fading Channel

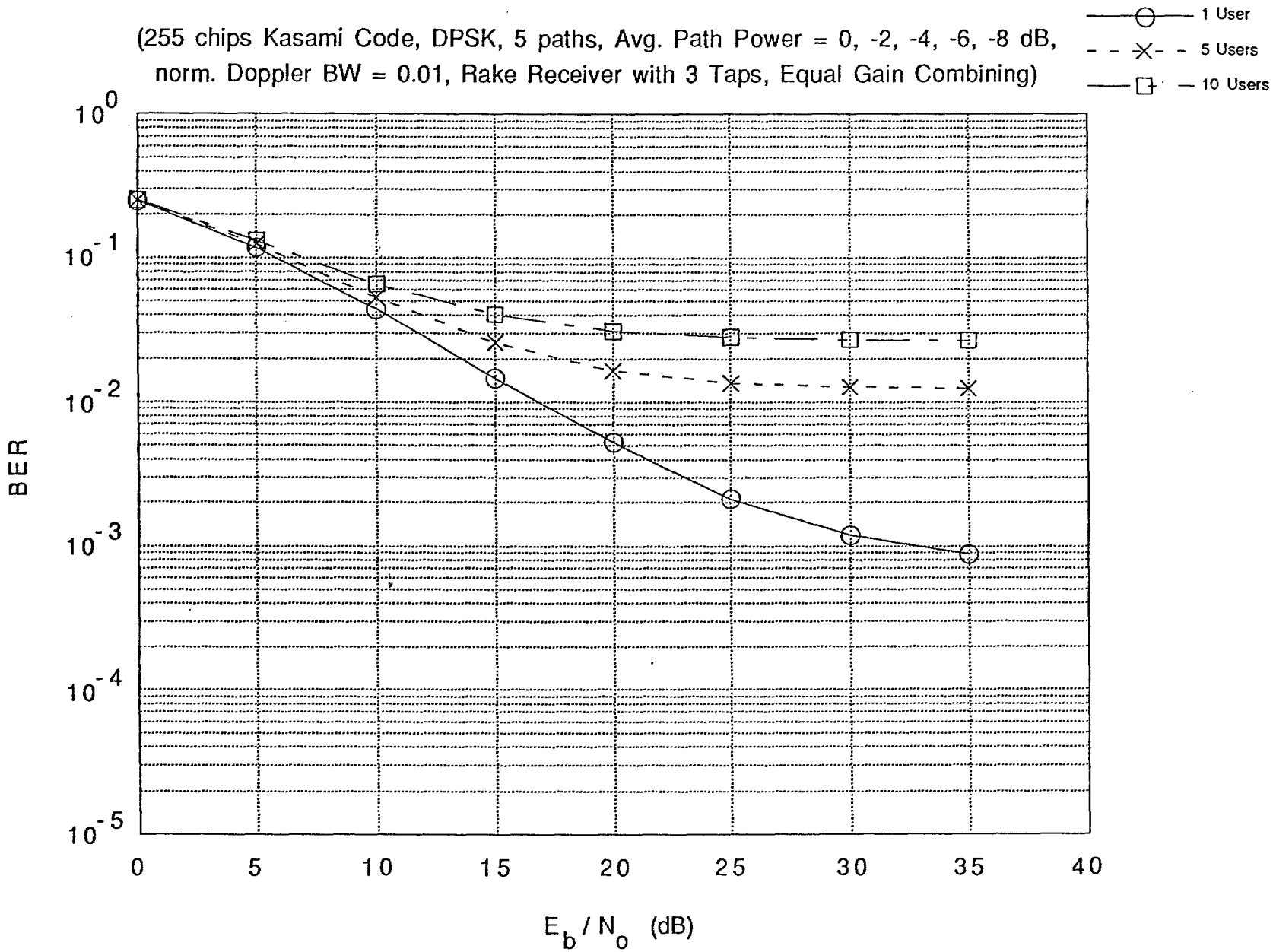

Fig. 24b Combined Effects of Multipath and Multiuser Interference on Rayleigh Frequency Selective Fading Channel

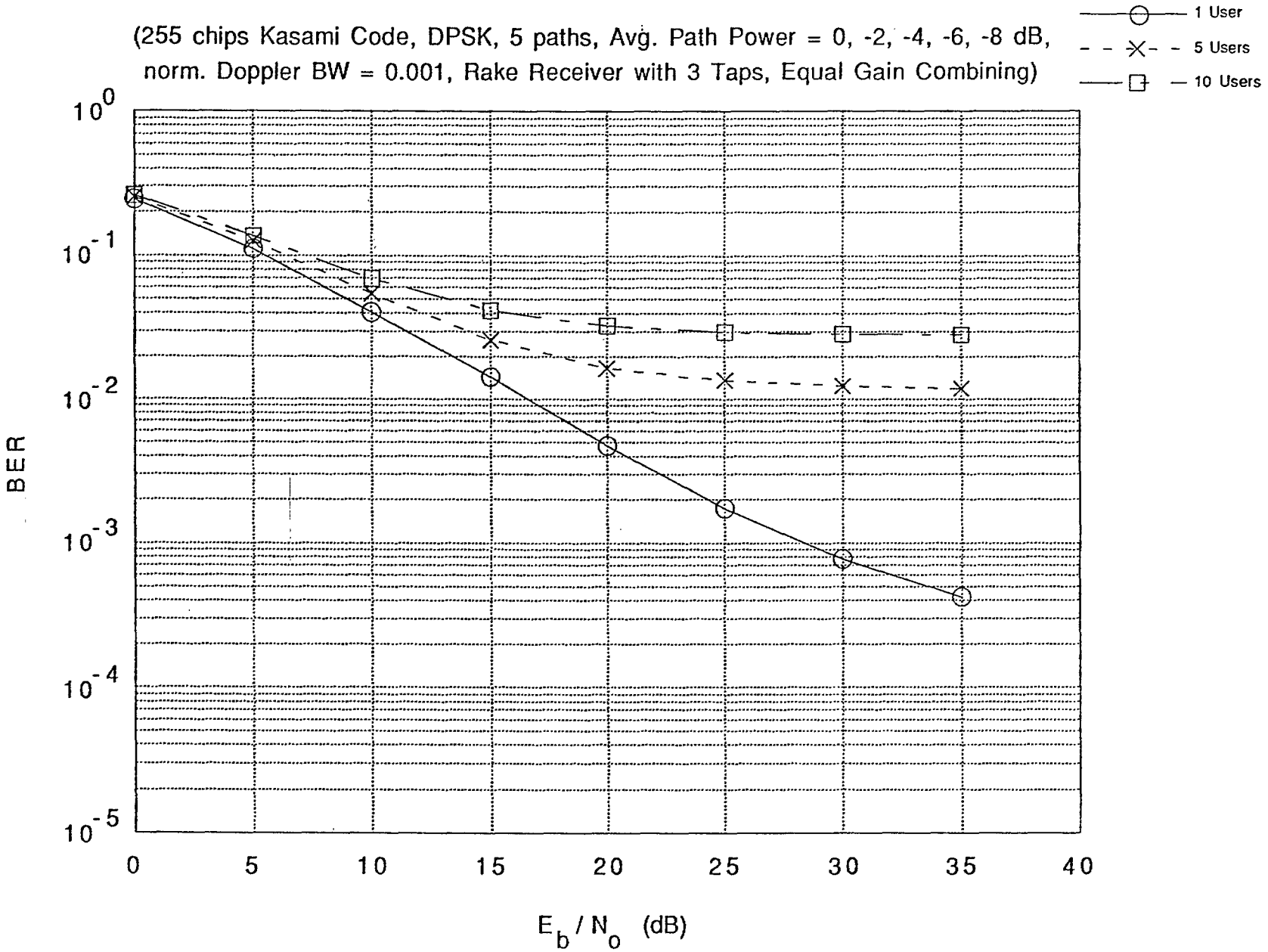

RAKE receiver with 10 taps (Fig. 11b). Similar observation also holds for the comparison between Figs. 23a and 19a where in Fig. 19a a known channel is assumed. For the 31-chip Gold sequence, the multipath interference (single user) and the combined multipath and multi-user interference is large enough so that the impact of unequal average path powers is not apparent. If 255-chip Kasami sequence is used instead, the advantage of unequal path power should begin to show. This is confirmed by comparing Fig. 24a with Fig. 13a where it is seen that the BER performance of a single user system in Rayleigh frequency selective fading with unequal average path power and a 3-tap RAKE receiver is slightly better than with equal average path power and a 10-tap RAKE receiver and is almost identical with that obtained for a 20-tap RAKE receiver. A similar observation is also made from a comparison of Fig. 21a with Fig. 24a.

In a system which takes into account the effects of multipath and multi-user interference, of interest to system designers is the number of users that can transmit simultaneously such that the communications quality of the desired user is not degraded below an acceptable level. At a typical value of 10^{-3} BER for acceptable voice quality, it is seen from Figs. 19 and 21 that a spread spectrum system in a Rayleigh frequency selective fading channel does not support 5 users because the best error floor attained is 1.7×10^{-2}. It is also obvious from Fig. 20a that a system in a Rician frequency selective fading channel (31-chip Gold sequence) does not support 5 users at Rice factors of -5 dB and -100 dB due to error floors of 5.3×10^{-2} and 2.7×10^{-2} respectively. From Fig. 20b however, 2 users are supported over a Rician frequency selective channel (Ω = -100 dB) at an E_b/N_0 requirement of 18 dB to achieve a BER of 10^{-3}. When 255-chip Kasami sequence is used instead (Fig. 22), the system does not support 5 users due to the error floor at 3.6×10^{-3} if Ω = -5 dB. If the Rice factor is then reduced to -100 dB, a system consisting of 5 users requires an E_b/N_0 of 8.5 dB to achieve a 10^{-3} BER; this requirement is respectively 1.3 dB and 1.8 dB more than the E_b/N_0 requirements in Fig. 18b (5 users in Rician flat fading channel, Ω = -100 dB and fading bandwidth equals 0.01) and Fig. 14 (1 user in Rician frequency selective fading channel, Ω = -100 dB and fading bandwidth of 0.01).

4.3 Symbol Statistics

The simulation package developed has been used to generate the statistics of symbol amplitude and phase. The symbol amplitude is calculated from $|\mathrm{Re}[\tilde{Z}(T)] + j\mathrm{Im}[\tilde{Z}(T)]|$ while the phase is computed using $\arctan(\mathrm{Im}[\tilde{Z}(T)]/\mathrm{Re}[\tilde{Z}(T)])$, where $\mathrm{Re}[\tilde{Z}(T)]$ and $\mathrm{Im}[\tilde{Z}(T)]$ are as defined for each receiver structure discussed in Section 2.5.3. Symbol amplitude and phase statistics of interest are the cumulative distribution function, probability density function and correlation (assuming the amplitude and phase processes are stationary). The procedure used in the statistical analysis is described as follows. At a specified BER, the corresponding E_b/N_0 is extracted from Figs. 11 to 24 which then serves as an input to the simulation and each simulation run is terminated after 50000 symbols have been transmitted. Sequences of detected symbol amplitudes and phases are formed and these sequences are then used for subsequent symbol statistical analysis. Representative results for the statistics of symbol amplitude and phase are presented in Figs. 25 to 31.

For a single user system in a Rayleigh flat fading channel (fading bandwidth set to 0.01) with differential single path receiver, Figs. 25 and 26 depict the symbol statistics corresponding to bit error rates of 0.1 and 0.01 respectively. At BERs of 0.1 and 0.01, the corresponding E_b/N_0's (extracted from Fig. 11a) are found to be 6 dB and 17.5 dB respectively. By comparing Figs. 25 and 26, it is seen that the probability density function (PDF) for symbol amplitude becomes slightly narrower and more peaked about zero amplitude at a BER of 0.01 than at 0.1. Also, the PDF for the symbol phase becomes narrower and more peaked about zero and π at BER of 0.01 than at 0.1. As such, the probability of symbol error is minimized at a BER of 0.01 than at 0.1. Finally, it is seen that the symbol amplitudes exhibit more correlation at BER of 0.01 (because of a reduction in AWGN at higher E_b/N_0) than at 0.1. However, there is no symbol phase correlation at BERs of 0.1 and 0.01, the lack of phase correlation is due partly to the independence between the phases of transmitted data symbols - which follows from the sign (+/-) of the transmitted symbols.

The symbol statistics of a 5-user CDMA system in a Rayleigh frequency selective fading channel with differential 10-tap RAKE receiver are shown in Figs. 27 and 28 assuming 31-chip Gold sequence and 255-chip Kasami sequence respectively.

Fig. 25a Symbol Amplitude Probability Density Function and Cumulative Distribution Function

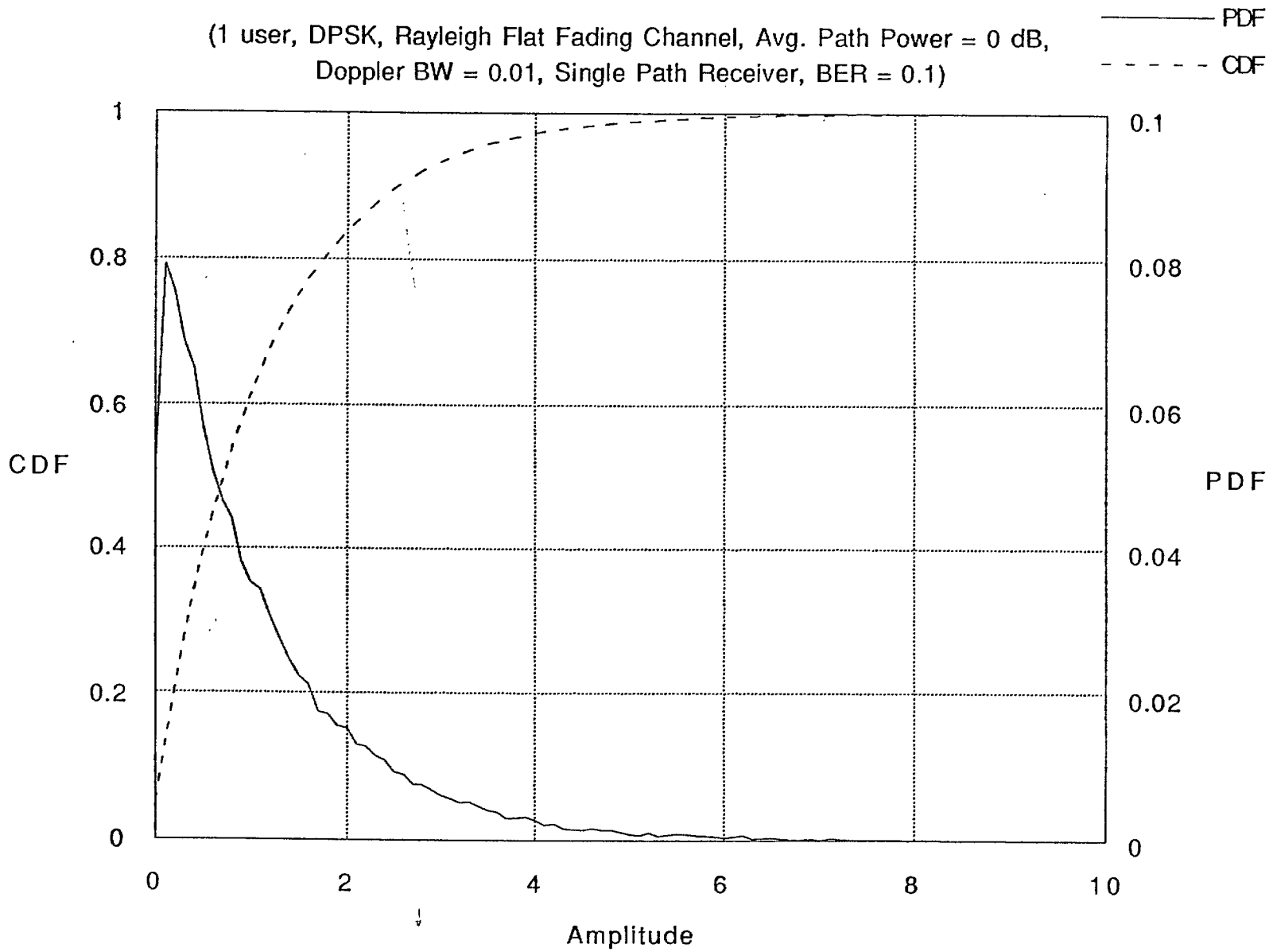

Fig. 25b Symbol Phase Probability Density Function and Cumulative Distribution Function

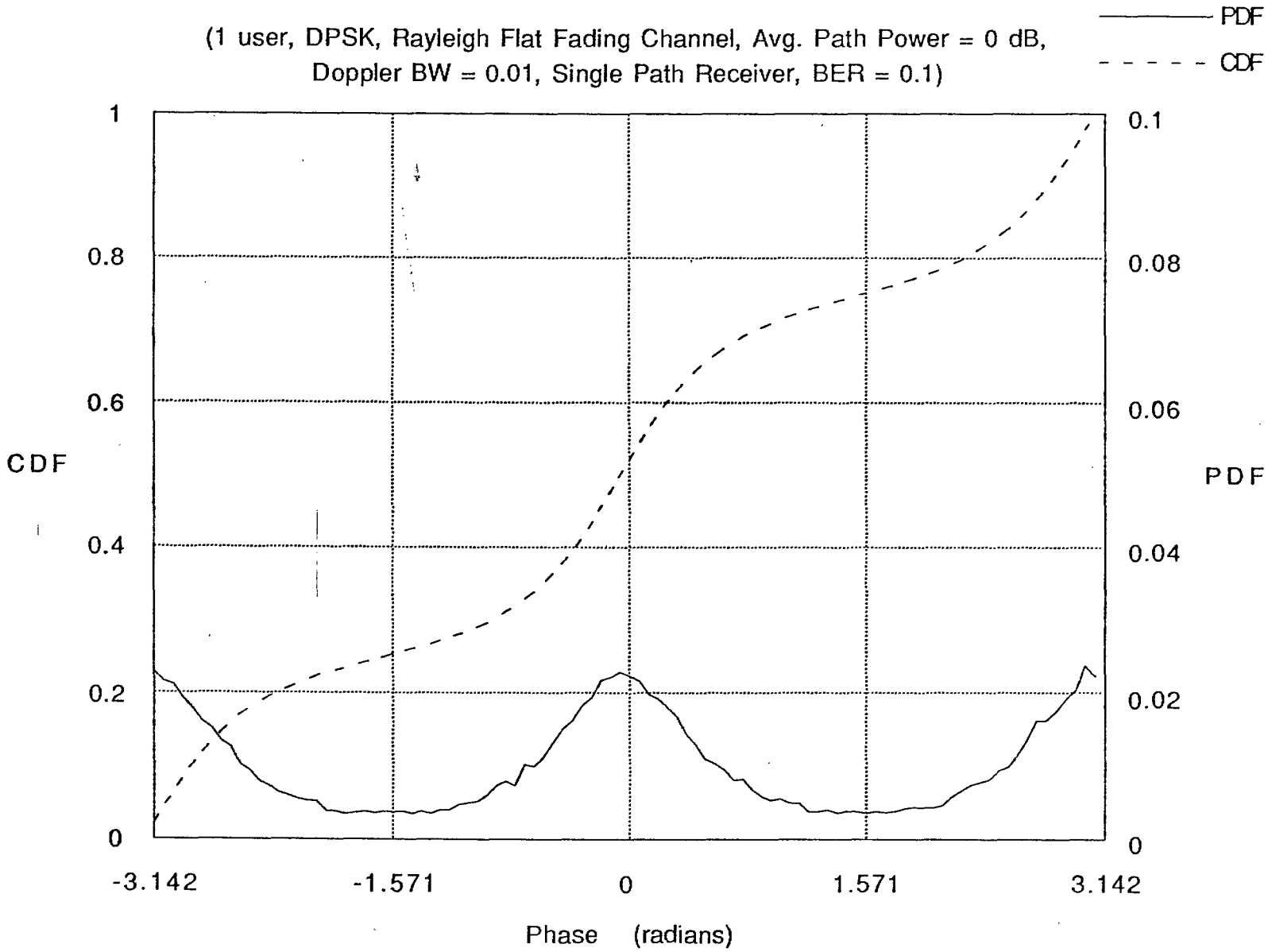

Fig. 25c Symbol Amplitude and Phase Correlation

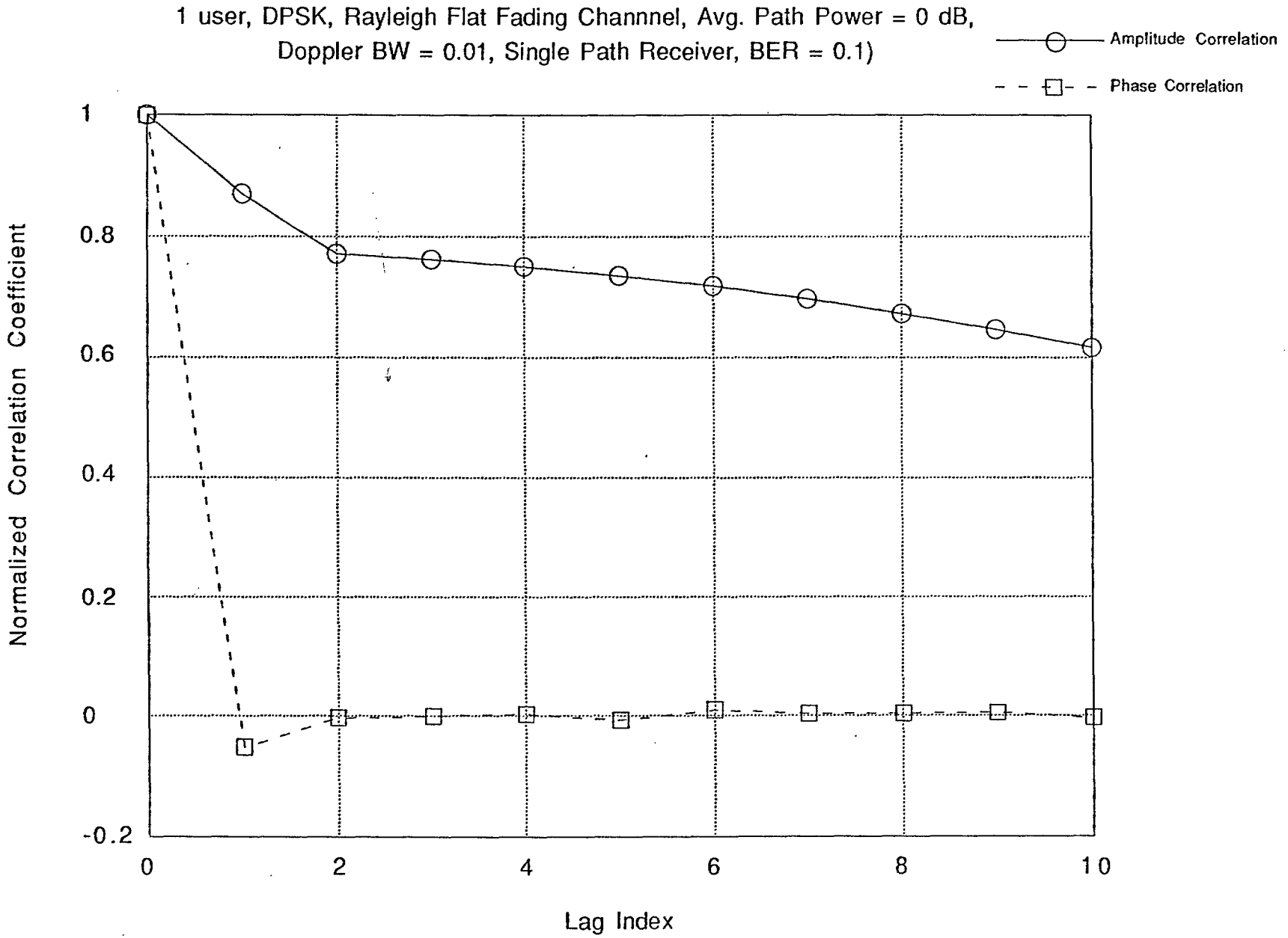

Fig. 26a Symbol Amplitude Probability Density Function and Cumulative Distribution Function

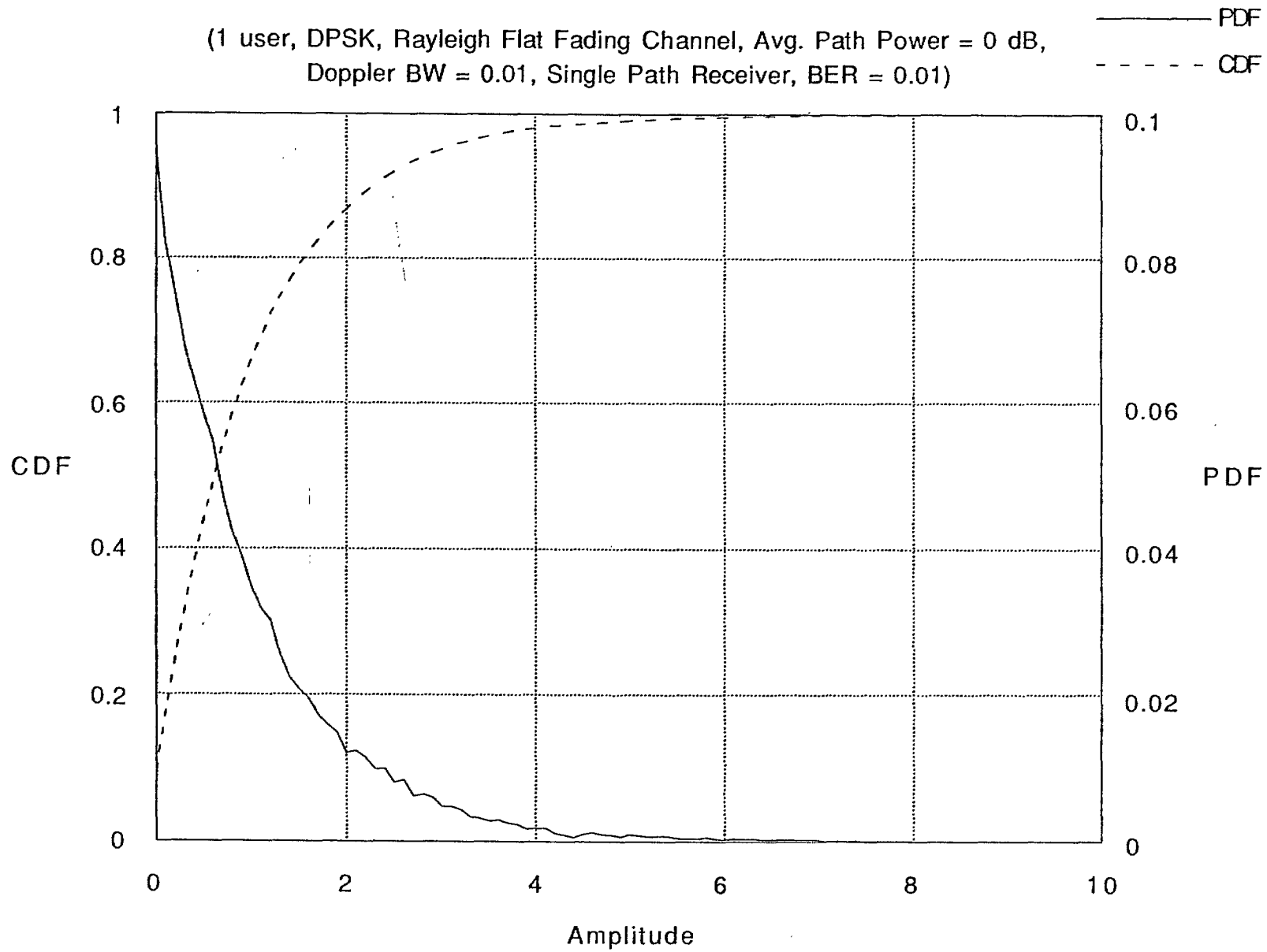

Fig. 26b Symbol Phase Probability Density Function and Cumulative Distribution Function

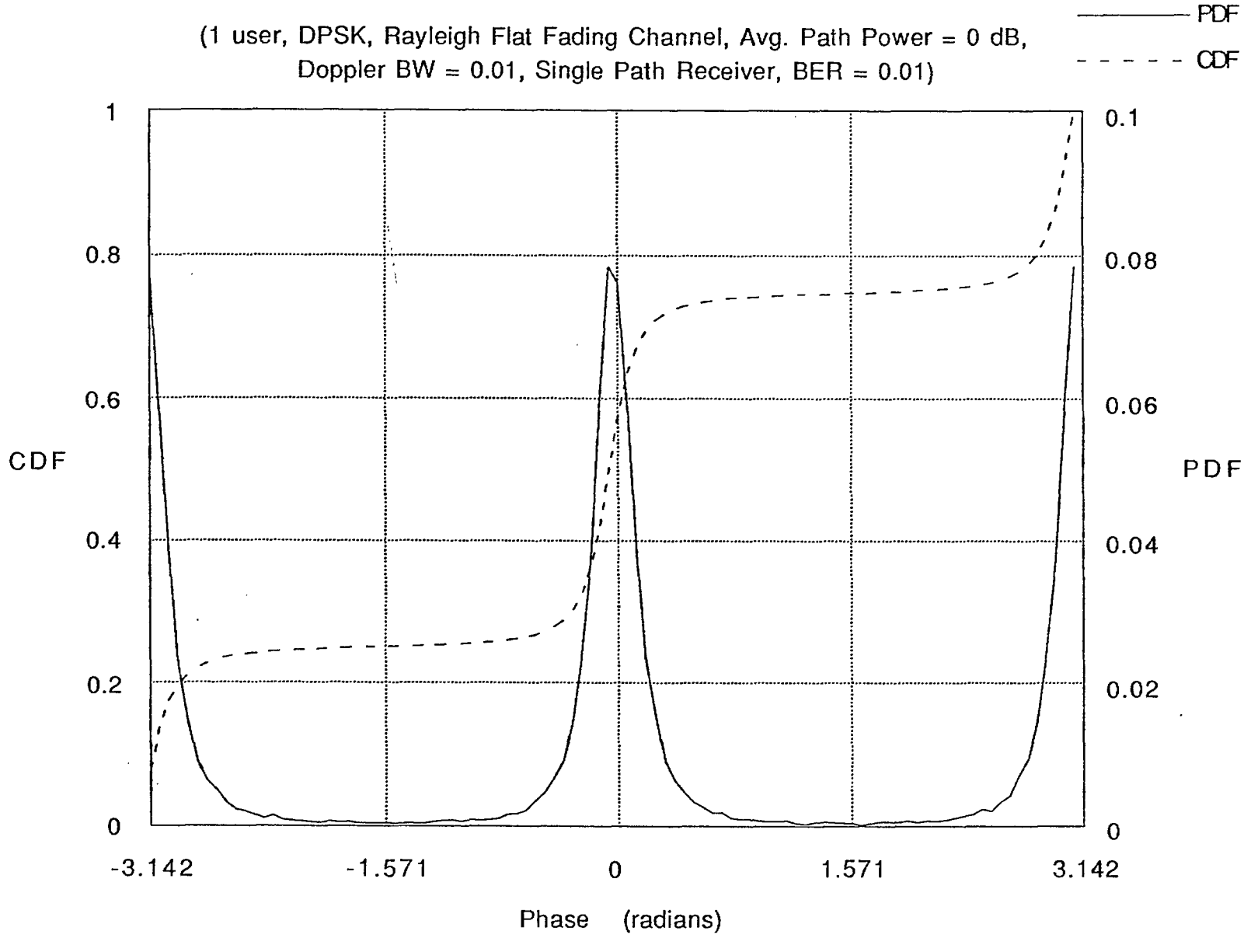

Fig. 26c Symbol Amplitude and Phase Correlation

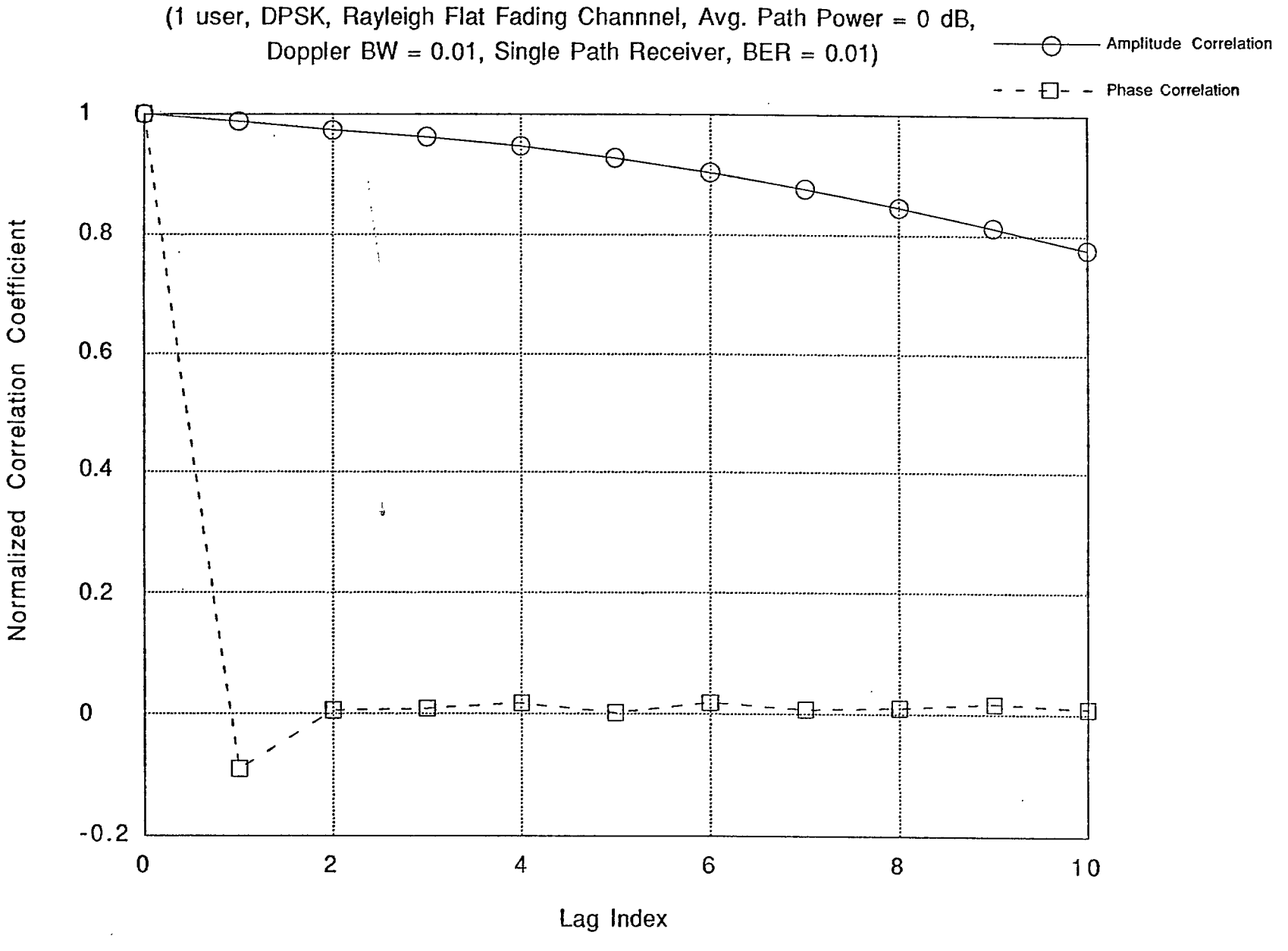

Figs. 27 and 28 assume a BER of 0.1 which translates to an E_b/N_0 of 5 dB (Fig. 19a) and 6 dB (Fig. 21a). The following observations are made. First, the symbol amplitude PDF now spreads over a wider range (because the overall decision variable is a vector sum of the weighted differential detector outputs for those paths whose delays fall within the RAKE window) than those seen in Fig. 25a. Notice that in Fig. 28a, the symbol amplitude PDF becomes narrower and more peaked (this implies higher probability of making correct decisions) for the 255-chip Kasami sequence than it is for the 31-chip Gold sequence. However, the symbol phase distribution, as well as the symbol amplitude and phase correlation are identical for both 31-chip Gold sequence and 255-chip Kasami sequence. The symbol amplitude correlation for the 10-tap differential RAKE receiver is less, and the symbol amplitude decorrelates at a much faster rate, compared to that for differential single path receiver (Fig. 25a). The less symbol amplitude correlation observed for the 5-user CDMA system in a Rayleigh frequency selective channel with 10-tap RAKE receiver is due to the added multi-user and multipath interference as well as the nature of the overall RAKE receiver decision variable, which as stated above, is determined by the paths whose delays fall within the RAKE window. For the single-user system in a Rayleigh flat fading channel with differential single path receiver, there is neither multi-user nor multipath interference effect and the decision variable is always determined by the characteristics of one path. As such, the symbol amplitude correlation for the single user system in a Rayleigh flat fading with differential single path receiver is higher than that for the 5-user system in a Rayleigh frequency selective channel with 10-tap differential RAKE receiver. It is also seen that the phase samples are uncorrelated.

For a single user system in a Rician flat fading channel (fading bandwidth set at 0.01 and Ω = -100 dB) with coherent single path receiver, Fig. 29 shows the symbol statistics at a BER of 0.01 (i.e. E_b/N_0 of 4 dB in Fig. 12a). It is seen that the symbol amplitude PDF (Fig. 29a) is centered about an amplitude of unity, and the cumulative distribution function (CDF) shows that the amplitude attains a value equal to or greater than 2 with an almost negligible probability. Observe from Fig. 29b that most of the symbol phases are distributed about 0 and π and Fig. 29c shows that neither the symbol amplitude nor phase is correlated. For the system scenario under consideration, the transmitted signal undergoes an almost zero fading and the decision variable is a sum of the transmitted signal (recall that two

Fig. 27a Symbol Amplitude Probability Density Function and Cumulative Distribution Function

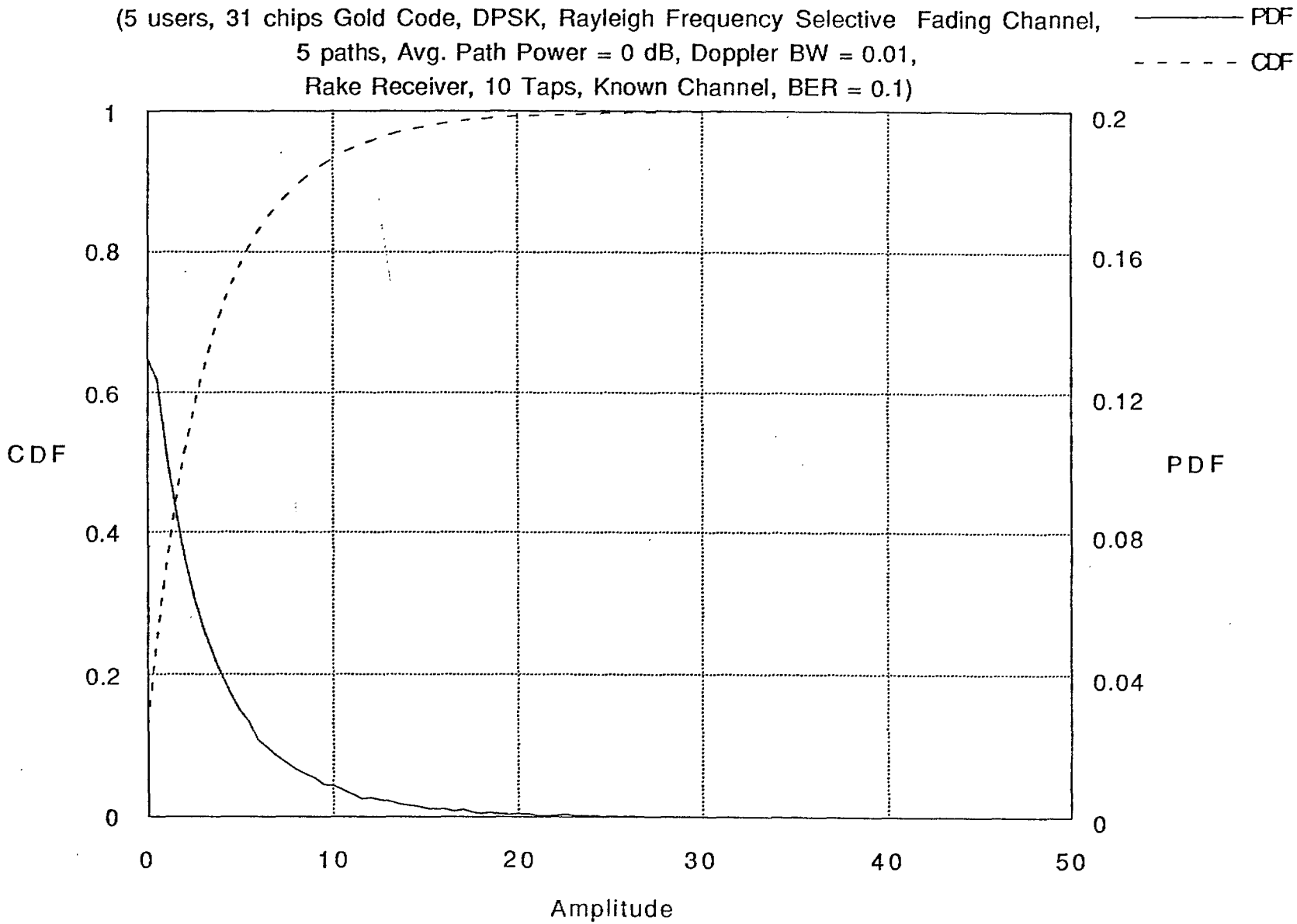

Fig. 27b Symbol Phase Probability Density Function and Cumulative Distribution Function

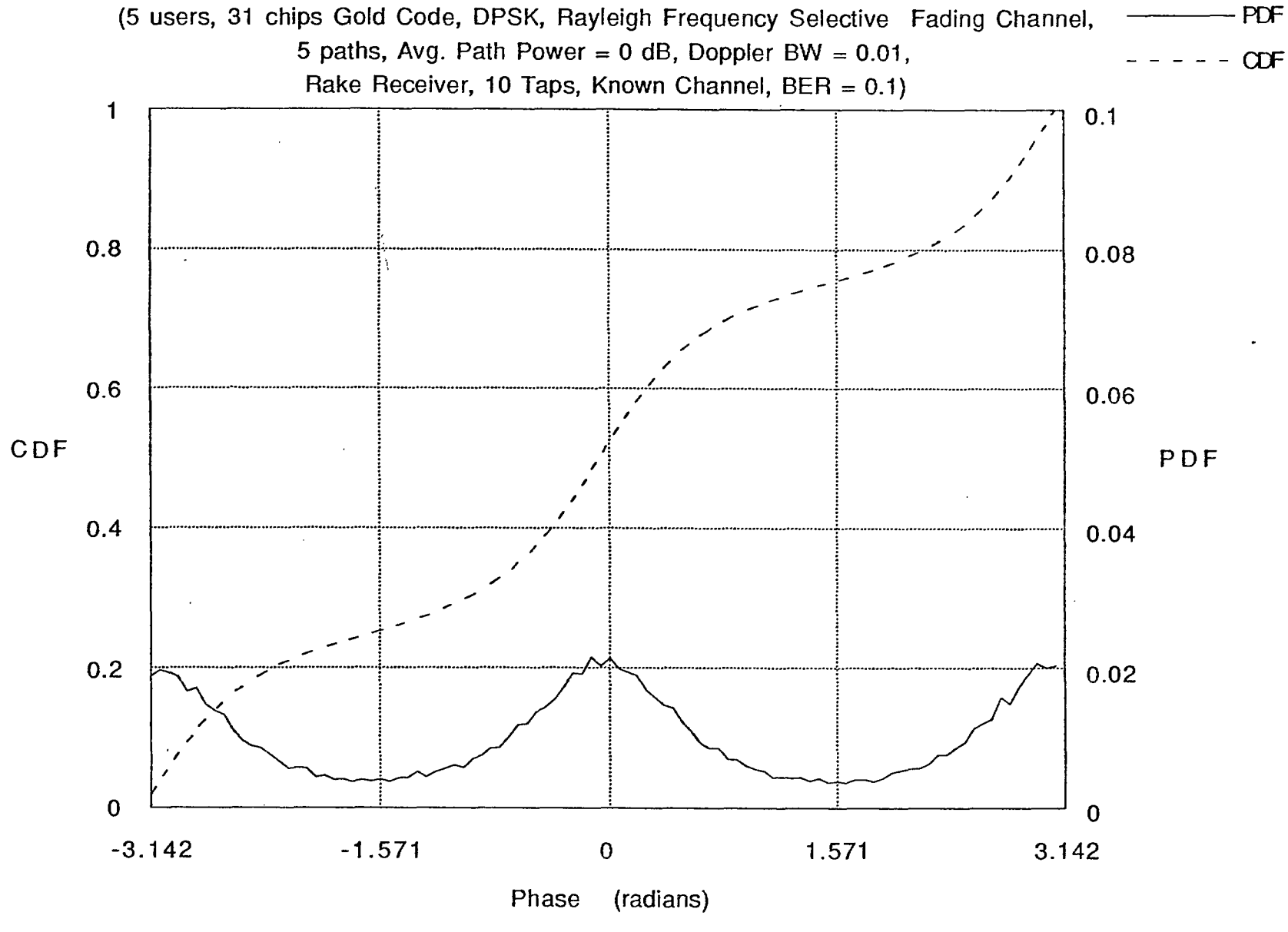

Fig. 27c Symbol Amplitude and Phase Correlation

(5 users, 31 chips Gold Code, DPSK, Rayleigh Frequency Selective Fading Channel,
5 paths, Avg. Path Power = 0 dB, Doppler BW = 0.01,
Rake Receiver, 10 Taps, Known Channel, BER = 0.1)

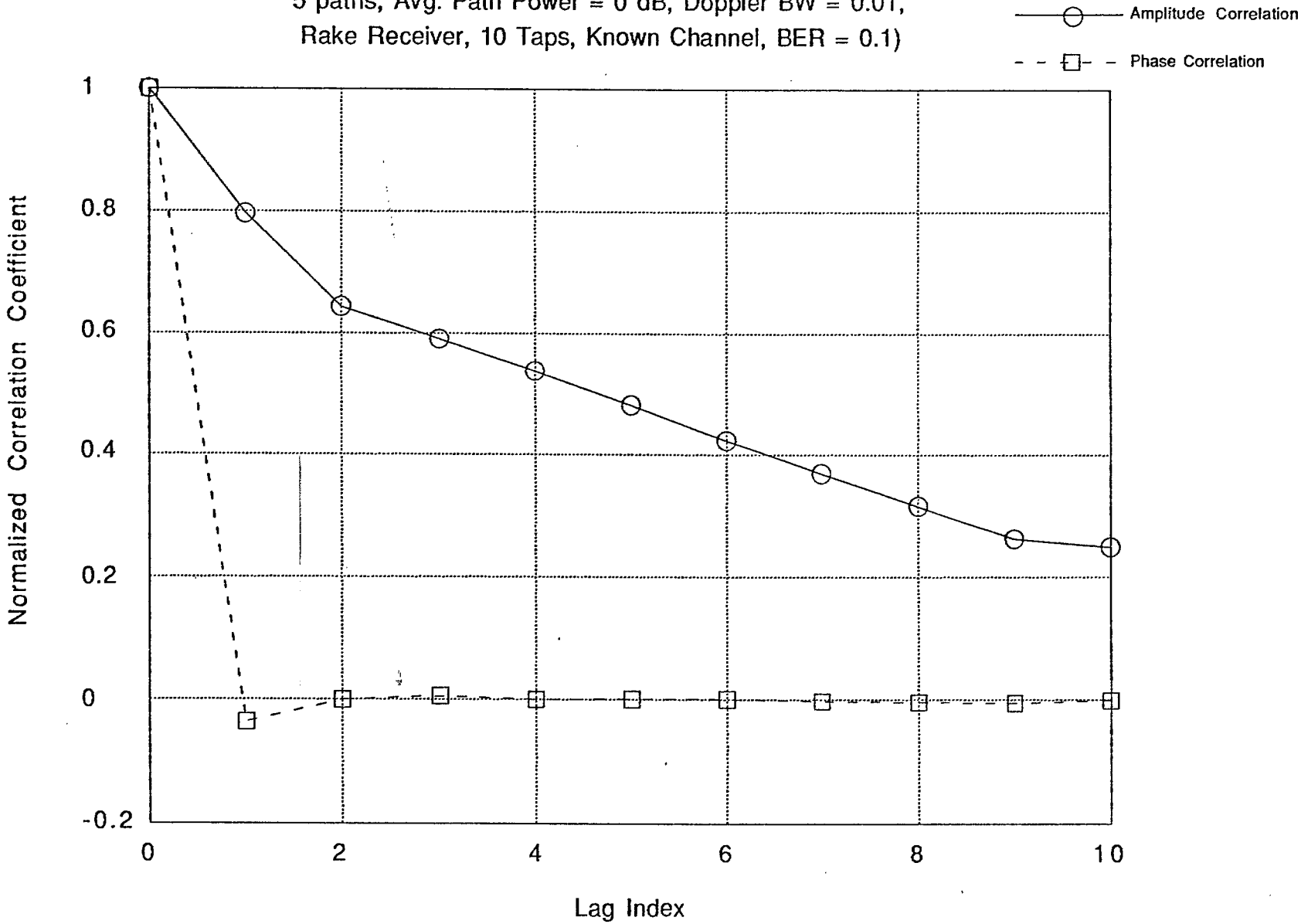

Fig. 28a Symbol Amplitude Probability Density Function and Cumulative Distribution Function

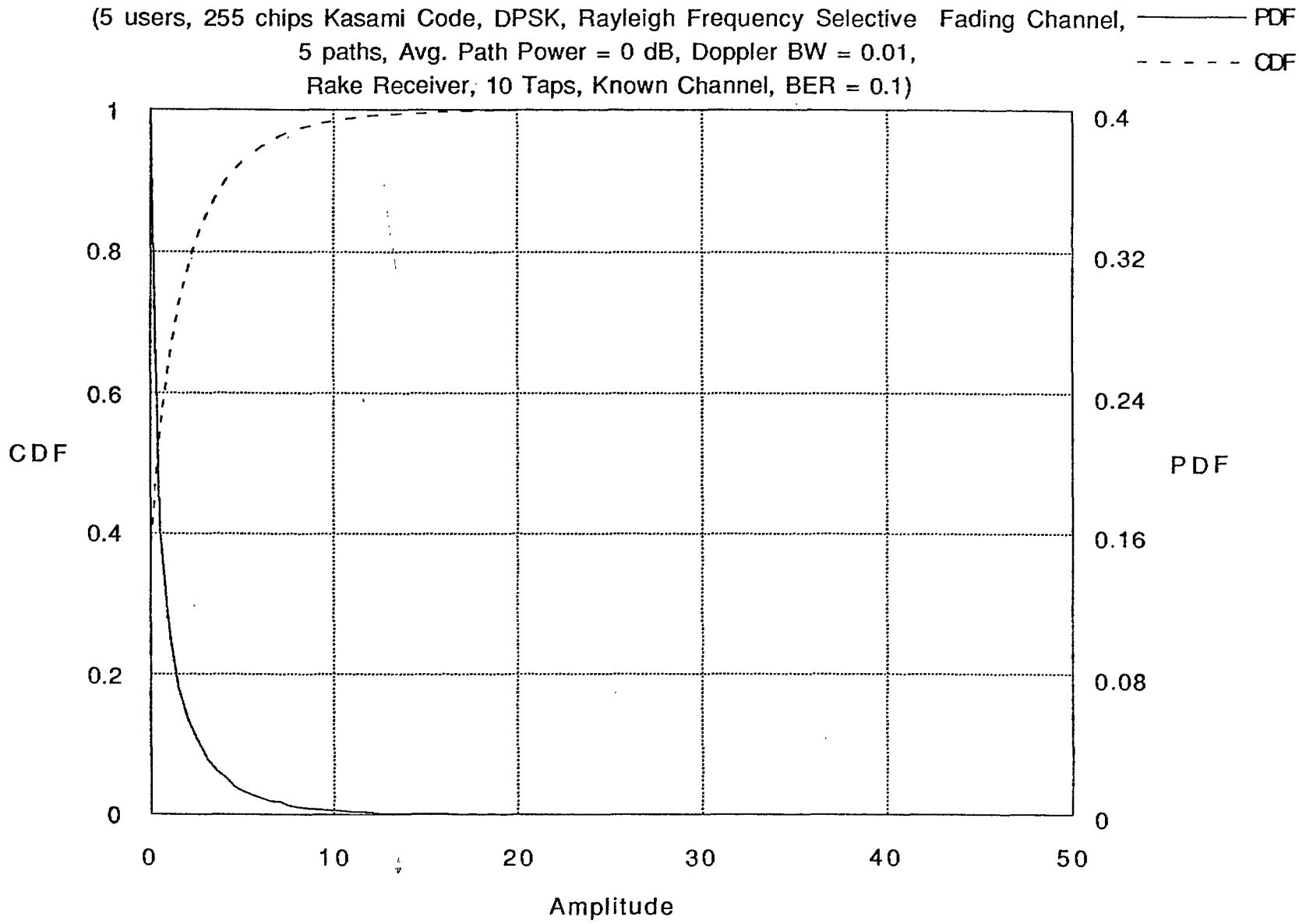

Fig. 28b Symbol Phase Probability Density Function
and Cumulative Distribution Function

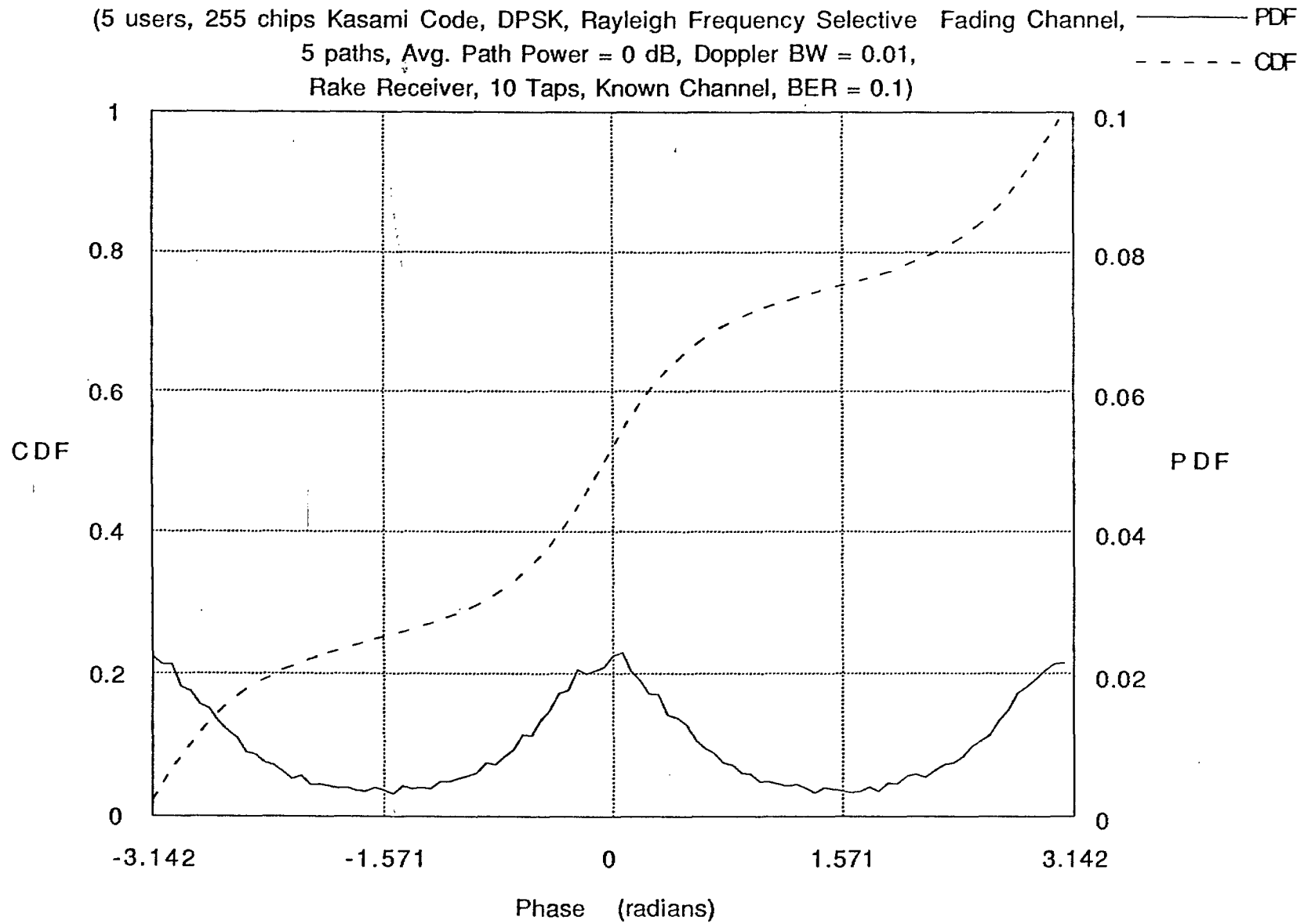

Fig. 28c Symbol Amplitude and Phase Correlation

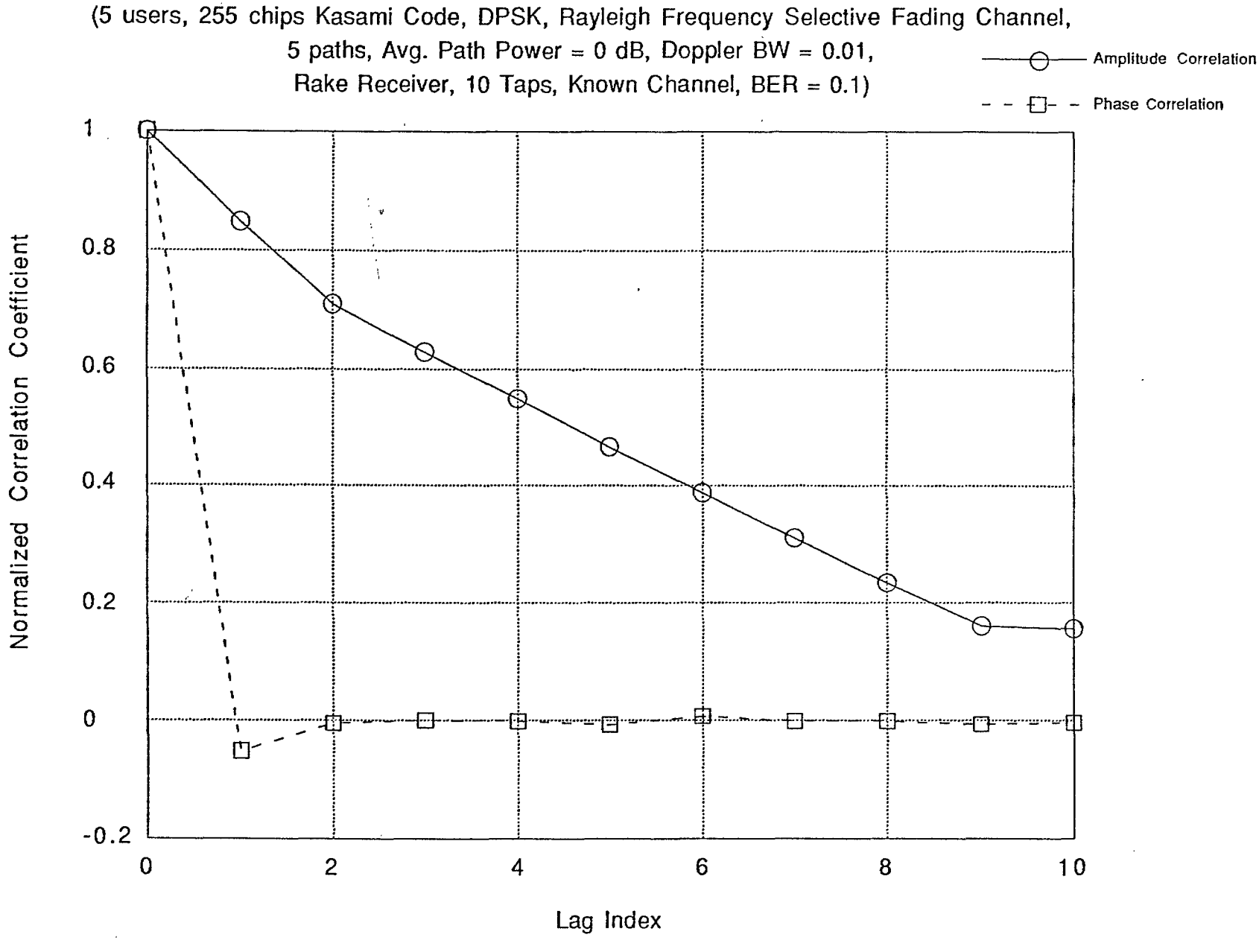

successive transmitted data symbols are independent) and AWGN (also of independent samples). Hence, the symbol amplitudes are independent and as such are uncorrelated. Contrast Fig. 29c with Fig. 26c which shows correlation of symbol amplitude because of the Rayleigh channel fading. In Fig. 29c, the symbol phases are uncorrelated because of the independence between the phases of successive transmitted symbols.

Finally, the symbol statistics of a 5-user system in a Rician frequency selective fading channel with coherent single-path receiver is shown in Figs. 30 and 31 for 31-chip Gold sequence and 255-chip Kasami sequence respectively. A BER of 0.1 is used in Fig. 30 - this implies an E_b/N_0 of 1.5 dB in Fig. 20a. In Fig. 31, only a BER of 0.01 is considered which corresponds to an E_b/N_0 of 5 dB in Fig. 22 (a BER of 0.1 is not considered because the BER is better than 0.1 at an E_b/N_0 of 0 dB). The symbol amplitude PDF becomes narrower and more peaked at a BER of 0.01 (255-chip Kasami sequence). The phase samples are concentrated about 0 and π and there is no correlation among the symbol amplitude samples as well as among the symbol phases. The lack of symbol amplitude correlation is explained partly by the reasons given above (Fig. 29c), as well as the added multi-user and multipath interference effects.

The stationarity of the autocorrelation functions for symbol amplitudes and phases (shown in Figs. 25c to 31c) is tested by using a procedure described below:
i) Generate a block of 50000 symbol amplitudes (or symbol phases)
ii) Divide the 50000 samples into 10 subblocks each of size 5000
iii) For each subblock, compute the correlation function over the first 10 lags
iv) Calculate the (mean) correlation function for the whole block of 50000 samples
v) For lag n, n = 0, 1, ..., 9:

- Calculate the standard deviation of the correlation functions for the subblocks from the correlation function for the whole block
- Calculate the percent coefficient of variation, defined here as a ratio of standard deviation of correlation for the subblocks to the (mean) correlation for the total block, expressed as a percentage

Ideally, the autocorrelation function for symbol amplitudes and phases is said to be stationary if the percentage coefficient of variation is zero at all lags. However, because of the finite number of samples used in the calculation, an

Fig. 29a Symbol Amplitude Probability Density Function and Cumulative Distribution Function

(1 user, Coherent BPSK, Rician Flat Fading Channel, Avg. Path Power = 0 dB, Ω = -100 dB, Doppler BW = 0.01, Single Path Receiver, BER = 0.01)

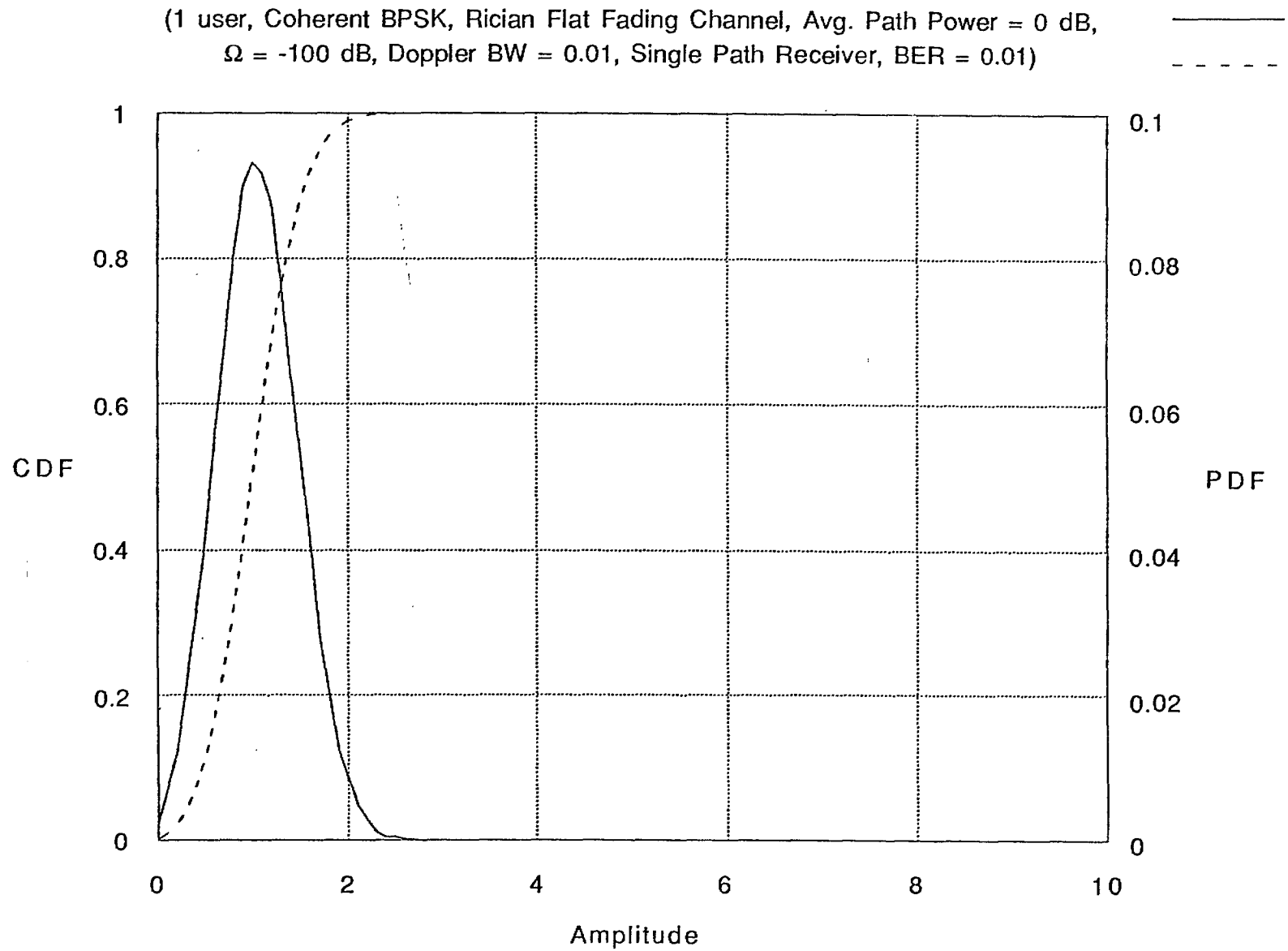

Fig. 29b Symbol Phase Probability Density Function and Cumulative Distribution Function

(1 user, Coherent BPSK, Rician Flat Fading Channel, Avg. Path Power = 0 dB, Ω = -100 dB, Doppler BW = 0.01, Single Path Receiver, BER = 0.01)

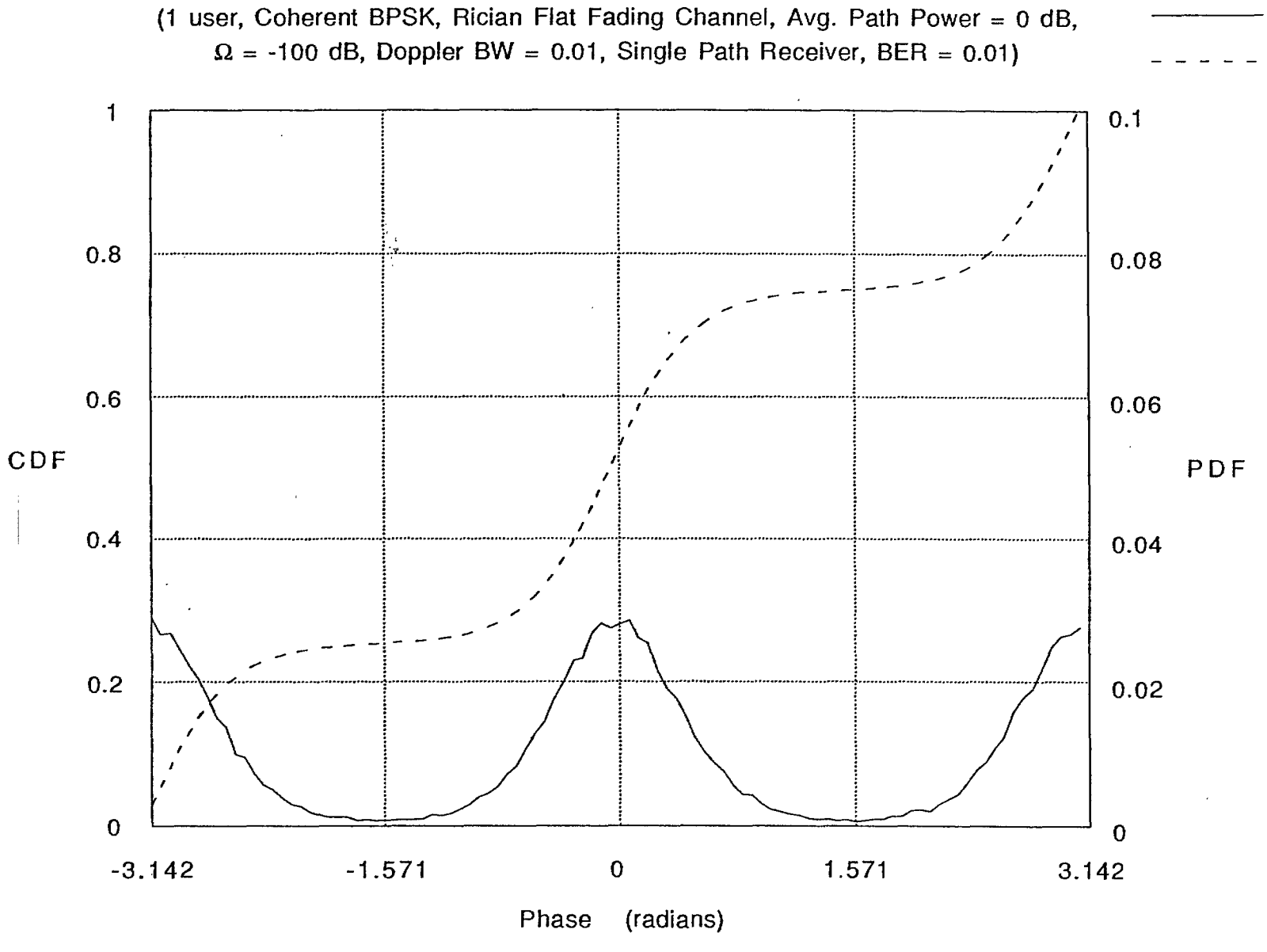

Fig. 29c Symbol Amplitude and Phase Correlation

(1 user, Coherent BPSK, Rician Flat Fading Channel, Avg. Path Power = 0 dB,
Ω = -100 dB, Doppler BW = 0.01, Single Path Receiver, BER = 0.01)

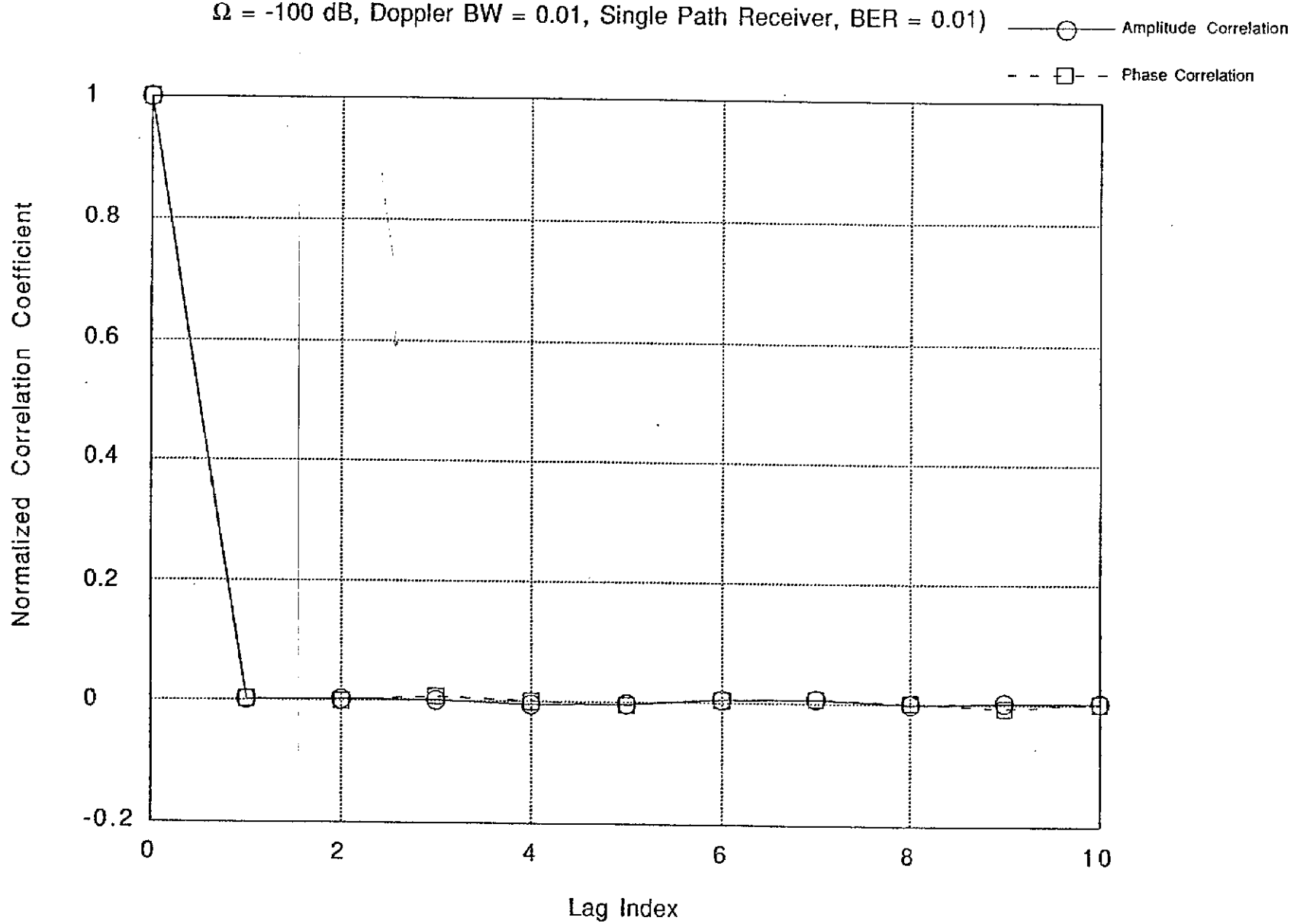

Fig. 30a Symbol Amplitude Probability Density Function and Cumulative Distribution Function

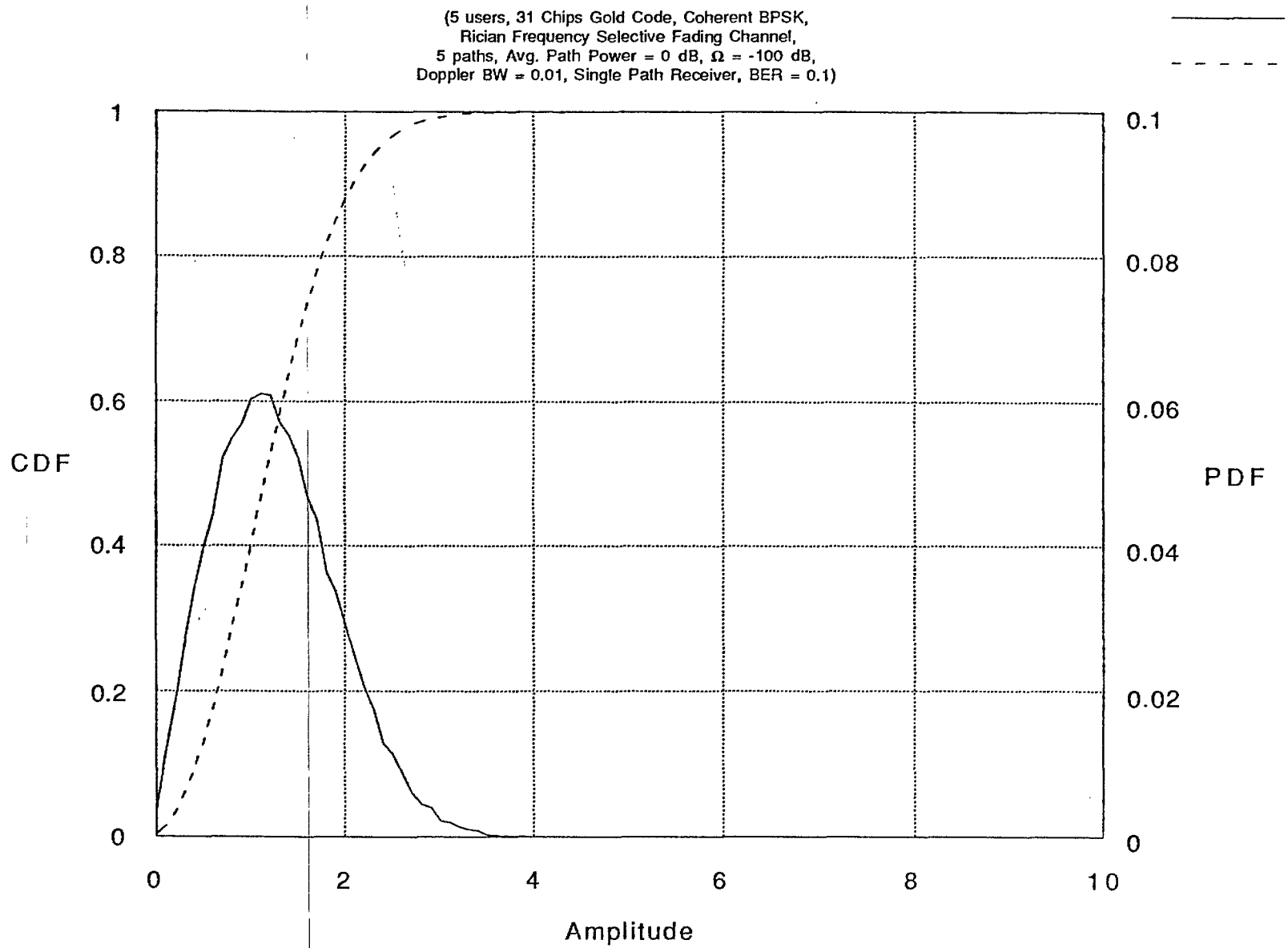

Fig. 30b Symbol Phase Probability Density Function and Cumulative Distribution Function

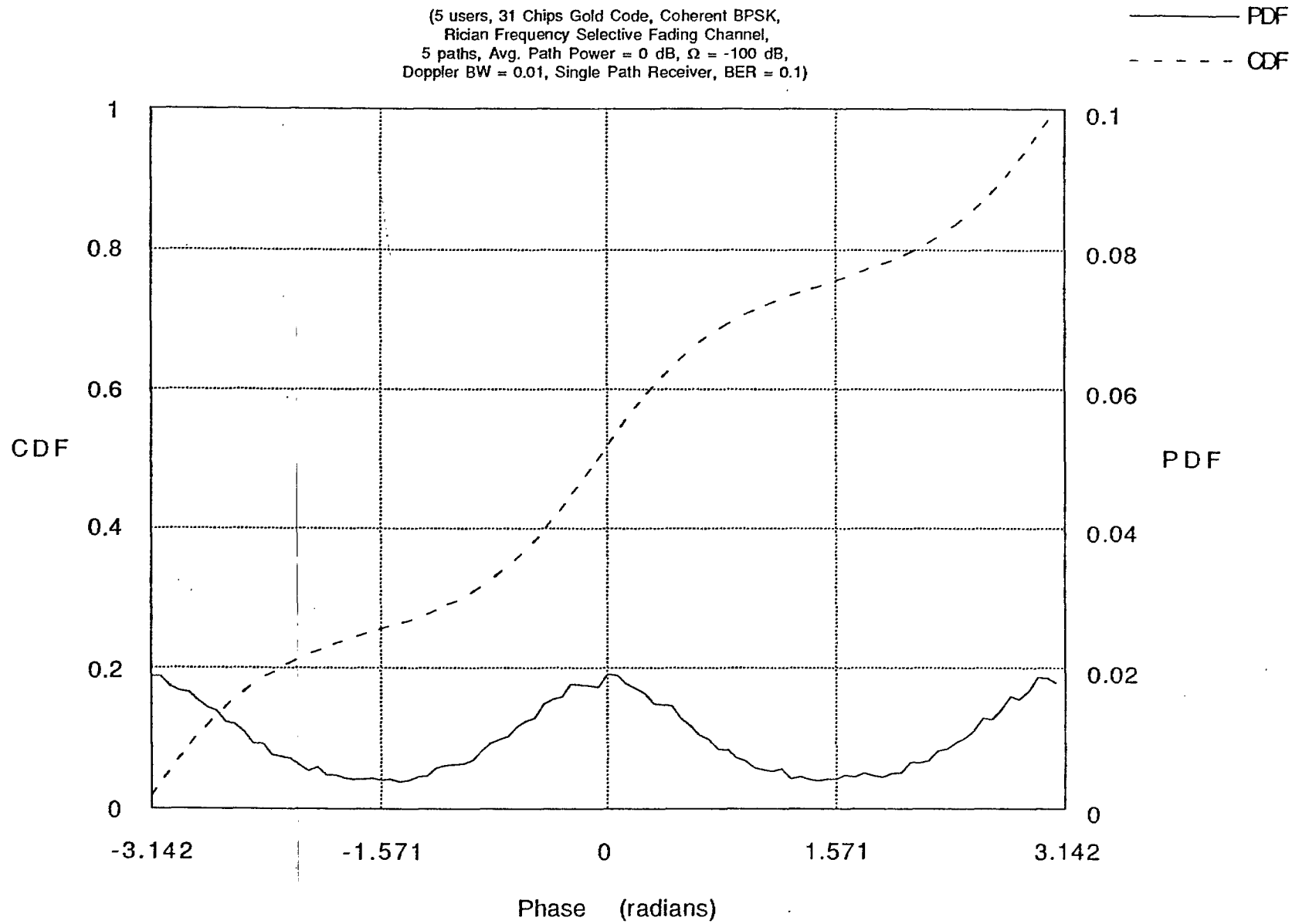

Fig. 30c Symbol Amplitude and Phase Correlation

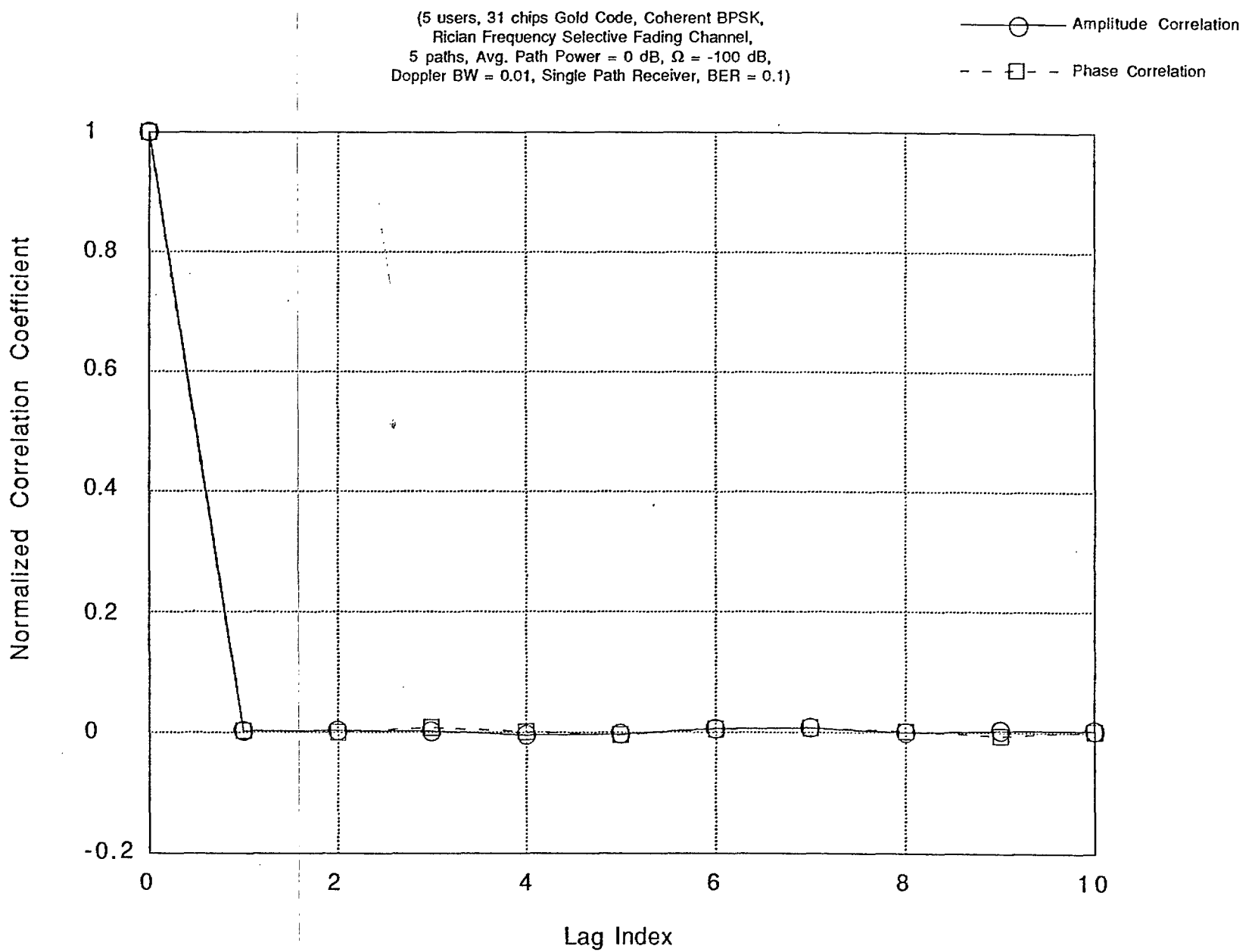

Fig. 31a Symbol Amplitude Probability Density Function and Cumulative Distribution Function

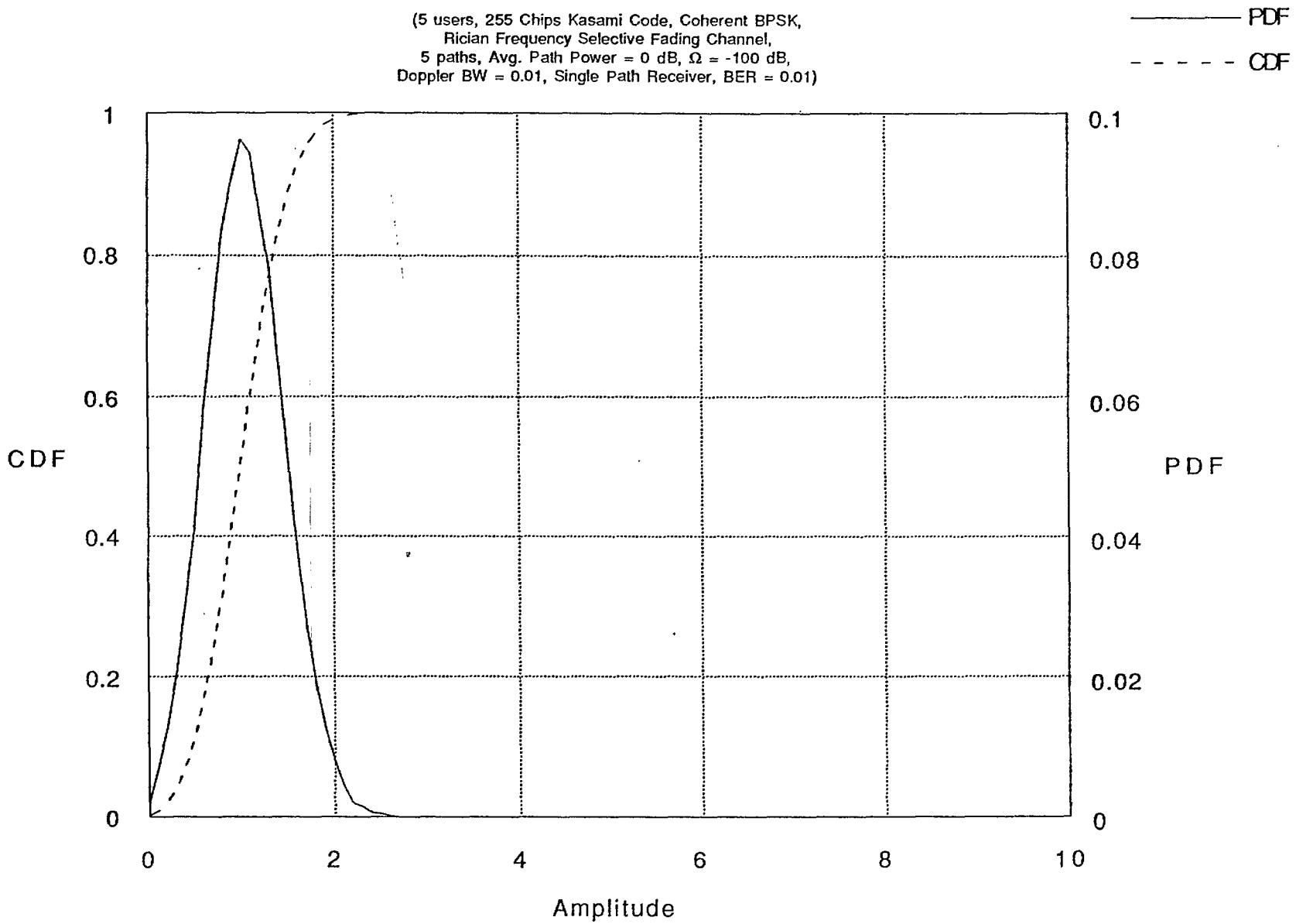

Fig. 31b Symbol Phase Probability Density Function and Cumulative Distribution Function

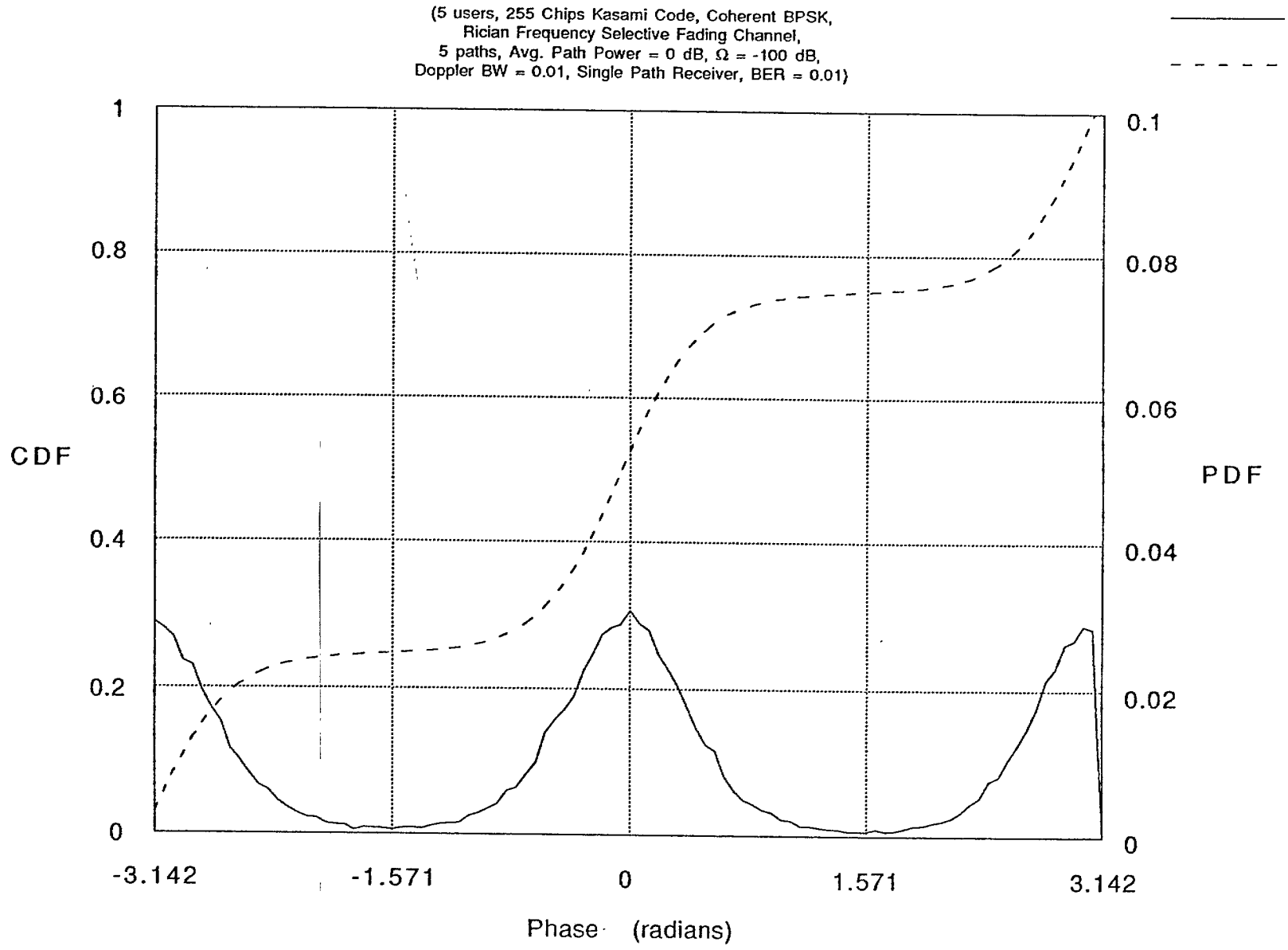

Fig. 31c Symbol Amplitude and Phase Correlation

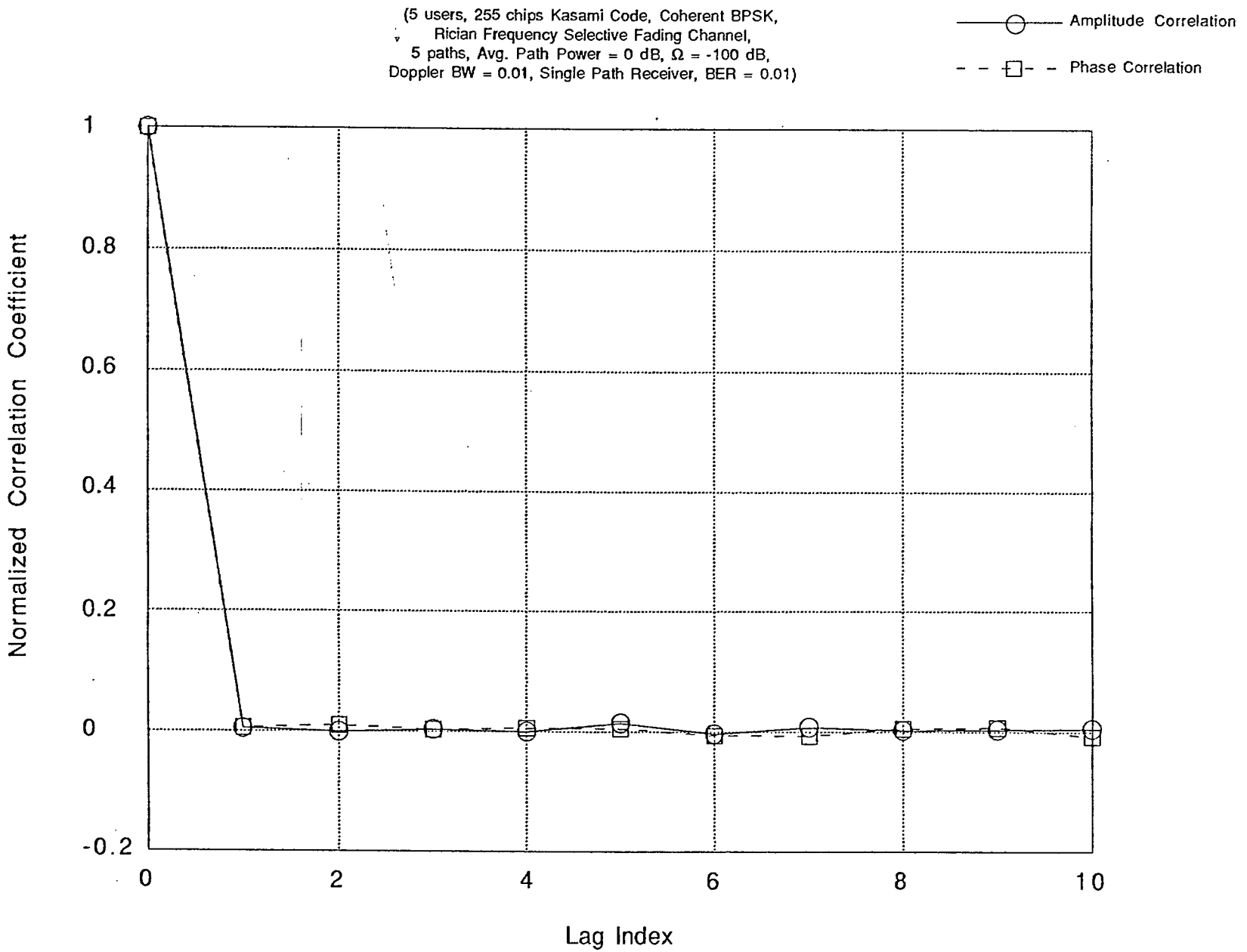

autocorrelation function for symbol amplitudes or phases is taken as stationary provided the percent coefficient of variation is within 10% at all lags. On the basis of this criterion, it is found that the autocorrelation function for the symbol amplitude processes shown in Figs. 25c, 26c and 27c are stationary while those in Fig. 28c to 31c are not. Also, none of the autocorrelation functions for the symbol phase processes shown in Figs. 25c to 31c is stationary.

5.0 Conclusions

The primary objective of this work is to study the effects of radio channel fading, multipath interference, multi-user interference and additive white Gaussian noise (AWGN) on the bit error rate performance of a BPSK/DPSK modulated, direct sequence spread spectrum code division multiple access mobile communication system. This objective is realized through the development of a computer simulation tool for predicting the bit error rate. The basis of the computer simulation tool are the expressions derived for the decision statistic for single path receiver (coherent and differential) and differential RAKE receiver structures.

The following conclusions are drawn from the bit error rates predicted using the simulation tool developed for the mobile to base link of a CDMA system operating in a fading environment:

- For a non-multiple access system in a flat fading channel, the bit error rate performance is affected by additive white-Gaussian noise and random FM noise caused by the random phase fluctuations of the fading channel. In the range of E_b/N_0 where the effects of AWGN become negligible, the random phase fluctuations give rise to an error floor which increases with fading bandwidth in a Rayleigh fading channel with differential single path receiver. For example, by increasing the fading bandwidth from 0.01 to 0.1 gives rise to an increase in the error floor from 5×10^{-4} to approximately 4.4×10^{-2}.

- The BER performance of a single-user CDMA system (assuming 31-chip

Gold sequence) in a Rayleigh frequency selective fading channel with differential single path receiver is independent of mobile speed because of the dominance of the multipath interference over the random FM noise. If 255-chip Kasami sequence is used instead, the multipath interference is reduced and a small dependence of the BER on fading bandwidth appears. The same conclusion also holds for a multiple access CDMA system in a Rayleigh frequency selective channel with differential single path receiver. For a multiple access CDMA system in a Rayleigh flat fading channel with differential single path receiver, increasing the fading bandwidth by an order of magnitude only shows a small increase in the error floor.

- The impact of multipath interference that arises from a single-user CDMA system (31-chip Gold sequence) in a Rayleigh frequency selective channel is minimized by using a multipath combining receiver such as the RAKE. For example, a system in a Rayleigh frequency selective channel and operating at an E_b/N_0 of 10 dB gives simulated bit error rates of 5.2×10^{-2}, 10^{-2} and 7.7×10^{-4} for differential single path receiver, 10-tap RAKE receiver and 20-tap RAKE receiver respectively. This BER improvement comes at a price of increased RAKE receiver design complexity. Alternatively, the simulation results show that multipath interference is also reduced by using 255-chip Kasami sequence which of course implies huge processing requirements. It is found that meaningful comparison between the performance for 31-chip Gold sequence and 255-chip Kasami sequence only holds for single path receiver structure or a multipath combining receiver having the same RAKE window. For a single-user system (255-chip Kasami sequence) in a Rician frequency selective channel (with almost zero fading) and coherent single path receiver, a BER of 10^{-3} is achieved at a value of E_b/N_0 which is about 0.5 dB less than that required assuming 31-chip Gold sequence. The BER performance of a single-user system in a Rician frequency selective channel (with almost zero fading) and coherent single path receiver is found to be better than that of a system in a Rayleigh frequency selective channel and differential 20-tap RAKE receiver. In fact, the simulation results show that the system in a Rician channel requires an E_b/N_0 which is 2.5 dB less than that required by a system in a Rayleigh channel.

- At a desired performance quality specification, multi-user interference limits the number of users that a multiple access CDMA system supports in a flat fading channel. If for example, the performance specification is set to a BER of 10^{-3} which is typical for acceptable voice quality, the simulation results show that five or more users cannot be supported in a Rayleigh flat fading channel with differential single path receiver because the error floor attained with 255-chip Kasami sequence is 5.5×10^{-3}. However, when the simultaneous transmission is over a Rician flat channel with almost zero fading and coherent single path receiver , a BER of 10^{-3} is achieved with 5 users at an E_b/N_0 of 13 dB and 7.2 dB assuming the transmitted signal is spread by 31-chip Gold sequence and 255-chip Kasami sequence respectively. Another finding from the results of a multiple signal transmission (each spread by 31-chip Gold sequence) in a Rician flat channel and detected by a coherent single path receiver is that multiple users in the system cause error floor even when the Rician path experiences almost zero fading, the error floor however disappears if the 31-chip Gold sequence is replaced by the 255-chip Kasami sequence.

- The combined effects of multipath and multi-user interference result in unacceptable performance for a multiple-access CDMA system in a Rayleigh frequency selective fading channel with differential single path receiver. For example, error floors of 0.15 and 0.025 are obtained assuming the transmitted signal is spread by 31-chip Gold sequence and 255-chip Kasami sequence respectively. If the differential single path receiver is replaced by a differential 20-tap RAKE receiver (31-chip Gold sequence) the error floor is reduced by approximately an order of magnitude.

- Another interesting finding from the simulation results of a CDMA system in Rayleigh frequency selective fading is that for 255-chip Kasami sequence, the improvement in BER performance with differential 10-tap and 20-tap RAKE receiver is not as dramatic as the corresponding improvement for 31-chip Gold sequence. This is so because if the code period (expressed in units of time) for both spreading sequences is assumed to be equal, then for a given number of RAKE taps, the RAKE window for the 255-chip Kasami

sequence is obviously less than that for the 31-chip Gold sequence. As a consequence, the probability that a path delay falls within the RAKE window is higher for the 31-chip Gold sequence than it is for the 255-chip Kasami sequence.

- For a multiple-access system in a frequency selective channel where one of the paths between each interfering transmitter and the coherent single path receiver is Rician, then the Rician paths (even at almost zero fading) from all the interfering transmitters contribute significant interference that results in an error floor. For example, a single-user system in a frequency selective fading channel consisting of five paths where one is Rician faded achieves a BER of 10^{-3} at an E_b/N_0 of 8.5 dB. If the number of users is increased to 5, the BER degrades and saturates at 2.8×10^{-2}.

- In a Rayleigh frequency selective fading channel where the average path power decreases with increasing path delay, the interference introduced is expected to be less. Assuming a differential RAKE receiver, the effectiveness of multipath combining is also expected to be reduced. The simulation results show an improvement in the BER performance for a differential 3-tap RAKE receiver in a Rayleigh fading channel (average power decreasing in 2 dB steps from 0 dB) compared to that for a differential 10-tap RAKE receiver in a Rayleigh frequency selective fading channel with constant average path power of 0 dB. It is inferred from this performance improvement that the reduction in the interference is greater than the reduction in the effectiveness of multipath combining.

- All the simulation results of a single-user or multiple-user CDMA system in a Rayleigh frequency selective fading channel with differential RAKE receiver show that the BER performance improves with the number of RAKE taps. However, the number of RAKE taps cannot be increased without limit because there exists an upper limit, which is determined by the maximum delay spread of the radio channel. In a practical system, the price to be paid for the improved performance is the complexity of the RAKE receiver design which depends on the technique adopted for demodulating the received signal. Either a passive or an active design can be used.

Passive design (implemented using SAW matched filter) requires no local spreading code generation at the receiver - hence no need for synchronization circuit design but suffers from low processing gain and very expensive SAW device. On the other hand, the active design (implemented using sliding correlator) requires local spreading code generation at the receiver (hence there is a need for acquisition and tracking circuit design), provides a large processing gain and can be built at lower cost than passive design. It is believed that the selection of a RAKE receiver design technique should be based on factors such as component/device cost, receiver circuitry design complexity and receiver performance in a multipath fading environment. Preliminary in-house studies on RAKE receiver design [13] seem to favor an active design technique because of its low component cost and robustness of performance in a multipath environment. However, as stated above, synchronization circuitry is required, satisfying this requirement may not be a trivial task especially in a fast fading environment.

Suggested below are three areas on the work reported in this report which require further study:

i) All the current simulation results have been generated assuming Rayleigh and Rician fading channels. It is of interest to investigate the performance of the CDMA multiple access system in a realistic urban radio propagation channel using for example the radio channel simulation package developed in [3].

ii) The simulated RAKE receiver structure in the current study assume "perfect" channel estimator or equal gain combining. Clearly, the BER performance with perfect channel estimator serves as a lower bound. A challenging problem is to devise practical or imperfect channel estimator(s) for the RAKE receiver. Availability of such a practical channel estimator will then allow us to measure its performance relative to that of a perfect channel estimator.

iii) Investigate other possible techniques that can be used to improve BER performance such as application of power control

where the mobiles transmit at different power levels (current study assume that all mobiles transmit at the same power level), application of antenna diversity at the base station and lastly, application of forward error correction encoding/decoding.

References

1. CRC: Revised Statement of work for CDMA Performance study, January 23, 1991.

2. M.B. Pursley, "Spread-spectrum multiple access communications," *in Multi-user Communications,* G. Longo (ed.), New York: Springer - Verlag, pp. 139 - 199, 1981.

3. H. Hashemi, "Simulation of the urban radio propagation channel," IEEE Trans. Veh. Tech., vol. VT-28, pp. 213 - 224, Aug. 1979.

4. E. Lutz and E. Plochinger, "Generating Rice Processes with given spectral properties," *IEEE Trans. Veh. Tech.*, vol. VT-34, pp. 178-181, Nov. 1985.

5. J.R. Ball , "A real-time fading simulator for mobile radio," *The Radio and Electronic Engineer*, vol. 52, pp. 475 - 478, Oct. 1982.

6. M. Schwartz, W.R. Bennett, and S. Stein , *Communication Systems and Techniques,* New York: McGraw-Hill, 1966.

7. G.L. Turin, "Introduction to spread-spectrum antimultipath techniques and their application to urban digital radio," *Proceedings of the IEEE,* vol. 68, pp. 328 - 353, March 1980.

8. J. Proakis, *Digital Communications*, 2nd ed., New York: McGraw-Hill, 1989.

9. M. B. Pursley and H.F.A. Roefs, "Numerical evaluation of correlation parameters for optimal phases of binary shift-register sequences," *IEEE Trans. Comm*, vol. COM-27, pp. 1597 - 1604, October 1979.

10. C. Jakes, Jr., *Microwave Mobile Communications,* New York: John Wiley & Sons, 1974.

11. W.H. Lam and R. Steele, "Performance of direct-sequence spread-spectrum multiple-access systems in mobile radio," *IEE Proceedings - I*, vol. 138, pp. 1 - 14, Feb. 1991.

12. E. A. Geraniotis and M. B. Pursley, "Performance of coherent direct-sequence spread spectrum communications over specular multipath fading channels," *IEEE Trans. Comm*, vol. COM-33, pp. 502 - 508, June 1985.

13. C. Tsien, "DS-CDMA system study with RAKE structure," *Internal Report, System Definition & Simulation Group, NovAtel,* August, 1991.